Symmetry Method for Limit Cycle Walking of Legged Robots

by

Seyed Hamed Razavi

A dissertation submitted in partial fulfillment
of the requirements for the degree of
Doctor of Philosophy
(Applied and Interdisciplinary Mathematics)
in The University of Michigan
2016

Doctoral Committee:

Professor Anthony Bloch, Co-Chair
Professor Jessy Grizzle, Co-Chair
Professor Peter Miller
Assistant Professor C. David Remy
Assistant Professor Shai Revzen

To My Dad

ACKNOWLEDGEMENTS

It might be me writing this thesis, but there are many others without whom this thesis would not have been possible.

I owe many thanks to my love of life, Maryam, for her support and sacrifices. Maryam, I cannot imagine that I could have done this without you. It is not even possible to thank you, but thank you!

I would like to thank Prof. Tony Bloch who has always been there for me, always supported me. I was very lucky to have him as my advisor. Working with Tony has been a milestone in my life. I learned a lot from him. Tony, I don't know how to thank you, but thank you!

I am also very grateful to my co-advisor, Prof. Jessy Grizzle. He showed me that there is another level of excellence to everything. He taught me the lesson that "whatever you do, do it extraordinary". Jessy, you made me raise my standards, and I learned a lot from you. I don't know how to thank you, but thank you!

I wish to thank my committee member, Prof. Peter Miller. I remember my first days here at Michigan, and I never forget how supportive he was. Peter, I don't know how to thank you, but thank you!

I am also very grateful to my other committee members, Prof. Revzen and Prof. Remy, for their valuable feedback and discussions in our meetings and in particular, in the legged robotics group meetings.

I wish to extend my thanks to Prof. Christine Chevallereau for her invaluable feedback on my work. Christine hosted me in IRCCyN, France during Fall 2015 and

made it possible for me to work with Romeo. It was a great experience for which I am very thankful to Christine. During this time, I also worked with Pierre-Alexandre Geraert to whom I want to express my thanks as well. I am also thankful to Prof. Yannick Aoustin for his insightful feedback on my work on symmetry.

I also would like to express my sincere thanks to my colleagues Xingye (Dennis) Da, Brent Griffin and Leo Colombo for the helpful discussions during the past years, and especially, would like to thank Dennis for providing me with MARLO's simulation codes.

I am grateful to National Science Foundation, Rackham Graduate School and International Institute of the University of Michigan for their support through research grants and fellowships.

Last, but not least, I would like to thank my Mom. If I am at this stage, it is because of you, Mom.

Hamed Razavi,

Ann Arbor, 2016

TABLE OF CONTENTS

LIST OF FIGURES

Figure

LIST OF TABLES

Table

LIST OF ABBREVIATIONS

COM Center of Mass

DOF Degrees of Freedom

ZMP Zero Moment Point

DIP Double Inverted Pendulum

SVF Symmetric Vector Field

SHS Symmetric Hybrid System

LIP Linear Inverted Pendulum

SLIP Spring Loaded Inverted Pendulum

HZD Hybrid Zero Dynamics

IP Inverted Pendulum

IPF Inverted Pendulum with Flywheel

CGB Compass-Gait Biped

SBP Symmetric Bézier Polynomial

PSBP Perturbed Symmetric Bézier Polynomial

URDF Unified Robot Description Format

MDH Modified Denviat-Hartenberg

PD Proportional-Derivative

ABSTRACT

Symmetry Method for Limit Cycle Walking of Legged Robots

by

Hamed Razavi

Chairs: Anthony Bloch and Jessy Grizzle

Dynamic steady-state walking or running gaits for legged robots correspond to periodic orbits in the dynamic model. The common method for obtaining such periodic orbits is conducting a numerical search for fixed points of a Poincaré map. However, as the number of degrees of freedom of the robot grows, such numerical search becomes computationally expensive because in each search trial the dynamic equations need to be integrated. Moreover, the numerical search for periodic orbits is in general sensitive to model errors, and it remains to be seen if the periodic orbit which is the outcome of the search in the domain of the dynamic model corresponds to a periodic gait in the actual robot.

To overcome these issues, we have presented the *Symmetry Method for Limit Cycle Walking*, which relaxes the need to search for periodic orbits, and at the same time, the limit cycles obtained with this method are robust to model errors.

Mathematically, we describe the symmetry method in the context of so-called Symmetric Hybrid Systems, whose properties are discussed. In particular, it is shown that a symmetric hybrid system can have an infinite number of periodic orbits that can be identified easily. In addition, it is shown how control strategies need to be

selected so that the resulting reduced order system still possesses the properties of a symmetric hybrid system.

The method of symmetry for limit cycle walking is successfully tested on a 12 Degrees of Freedom (DOF) 3D model of the humanoid robot Romeo.

CHAPTER I

Introduction

1.1 Why Legged Robots?

Aside from the fact that legged robots are fun and interesting to study, there are three reasons why research on legged robots is necessary.

First, there is a need for vehicles that can travel on uneven terrains where wheeled vehicles cannot operate. Wheeled vehicles can only perform well on prepared surfaces such as roads and rails. Unlike the wheeled vehicles which need a continuos path for travel, legged robots have the choice of choosing their footholds to optimize their traction and stability (*Raibert*, 1986a). Stairs or ladders are examples where legged robots outperform wheeled vehicles.

Second, a study of legged robots and control strategies, which can lead to stable walking, directly applies to the research on exoskeletons and rehabilitation robotics (see (*Gregg et al.*, 2014) as an example).

Finally, building legged robots and analyzing their gaits and their energy aspects can help one understand the biological aspects of the locomotion of animals (*Ijspeert*, 2014).

1.2 From Static Walking to Dynamic Walking

One of the main challenges in the path toward having legged robots as reliable as the wheeled vehicles is the issue of stability in legged locomotion. Unlike a car which is hardly unstable, a bipedal robot, without control, is hardly stable; in particular, during the walking, in a period of time a bipedal robot has only one foot as the support. With this in mind, the first research approaches on legged robots were focused on maximizing the support polygon[1] to make stability of the legged robot as simple as that of a car or a table standing still. The control strategy was simply to ensure that the projection of the Center of Mass (COM) on the ground lies on the support polygon. In order for this criterion to lead to stability, the legs and body move slowly enough such that if the legs stop moving at any point, the robot does not fall. This is why these robots are referred to as *static crawlers*, and the stability which is achieved by this strategy is called *static stability*. One of the first successful examples of a static crawler is Robert McGhee's hexapod (*McGhee*, 1985) as shown in Fig. 1.2.

A step taken toward getting more dynamic locomotion was the notion of Zero Moment Point (ZMP). The ZMP is a point on the ground where the resultant of the ground-reaction forces acts (*Goswami*, 1999). A walking gait is said to be ZMP stable if the ZMP stays within the area of the support polygon (not on the edge). Since the ZMP stays within the support polygon, for bipedal robots, ZMP criterion only allows flat-footed walking. Today, most of the research on legged locomotion is based on the ZMP criterion. Unlike static stability, ZMP criterion allows dynamic walking, in the sense that there are successful walking gaits that are ZMP stable but not statically stable. Despite the fact that ZMP allows dynamic locomotion, there are a number of downsides to this method. First, there are many gaits in humans,

[1]Support polygon is the convex hull formed by all of the contact points with the ground (*Westervelt et al.*, 2007), for example, with three point feet on the ground the support polygon is a triangle.

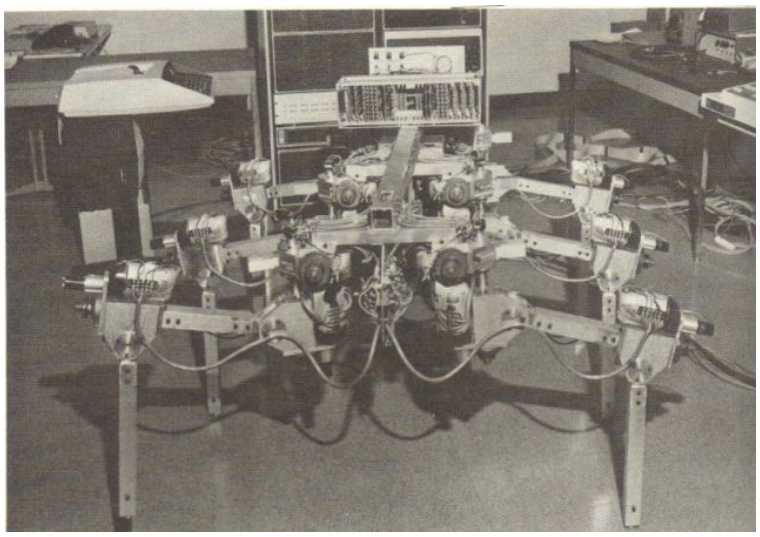

Figure 1.1: Robert McGhee's hexapod, Ohio State University, 1977.

animals and some legged robots that are dynamically stable but not ZMP stable. For instance, Raibert's hopper (*Raibert*, 1986b) or the bipedal robot MABEL (*Grizzle et al.*, 2009; *Sreenath et al.*, 2011) are both point-feet robots that have achieved many stable walking and/or running gaits, which because of the point-feet, none of them are ZMP stable. Another issue with the ZMP method is that the ZMP stable gaits are not the most energy optimal walking gaits as all the actuators including the stance leg ankle are engaged during the walking gait; in fact, all ZMP stable bipedal robots are fully actuated robots. Finally, the ZMP stable gaits don't allow the full extent of agility that a legged robot can reach. As an example, the dynamically stable bipedal robot MABEL has reached a peak speed of 3.06 m/s (*Sreenath et al.*, 2013), while the ZMP stable bipedal robots have a far lower pick speed.

In contrast to static and ZMP walking, which respectively require the projection of the COM and the ZMP to lie on the support polygon all the time, the highly dynamic walking or running gaits only require an average stable behavior; the legged robot places its leg(s) fast enough to prevent the robot from falling. That is, the robot is falling and catching itself so that on average the COM is not diverting much from

Figure 1.2: The Bipedal Robot MABEL, University of Michigan, 2009. MABEL has reached a pick speed of 3.06 m/s (*Sreenath et al.*, 2013).

a reasonable trajectory. As a means of illustration, look at Fig. 1.3 which shows a simple inverted pendulum with a point support (point O in Fig. 1.3). With an initial velocity and under gravity the point mass travels from point $-x_0$ to x_0. Even though the mass spends almost all of the time away from the support point (i.e., $x \neq 0$), *on average* it stays on the point O. In other words, if $x(t)$ is the position of the point and the whole motion from $-x_0$ to x_0 takes T seconds, then

$$\bar{x} = \frac{1}{T} \int_0^T x(t) \, \mathrm{d}t = 0.$$

If there is a control strategy that can keep this average close to zero or converging to zero in the subsequent steps, then the walking is considered as being dynamically stable; however, from the static stability or ZMP criterion this motion is not considered as being stable because the support polygon is a single point.

Compared to static or ZMP criterion, even though the dynamic stability has the least requirement for a gait to be considered as being stable, mathematical modeling

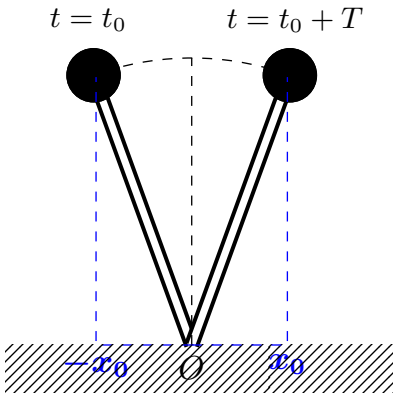

Figure 1.3: Simple Inverted Pendulum Biped With Massless Legs.

of a criterion for average stable behavior that can realize a control strategy is not easy. However, a notion which can capture the agility that dynamic stability criterion provides and at the same time is mathematically easier to model and test is the notion of limit cycle legged locomotion.

In limit cycle legged locomotion, a walking or running gait is modeled as a periodic orbit of the associated dynamical system, and the walking is considered as being stable if the associated periodic orbit is stable.

The problem of stable limit cycle walking is the main focus of this thesis. The two main challenges in this problem are (i) how to obtain periodic walking gaits for a given legged robot, and (ii) how to ensure their stability.

Periodic locomotion is primarily studied by a Poincaré map analysis. The common method for obtaining stable periodic gaits of a legged robot is to search for fixed points of the Poincaré map (a.k.a. stride function) such that the eigenvalues of the linearization of the Poincaré map are within the unit circle (*McGeer*, 1990; *Grizzle et al.*, 2001; *Wisse et al.*, 2005; *Geng et al.*, 2006; *Gregg and Righetti*, 2013; *Dingwell and Kang*, 2007).

To reduce the computational costs of the numerical search, Grizzle et al. (*Grizzle*

et al., 2001) have used the notion of virtual constraints and Hybrid Zero dynamics (HZD) to conduct the search on a lower dimensional system. Virtual constraints are relations between the generalized coordinates of the system that are enforced by controllers. By using a class of Bézier polynomials for virtual constraints, Grizzle et al. (*Grizzle et al.*, 2008) have demonstrated the possibility of gait design together with optimization on energy, torque limit, etc.

Search methods, however, have two main drawbacks: namely, high computational costs and the robustness issue. The high computational cost is due to the fact that in each trial the equations of motion need to be integrated to check if the solution returns back to the starting point, and the robustness issue is due to the fact that the search for fixed points of the Poincaré map is performed based on a model of the legged robot, and it remains to be seen whether with model errors, which always more or less exist, the fixed point still corresponds to a periodic orbit of the actual system. Moreover, since the stability is based on the eigenvalues of the Jacobian of the Poincaré map, the periodic orbit is only locally stable. With local stability it is challenging to have the actual robot start walking or running from rest.

The main contribution of this thesis is to introduce the method of *Symmetry for Limit Cycle Walking* for legged robots which relaxes the need for searching for periodic orbits; at the same time, since this method relies only on general symmetry principles that all legged robots possess, naturally, robustness issue will be resolved. In the next section we present a brief overview of this method.

1.3 Symmetry Method for Stable Periodic Walking

The simplest example that can capture some important properties of legged robots is a Linear Inverted Pendulum (LIP) as depicted in Fig. 1.4. As will be discussed

later, the equation of motion of a 2D LIP can be written as

$$\ddot{x} = \omega^2 x \tag{1.1}$$

for $\omega \in \mathbb{R}$, where x is the position of the point mass projected to the ground in the inertial frame attached to the support point (point O in Fig. 1.4). Consider a solution of this system starting from $x(t_0) = -x_0$ and $\dot{x}(t_0) = \dot{x}_0 > 0$. Multiplying the two sides of (1.1) by $\dot{x}$ yields

$$\ddot{x}\dot{x} = \omega^2 x\dot{x}.$$

Suppose that $x(t_0 + T) = x_0$ for some $T > 0$. Integrating this equation from t_0 to $t_0 + T$ results in

$$\int_{t_0}^{t_0+T} \ddot{x}\dot{x}\mathrm{d}t = \int_{t_0}^{t_0+T} \omega^2 x\dot{x}\ \mathrm{d}t, \tag{1.2}$$

from which we conclude that

$$\frac{1}{2}(\dot{x}^2(t_0 + T) - \dot{x}^2(t_0)) = \int_{-x_0}^{x_0} \omega^2 x\mathrm{d}x, \tag{1.3}$$

where $\dot{x}\mathrm{d}t$ on the ride-hand-side of (1.2) is replaced with $\mathrm{d}x$. Since $\int_{-x_0}^{x_0} \omega^2 x\mathrm{d}x = 0$, from (1.3) we conclude that $\dot{x}(t_0 + T) = \dot{x}(t_0)$; that is, the velocity at the end of step is equal to that of the beginning of step. Since the LIP moves on a plane of constant height z_0, there will be no impact loss when the swing leg hits the ground[2] and the velocity of the point mass at the beginning of next step will be $\dot{x}(t_0)$; as a result, if at the beginning of each step $x = -x_0$, the motion is periodic.

Indeed, in (1.3) if x on the right-hand-side is replaced with any other odd function,

[2]This will be discussed in details in Chap III.

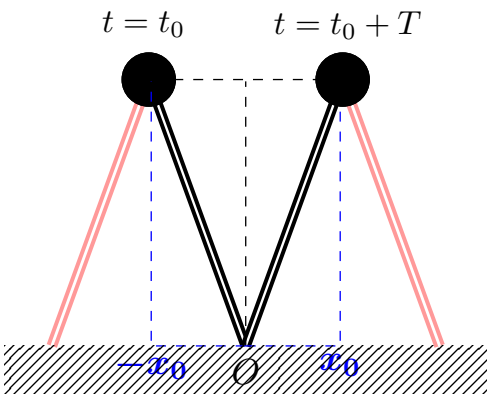

Figure 1.4: 2D Linear Inverted Pendulum. The point mass moves on a line of constant height.

$f(x)$, the solution is periodic. Thus, all that really matters for periodicity of solutions of an equation in the form $\ddot{x} = \omega^2 f(x)$ with a trivial impact map (i.e., similar to that of LIP) is the oddness of the function $f(x)$. Similar symmetries exist in the equations of motion of more complex models of legged robots. For instance, the kinetic and potential energies of the 2D Double Inverted Pendulum (DIP) depicted in Fig. 1.5 are invariant under the map G which sends $(\theta_1, \theta_2, \dot{\theta}_1, \dot{\theta}_2)$ to $(-\theta_1, -\theta_2, \dot{\theta}_1, \dot{\theta}_2)$. As a result, in the equations of motion of the 2D DIP, which can be written as

$$\begin{aligned} \ddot{\theta}_1 &= f(\theta_1, \theta_2, \dot{\theta}_1, \dot{\theta}_2), \\ \ddot{\theta}_2 &= g(\theta_1, \theta_2, \dot{\theta}_1, \dot{\theta}_2), \end{aligned}$$

we have $f(-\theta_1, -\theta_2, \dot{\theta}_1, \dot{\theta}_2) = -f(\theta_1, \theta_2, \dot{\theta}_1, \dot{\theta}_2)$ and $g(-\theta_1, -\theta_2, \dot{\theta}_1, \dot{\theta}_2) = -g(\theta_1, \theta_2, \dot{\theta}_1, \dot{\theta}_2)$.

Similarly, the Spring Loaded Inverted Pendulum (SLIP) and the 5-DOF biped as explained in Fig. 1.6 and Fig. 1.7 are symmetric under the specified transformations.

In the following chapters, we discuss the symmetry method in details and show how these existing symmetries can be exploited to generate stable limit cycle walking

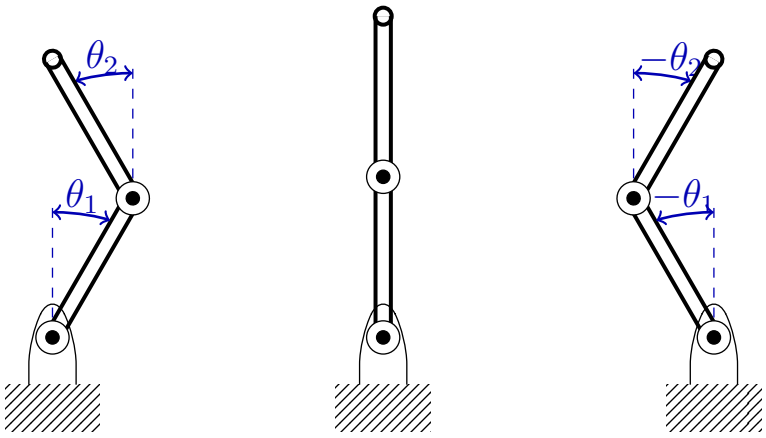

Figure 1.5: The kinetic and potential energy of the Double Inverted Pendulum (DIP) is invariant under the map $(\theta_1, \theta_2, \dot{\theta}_1, \dot{\theta}_2) \mapsto (-\theta_1, -\theta_2, \dot{\theta}_1, \dot{\theta}_2)$. The fixed points of this map, as shown in the middle figure, occurs at $\theta_1 = 0$ and $\theta_2 = 0$, with arbitrary $\dot{\theta}_1^*$ and $\dot{\theta}_2^*$.

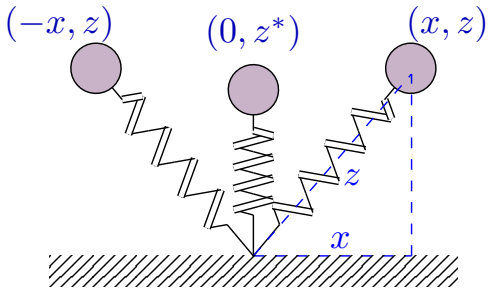

Figure 1.6: The kinetic energy and potential energy of the SLIP are invariant under the map $(x, z, \dot{x}, \dot{z}) \mapsto (-x, z, \dot{x}, -\dot{z})$, where z is the length of the spring. The fixed points of the map G, which correspond to the configuration in the middle figure the middle SLIP model in the figure above, are $(0, z^*, \dot{x}^*, 0)$ for arbitrary z^* and $\dot{x}^*$.

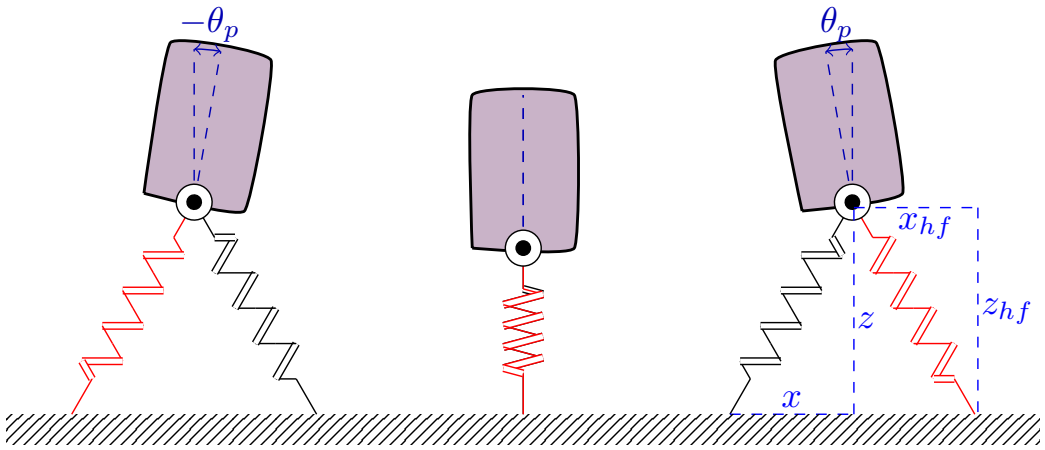

Figure 1.7: If $(x, z, \theta_p, x_{hf}, z_{hf})$ denotes the generalized coordinates, where (x, z) is the position of the hip, θ_p is the pitch angle and (x_{hf}, z_{hf}) is the swing leg end position relative to hip. Assuming that the legs are identical and the mass distribution is uniform, the Lagrangian is invariant under the map G which maps $(x, z, \theta_p, x_{hf}, z_{hf}) \mapsto (-x, z, -\theta_p, -x_{hf}, z_{hf})$.

gaits for legged robots.

Fig 1.8 shows an overview of the symmetry method for limit cycle walking. Based on this method, given a legged robot, first the natural symmetries of the legged robot are detected. Then virtual constraints are chosen such that the symmetry is preserved while the dimension of the system is reduced (i.e., the resulting HZD is symmetric) by enforcing the virtual constraints using controllers. Such virtual constraints are called Symmetric Virtual Constraints (SVCs). It is then shown that the resulting HZD is a Symmetric Hybrid System (SHS) (*Razavi et al.*, 2016), and consequently, has an infinite number of symmetric periodic orbits, which can be identified easily (i.e., without any searches). The SVCs also allow gait design (with possible optimization on energy, torque limit, etc.). The last two steps of the symmetry method for limit cycle walking include introducing asymmetries and augmenting foot placement for achieving asymptotically stable limit cycles with relatively large basins of attractions.

The rest of this thesis is organized as follows. In Chapter II, we discuss Symmetric Vector Fields and SHSs. It will be shown that a Symmetric Hybrid System can possess

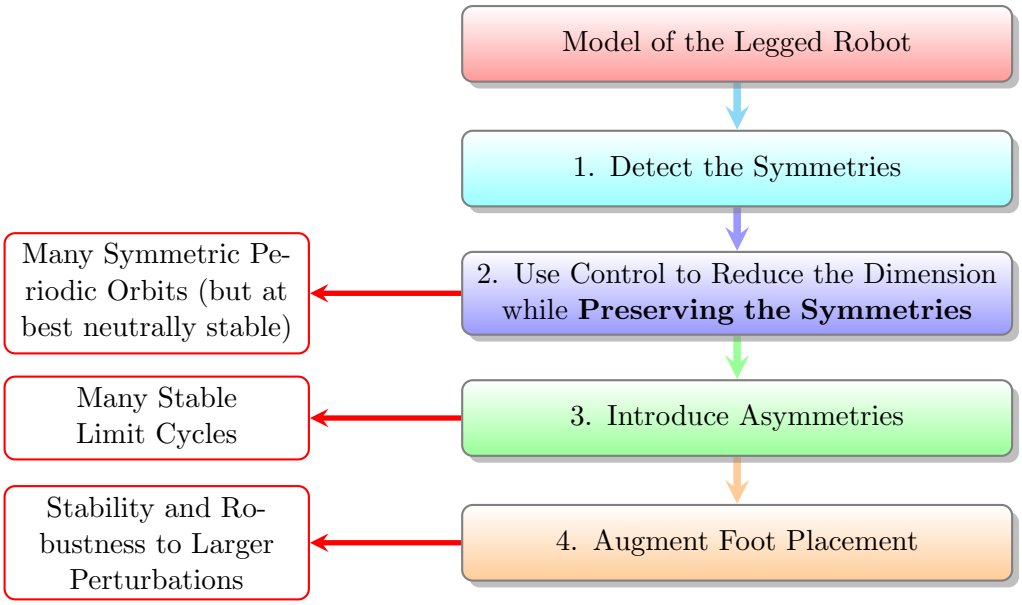

Figure 1.8: High-level control algorithm of the symmetry method for stable limit cycle walking.

an infinite number of symmetric periodic orbits. In Chapter III, examples of legged robots which are SHSs are given. Chapter V discusses in detail the second step in Fig. 1.8; the notion of SVCs and symmetric HZD is introduced in this chapter. It will be shown how SVCs can realize feedback control laws which reduce the dimension of the system while preserving the symmetry so that the resulting system can have an infinite number of symmetric periodic orbits. As a tool for gait design, the notion of a Symmetric Bézier Polynomial (SBP) is introduced. SBPs can be easily utilized to produce SVCs. Chapter VI discusses the stability of symmetric periodic orbits and presents two methods for stabilization of symmetric periodic orbits: introducing asymmetry and foot placement. The notion of Perturbed SBPs (PSBPs) is introduced as a means of systematic introduction of asymmetry as well as augmentation of foot placement algorithms to a symmetric system. Chapter VII includes an example of a 12-DOF 3D biped, Romeo, on which the symmetry method for limit cycle walking is successfully tested in simulations. Chapter VIII includes the conclusions.

CHAPTER II

Symmetric Vector Fields and Symmetric Hybrid Systems

2.1 Symmetric Vector Fields

The notion of symmetry, which was pointed out in Section 1.3, can be mathematically described by the notion of a *Symmetric Vector Field (SVF)* as defined below.

Definition II.1. Suppose that X is a smooth vector field on the manifold $\mathcal{X}$, and let $G : \mathcal{X} \to \mathcal{X}$ be a smooth map which is an involution, that is, $G \circ G = \mathrm{id}$, where id is the identity map on $\mathcal{X}$. If

$$X \circ G = -\mathrm{d}G \cdot X, \tag{2.1}$$

then X is said to be symmetric under G or simply G-symmetric, and G is said to be a symmetry map for X.

Such symmetry of a vector field, which has been referred to as time reversal symmetry in (*Altendorfer et al.*, 2004), is closely related to the notion of equivariant vector fields (*Buono et al.*, 2008).

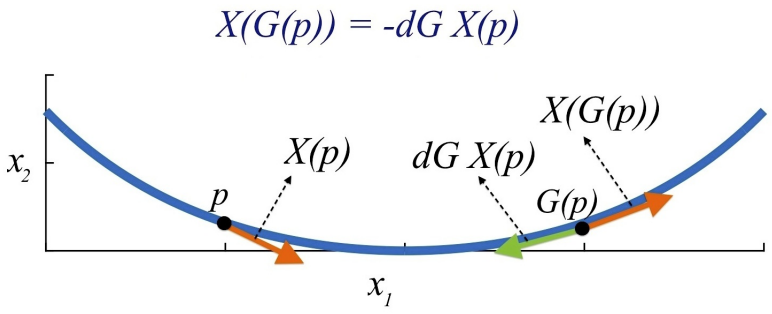

Figure 2.1: Graphical illustration of the SVF in Example II.2.

Example II.2. Consider the vector field

$$X(x_1, x_2) = \begin{bmatrix} x_2 \sin(x_2) + x_2 x_1^2 \\ x_1^2 \sin(x_1) + 2x_1 x_2 \end{bmatrix},$$

defined on $\mathbb{R}^2$. Define $G : \mathbb{R}^2 \to \mathbb{R}^2$ by $G(x_1, x_2) = (-x_1, x_2)$. Since $X \circ G(x_1, x_2) = X(-x_1, x_2) = (x_2 \sin(x_2) + x_2 x_1^2; -x_1^2 \sin(x_1) - 2x_1 x_2)$, and

$$\begin{aligned} -\mathrm{d}G \cdot X(x_1, x_2) &= \begin{pmatrix} 1 & 0 \\ 0 & -1 \end{pmatrix} \begin{bmatrix} x_2 \sin(x_2) + x_2 x_1^2 \\ x_1^2 \sin(x_1) + 2x_1 x_2 \end{bmatrix} \\ &= \begin{bmatrix} x_2 \sin(x_2) + x_2 x_1^2 \\ -x_1^2 \sin(x_1) - 2x_1 x_2 \end{bmatrix}, \end{aligned}$$

we conclude that $X \circ G = -\mathrm{d}G \cdot X$; hence, X is G-symmetric. Fig. **??** presents a graphical illustration of the symmetry $X \circ G = -\mathrm{d}G \cdot X$.

The following proposition shows that the symmetry of an SVF leads to the existence of a set of solutions which are invariant under G.

Proposition II.3. *Let X be an SVF defined on a manifold $\mathcal{X}$, and let $G : \mathcal{X} \to \mathcal{X}$ be a symmetry map for X with a fixed point x^*, that is, $G(x^*) = x^*$. Then every solution $x(t)$ of X (a.k.a. integral curve of X) for which $x(0) = x^*$ and is defined*

on a symmetric interval of the form $\mathcal{I} = (-a, a) \subset \mathbb{R}$ *for some* $a > 0$ *satisfies the following identity:*

$$G(x(t)) = x(-t), \quad \forall t \in \mathcal{I}.$$

Moreover, the maximal solution $x_M(t)$ *for which* $x_M(0) = x^*$ *is defined on the maximal interval* $\mathcal{I}_{x^*} = (-a_M, a_M)$ *for some* $a_M > 0$.

Proof. Let $x(t)$ be a solution of X satisfying the conditions of the proposition. Define $\hat{x}(t) = G(x(-t))$ for $t \in \mathcal{I}$. We have $\hat{x}(0) = G(x(0)) = G(x^*) = x^*$. Therefore, $\hat{x}(t)$ and $x(t)$ satisfy the same initial conditions. Next, we show that $\hat{x}(t)$ is an integral curve of X. By definition of $\hat{x}(t)$, $\dot{\hat{x}}(t) = -\mathrm{d}G \cdot \dot{x}(-t)$. Thus, since $x(t)$ is a solution of X, $\dot{\hat{x}}(t) = -\mathrm{d}G \cdot X(x(-t))$. From (2.1), $\dot{\hat{x}}(t) = X(G(x(-t))$, and by definition of $\hat{x}(t)$, $\dot{\hat{x}}(t) = X(\hat{x}(t))$, which proves that $\hat{x}(t)$ is a solution of X. By uniqueness of the solution of the initial value problem, $\hat{x}(t) = x(t)$, that is, $G(x(-t)) = x(t)$ for all $t \in \mathcal{I}$; equivalently, $G(x(t)) = x(-t)$ for all $t \in \mathcal{I}$.

In the appendix we show that $x_M(t)$ is defined on a maximal interval of the form $\mathcal{I}_{x^*} = (-a_M, a_M)$. □

Definition II.4. A solution $x(t)$ of a G-symmetric vector field is said to be a *symmetric solution* if it is defined on an interval $\mathcal{I} = (-a, a)$ for some $a > 0$ and $G(x(t)) = x(-t)$ for all $t \in \mathcal{I}$.

Based on Proposition II.3, the maximal solution $x_M(t)$ of X, for which $x_M(0) = x^*$ such that $G(x^*) = x^*$, is a symmetric solution of X. Since the maximal solution of an initial value problem (with sufficient smoothness conditions) is unique, we conclude that there is a one-to-one correspondence between the number of maximal symmetric solutions and the number of fixed points of G.

Corollary II.5. *There is a one-to-one correspondence between the set of maximal symmetric solutions of a* G*-symmetric vector field and the set of fixed points of* G.

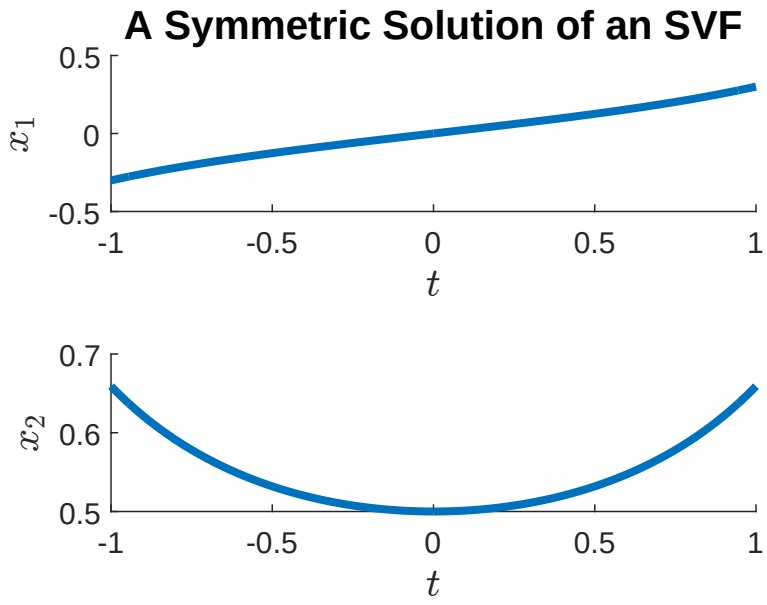

Figure 2.2: A symmetric solution of the SVF in Example II.6 passing through the fixed point $x^* = (0, 0.5)$ of the symmetry map.

Example II.6. In Example II.2, $G(x_1, x_2) = (-x_1, x_2)$. Thus, the fixed points of G are in the form $x^* = (0, x_2^*)$ for $x_2^* \in \mathbb{R}$. Based on Proposition II.3, the solutions passing through x^* are invariant under G. That is, if $x(t) = (x_1(t), x_2(t))$ is a solution for which $x_1(0) = 0$ and $x_2(0) = x_2^*$, then $G(x_1(t), x_2(t)) = (x_1(-t), x_2(-t))$; as a result, by definition of G,

$$(-x_1(t), x_2(t)) = (x_1(-t), x_2(-t)).$$

So, $x_1(t)$ is an odd function and $x_2(t)$ is an even function. Fig. 2.2 shows such a symmetric solution passing through $(0, 0.5)$.

2.2 Symmetric Hybrid Systems

In this section, we first define a *hybrid system*, and then a *Symmetric Hybrid System* will be defined.

In contrast to a simple dynamical system which is described by a set of ordinary differential equations, hybrid systems include discrete phases and continuous phases as well as the rules which determine the transitions between the continuous and discrete phases. Here, however, as described in the following definition, we only discuss hybrid systems with one continuous phase and one discrete phase.

Definition II.7. (**Hybrid System**) Let X be a smooth vector field defined on a manifold $\mathcal{X}$ and let $\mathcal{S}$ be an embedded submanifold of $\mathcal{X}$ with co-dimension one. Moreover, assume that $\Delta : \mathcal{S} \to \mathcal{X}$ is a smooth map such that $\Delta(\mathcal{S}) \cap \mathcal{S} = \emptyset$. A hybrid system $\Sigma = (X, \Delta, \mathcal{X}, \mathcal{S})$ is defined as

$$\Sigma = \begin{cases} \dot{x} = X(x), & x^- \notin \mathcal{S}, \\ x^+ = \Delta(x^-), & x^- \in \mathcal{S}, \end{cases} \tag{2.2}$$

and by definition, $x(t)$ is a solution of the hybrid system Σ if $\dot{x}(t) = X(x(t))$ when $x(t) \notin \mathcal{S}$, and if $x(t_I) \in \mathcal{S}$, then the solution is re-initialized to $x^+ = \Delta(x^-)$, where $x^- = \lim_{x \to t_I^-} x(t)$. We assume that the solution is left continuous at t_I, that is, $x(t_I) = x^-$. Fig 2.3 shows how a solution of a hybrid system is re-initialized after impact with $\mathcal{S}$.

In the above definition $\mathcal{S}$ is called the *switching surface*, and Δ is said to be the *transition map* or *impact map*. For a bipedal robot which is modeled as a hybrid system, switching occurs when the swing leg hits the ground.

It should be noted that in a general hybrid system complicated phenomena such as Zeno solutions can occur, however, we adopt the notion of hybrid systems as in (*Westervelt et al.*, 2007), where such behaviors are excluded.

Below, we define the so-called feasible solution of a hybrid system which will be helpful in the definition of an SHS which follows.

Definition II.8. A solution $x(t)$ of a hybrid system $\Sigma = (X, \Delta, \mathcal{X}, \mathcal{S})$ with $x(0) = x_0$

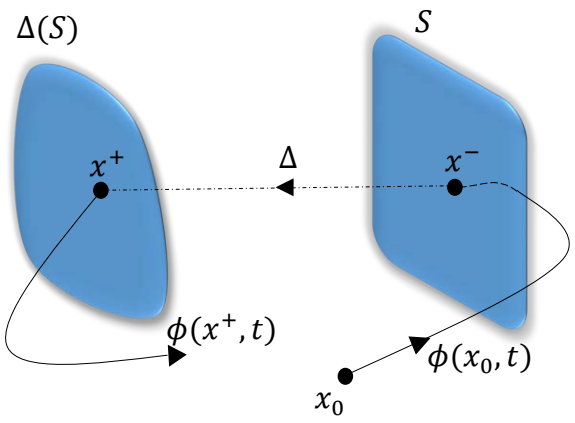

Figure 2.3: A solution of a hybrid system starting from $x_0 \in \mathcal{X}$.

is said to be a *feasible solution* if there exists $t_0 < 0$ such that $x_M(t_0) \in \Delta(\mathcal{S})$, where x_M is the maximal solution starting from x_0.

Definition II.9. (**Symmetric Hybrid System**) A hybrid system $\Sigma = (X, \Delta, \mathcal{X}, \mathcal{S})$ is said to be a *Symmetric Hybrid System (SHS)* if there exists a smooth map $G : \mathcal{X} \to \mathcal{X}$ such that

1. X is G-symmetric, that is,

$$X \circ G = -\mathrm{d}G \cdot X.$$

2. If $x_s(t)$ is a feasible symmetric solution of X which crosses the switching surface at t_I, then

$$\Delta(x_s(t_I)) = G(x_s(t_I)).$$

In the above definition, Σ is said to be an SHS under the symmetry map G, or simply a *G-SHS*. Moreover, $x_s(t)$ is said to be a symmetric solution of Σ.

A special case where the second condition is easily checked is presented in the following proposition.

Proposition II.10. *Let $\Sigma = (X, \Delta, \mathcal{X}, \mathcal{S})$ be a hybrid system such that X is G-symmetric for a smooth map $G : \mathcal{X} \to \mathcal{X}$. If $\Delta = G$ on $\mathcal{S}$, then Σ is a G-SHS.*

Proof. Clearly, the first condition of Definition II.9 is satisfied. Since $\Delta(x) = G(x)$ for all $x \in \mathcal{S}$, the second condition of Definition II.9 always hold true as well. Consequently, Σ is a G-SHS. □

Example II.11. The hybrid system $\Sigma = (X, \Delta, \mathcal{X}, \mathcal{S})$ with X as in Example II.2, that is,

$$X(x_1, x_2) = \begin{bmatrix} x_2 \sin(x_2) + x_2 x_1^2 \\ x_1^2 \sin(x_1) + 2x_1 x_2 \end{bmatrix},$$

$\mathcal{X} = \mathbb{R}^2$, $\mathcal{S} = \{(x_1, x_2) \in \mathbb{R}^2 | x_1 = x_0\}$ for some $x_0 > 0$, and $\Delta(x_1^-, x_2^-) = (-x_0, x_2^-)$ is an SHS under the map $G(x_1, x_2) = (-x_1, x_2)$ because first, as shown in Example II.2, X is symmetric under G and second, by definition of Δ, we have $\Delta(x_1^-, x_2^-) = (-x_0, x_2^-) = G(x_0, x_2^-)$, that is $\Delta = G$ on $\mathcal{S}$.

Example II.12. (2D LIP Biped) As shown in (*Razavi et al.*, 2016), the 2D LIP biped, shown in Fig. 1.4, taking constant swing foot end to hip strides of length x_0 (thus, the the point mass position after impact is always x_0) is a hybrid system with the following equations.

$$\begin{aligned} \ddot{x} &= \omega^2 x, \\ \mathcal{S} &= \{(x, \dot{x}) | x = x_0 > 0\}, \\ \Delta(x^-, \dot{x}^-) &= (-x_0, \dot{x}^-). \end{aligned}$$

In the state-space representation of this system with $x_1 = x$ and $x_2 = \dot{x}$, the vector field $X(x_1, x_2) = (x_2, \omega^2 x_1)$ is symmetric under the map $G(x_1, x_2) = (-x_1, x_2)$. Moreover, for all $\dot{x}^- \in \mathbb{R}$ we have $G(x_0, \dot{x}^-) = (-x_0, \dot{x}^-) = \Delta(x_0, \dot{x}^-)$, thus, $\Delta = G$

on $\mathcal{S}$. Consequently, by Proposition II.10, the 2D LIP model is a G-SHS.

Symmetric solutions of an SHS are of particular interest because as shown in the following proposition, under a simple condition, they are always periodic.

Proposition II.13. *If $x_s(t)$ is a feasible symmetric solution of a G-SHS, that crosses the switching surface, then $x_s(t)$ is a periodic solution of Σ. Moreover, if $x_s(0)$ is a fixed point of G, and*

$$t_I = \inf\{t > 0 | x_s(t) \in \mathcal{S}\}, \tag{2.3}$$

then the period of $x_s(t)$ is $T = 2t_I$.

Proof. Assume that $x_s(0)$ is a fixed point of G. Suppose that $x_s(t)$ crosses the switching surface at t_I, and t_I is defined as in (2.3). Since $x_s(t)$ is symmetric, $x_s(-t) = G(x_s(t))$. Thus, for $t = t_I$, $x_s(-t_I) = G(x_s(t_I))$. On the other hand, by the second condition in Definition II.9, $x_s(t_I^+) = G(x_s(t_I))$. Therefore, from the last two equalities, we conclude that $x_s(t_I^+) = x_s(-t_I)$; that is, after impact with the switching surface, $x_s(t)$ is re-initialized back to $x_s(-t_I)$, hence is periodic with period $T = 2t_I$. □

A symmetric solution of an SHS which is a periodic orbit is called a *symmetric periodic orbit*. Fig. 2.4 shows a symmetric periodic orbit of the SHS in Example II.11.

Remark II.14. Obtaining periodic orbits of a hybrid systems normally relies on extensive numerical search for fixed points of a Poincaré map (*McGeer*, 1990; *Grizzle et al.*, 2001; *Wisse et al.*, 2005; *Geng et al.*, 2006; *Gregg and Righetti*, 2013; *Dingwell and Kang*, 2007). However, according to Proposition II.13, if the system is an SHS, under a simple condition, it can automatically have many symmetric periodic orbits which can be identified easily (i.e., without any searches) by fixed points of the sym-

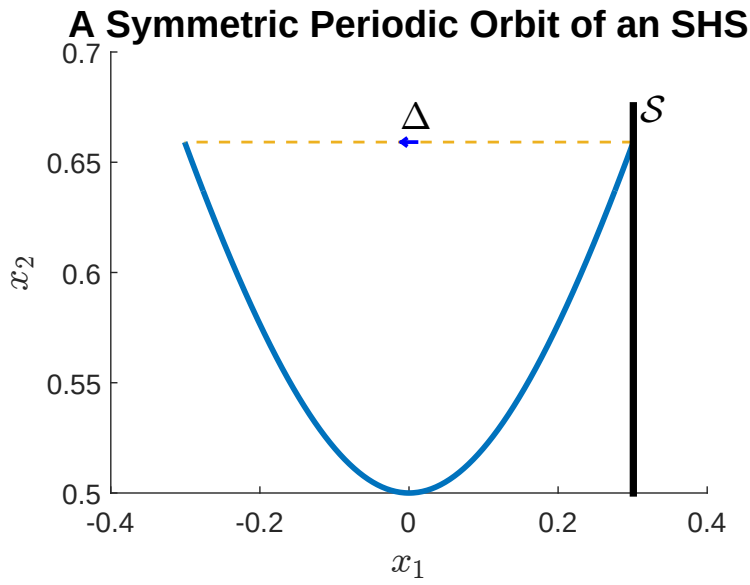

Figure 2.4: A symmetric periodic orbit of the SHS in Example II.11. Once the symmetric solution crosses the switching surface $\mathcal{S}$ at x^-, the impact map Δ sends it back to $G(x^-)$.

metry map. In the following chapters, this property of SHSs shall be used to generate periodic walking gaits for bipedal robots.

In the following example, we show that the 2D SLIP is an SHS.

Example II.15. (2D Spring Loaded Inverted Pendulum (SLIP)) Consider the 2D SLIP model as depicted in Fig. 2.5. Let z denote the length of the spring, and let θ denote the angle of the leg with respect to the center-line. Suppose that $V(\theta, z)$ denotes the potential and $K(\theta, z)$ the kinetic energy of the system. If k is the spring constant, and l_0 is the no-load length of the spring, then

$$\begin{aligned} V &= mgz\cos(\theta) + \tfrac{1}{2}k(z - l_0)^2, \\ K &= \tfrac{1}{2}m(\dot{z}^2 + z^2\dot{\theta}^2). \end{aligned}$$

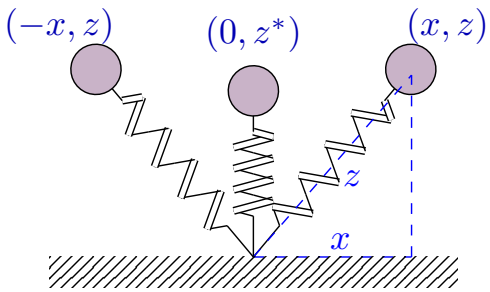

Figure 2.5: 2D SLIP.

The Euler-Lagrange equations of motion result in

$$\ddot{\theta} = -2\frac{\dot{z}}{z}\dot{\theta} - \frac{\mathrm{g}}{z}\sin(\theta), \tag{2.4}$$

$$\ddot{z} = z\dot{\theta}^2 + \omega^2(l_0 - z) - \mathrm{g}\cos(\theta), \tag{2.5}$$

where $\omega^2 = k/m$.

To derive the equation of the transition map, we note that the flight phase starts when the spring length reaches its no-load length (i.e., $z = l_0$); therefore, the switching surface is defined as

$$\mathcal{S} = \{(\theta, z, \dot{\theta}, \dot{z}) | z = l_0\}.$$

The flight phase consists of a projectile motion (where the only external force is gravity) at the end of which, when $z = l_0$, the next stance phase starts. We assume that at the beginning of each step the leg is at an angle[1] $-\theta_0$. Therefore,

$$\theta^+ = -\theta_0, \quad z^+ = l_0. \tag{2.6}$$

Hence, the transition occurs when the height of the mass is $l_0\cos(\theta_0)$. Writing the

[1]This can be done by sweeping the swing leg to angle θ_0 during the flight phase.

equations of motion of a projectile yields:

$$\begin{aligned} \dot{x}^+ &= \dot{x}^-, \\ \dot{y}^+ &= -((\dot{y}^-)^2 - 2\mathrm{g}(y^- - y_0))^{1/2}, \end{aligned} \tag{2.7}$$

where, $x = z\sin(\theta)$, $y = z\cos(\theta)$ and $y_0 = l_0\cos(\theta_0)$. Equation (2.7) implicitly defines the transition map of the SLIP. Equations (2.4) to (2.7) define the equations of motion of the SLIP, excluding the flight phase.

Writing (2.4) and (2.5) in the form $\dot{x} = X(x)$, it is easy to check that the corresponding vector field is symmetric under the map $G(\theta, z, \dot{\theta}, \dot{z}) = (-\theta, z, \dot{\theta}, -\dot{z})$. The fixed points of G are of the form $\chi^* = (0, z^*, \dot{\theta}^*, 0)$. Let $\phi(t, \chi^*) = (\theta(t), z(t), \dot{\theta}(t), \dot{z}(t))$ be the solution for which $\phi(0, \chi^*) = \chi^*$. Based on Proposition II.3, $\phi(t, \chi^*)$ is invariant under G, in the sense that $G(\phi(t, \chi^*)) = \phi(-t, \chi^*)$. Thus, $(-\theta(t), z(t), \dot{\theta}(t), -\dot{z}(t)) = (\theta(-t), z(-t), \dot{\theta}(-t), \dot{z}(-t))$; equivalently, $\theta(t)$ is an odd function, and $z(t)$ is an even function of t:

$$\theta(-t) = -\theta(t),\ z(-t) = z(t).$$

By numerical simulations, it can be shown that there are infinitely many symmetric solutions $\phi(t, \chi^*)$ which cross the switching surface for different values of χ^*. Let $\chi(t)$ denote one of those solutions and assume that $\chi(t)$ crosses $\mathcal{S}$ at $\chi^- = (\theta_0, l_0, \dot{\theta}^-, \dot{z}^-)$. To prove that the 2D SLIP is an SHS, by Proposition II.10, it suffices to show that $\Delta(\chi^-) = G(\chi^-)$. By definition of y and y_0 given right after (2.7), at χ^- we have $y^- = y_0$, therefore, from (2.7), $\dot{x}^+ = \dot{x}^-$ and $\dot{y}^+ = -\dot{y}^-$. On the other hand, from definitions of x and y,

$$\begin{aligned} \dot{z} &= \dot{x}\sin(\theta) + \dot{y}\cos(\theta), \\ z\dot{\theta} &= \dot{x}\cos(\theta) - \dot{y}\sin(\theta). \end{aligned}$$

Therefore, since $\dot{x}^+ = \dot{x}^-$ and $\dot{y}^+ = -\dot{y}^-$,

$$\begin{aligned} \dot{z}^+ &= \dot{x}^- \sin(-\theta_0) - \dot{y}^- \cos(-\theta_0), \\ &= -(\dot{x}^- \sin(\theta_0) + \dot{y}^- \cos(\theta_0)), \\ &= -\dot{z}^-. \end{aligned}$$

Similarly, with $\theta = \theta_0$ and $z = l_0$ one can show that $\dot{\theta}^+ = \dot{\theta}^-$. As a result, $\Delta(\theta_0, l_0, \dot{\theta}^-, \dot{z}^-) = (-\theta_0, l_0, \dot{\theta}^-, -\dot{z}^-)$ which is equal to $G(\theta_0, l_0, \dot{\theta}^-, \dot{z}^-)$. Therefore, by Definition II.9, the 2D SLIP is a G-SHS with $G(\theta, z, \dot{\theta}, \dot{z}) = (-\theta, z, \dot{\theta}, -\dot{z})$. Moreover, by Proposition II.13, $\chi(t)$ is a periodic solution.

In Chapter III, we present more examples of legged robots which are SHSs.

CHAPTER III

Symmetric Lagrangian Systems and Symmetric Legged Robots

3.1 Symmetric Lagrangian Systems

For Lagrangian systems, as stated in the following proposition, the notion of symmetry can directly be defined by looking at the Lagrangian L.

Proposition III.1. *Let L be the Lagrangian defined on the tangent bundle of the configuration space $\mathcal{Q}$, and let $F : \mathcal{Q} \to \mathcal{Q}$ be a smooth map which is an involution. Define $G : \mathcal{TQ} \to \mathcal{TQ}$ by*

$$G(q, \dot{q}) = (F(q), -\mathrm{d}F(q) \cdot \dot{q}).$$

If L is invariant under G, that is,

$$L \circ G(q, \dot{q}) = L(q, \dot{q}),$$

and if $x^* = (q^*, \dot{q}^*)$ is a fixed point of G, then for the solution $x(t) = (q(t), \dot{q}(t))$ defined on $\mathcal{I} = (-a, a)$ for $a > 0$, with $x(0) = x^*$, we have $G(x(t)) = x(-t)$. Equivalently,

$$F(q(t)) = q(-t). \tag{3.1}$$

Finally, if X is the vector field defining the state-space representation of the Lagrangian system, then X is symmetric under G.

Proof. Suppose that $x(t) = (q(t), \dot{q}(t))$ is the solution of the Lagrangian system for which $x(0) = x^*$, where x^* is a fixed point of G. Define $\hat{x}(t) = G(x(-t))$. At $t = 0$, $\hat{x}(0) = G(x(0)) = G(x^*) = x^*$. Therefore, $\hat{x}(t)$ and $x(t)$ satisfy the same initial conditions. To prove that $\hat{x}(t) = x(t)$ for all $t \in \mathcal{I}$, we show that $\hat{x}(t)$ satisfies the Euler-Lagrange equations of motion. To this end, from the Hamilton's principle (*Bloch et al.*, 2003), it suffices to show that $\delta \int_{-t_i}^{t_i} L(\hat{x}(t))dt = 0$. However, by definition of $\hat{x}(t)$, $\delta \int_{-t}^{t} L(\hat{x}(t))dt = \delta \int_{-t}^{t} L(G(x(-t)))dt$. Invariance of L under G yields $L(G(x(-t)) = L(x(-t))$. Thus for any $t_i \in (-a, a)$ we have $\delta \int_{-t_i}^{t_i} L(\hat{x}(t))dt = \delta \int_{-t_i}^{t_i} L(x(-t))dt = \delta \int_{-t_i}^{t_i} L(x(t))dt = 0$, where the second equality is obtained by simple substitution of $t \to -t$, and the last equality follows from the fact that $x(t)$ is a solution to the Lagrangian system. Therefore, $\hat{x}(t)$ satisfies the Euler-Lagrange equations as $x(t)$ does, and since $\hat{x}(t)$ and $x(t)$ both satisfy the same initial conditions, by uniqueness of the solution of the initial value problem, we have $\hat{x}(t) = x(t)$; thus, $G(x(-t)) = x(t)$, as desired. □

It should be noted that in the above proposition G is not a coordinate transformation because G is defined as $(F, -\mathrm{d}F)$ not $(F, \mathrm{d}F)$.

Example III.2. (2D Double Inverted Pendulum (2D DIP) Consider the double inverted pendulum depicted in Fig. 1.5. In the coordinates (θ_1, θ_2), its kinetic and potential energies are

$$\begin{aligned} K &= \frac{1}{2} m_1 (l_1^2 \dot{\theta}_1^2) + \frac{1}{2} m_2 (l_1^2 \dot{\theta}_1^2 + l_2^2 \dot{\theta}_2^2 + 2 l_1 l_2 \dot{\theta}_1 \dot{\theta}_2), \\ V &= m_1 l_1 \cos(\theta_1) + m_2 (l_1 \cos(\theta_1) + l_2 \cos(\theta_2)). \end{aligned}$$

Let $F(\theta_1, \theta_2) = (-\theta_1, -\theta_2)$. Thus, as defined in Proposition III.1, $G(\theta_1, \theta_2, \dot{\theta}_1, \dot{\theta}_2) = (-\theta_1, -\theta_2, \dot{\theta}_1, \dot{\theta}_2)$. It immediately follows that the Lagrangian $L = K - V$ is invari-

ant under G. By Proposition II.3, since $x^* = (0, 0, \dot{\theta}_1^*, \dot{\theta}_2^*)$ for $\dot{\theta}_1^*, \dot{\theta}_2^* \in \mathbb{R}$ are fixed points of G, the solutions $x(t) = (\theta_1(t), \theta_2(t), \dot{\theta}_1(t), \dot{\theta}_2(t))$ for which $x(0) = x^*$ satisfy the equation $F(\theta_1(t), \theta_2(t)) = (-\theta_1(t), -\theta_2(t))$; equivalently, $\theta_1(-t) = -\theta_1(t)$ and $\theta_2(-t) = -\theta_2(t)$.

Example III.3. (2D SLIP) Next we revisit the 2D SLIP which was introduced in Example II.15. This time by just looking at its Lagrangian we determine the symmetry map. From Example II.15,

$$\begin{aligned} V &= mgz\cos(\theta) + \tfrac{1}{2}k(z - l_0)^2, \\ K &= \tfrac{1}{2}m(\dot{z}^2 + z^2\dot{\theta}^2). \end{aligned}$$

Looking at K and V, it is clear that the Lagrangian $L = K - V$ is invariant under the map $F(\theta, z) = (-\theta, z)$. According to Proposition III.1, $G(\theta, z, \dot{\theta}, \dot{z}) = (-\theta, z, \dot{\theta}, -\dot{z})$, which is the same symmetry map which was obtained in Example II.15 by looking at the equations of motion.

3.2 Symmetric Legged Robots

The equations of motion of legged robots, under some conditions, may be described as hybrid systems. For instance, if the double support phase, where both legs are simultaneously on the ground, can be approximated as being instantaneous (e.g., in a point-foot biped), the equations of motion can be written as a hybrid system as in Definition II.7. Based on the discussion in Chapter II, if the hybrid system describing the legged robot turns out to be an SHS, then one not only can guarantee the existence of symmetric periodic orbits, but also can find such orbits easily (i.e., without any numerical searches). In this section, we present examples of legged robots whose governing equations can be considered as SVFs.

Model	DOF	Symmetry Map, F
3D LIP	2	$(x, y) \mapsto (-x, y)$
3D IP	2	$(x, y) \mapsto (-x, y)$
2D SLIP	2	$(x, l) \mapsto (-x, l)$
3D SLIP	3	$(x, y, z) \mapsto (-x, y, z)$
3D LIPF	4	$(x, y, \theta_x, \theta_y) \mapsto (-x, y, -\theta_x, \theta_y)$
3D CGB	4	$(x, y, x_{hf}, y_{hf}) \mapsto (-x, y, -x_{hf}, y_{hf})$

Table 3.1: Symmetry maps of the simple models. The map G which is defined on $\mathcal{TQ}$, i.e., on the tangent bundle of the configuration space, is defined as $G = (F, -\mathrm{d}F)$.

Definition III.4. A legged robot with configuration space $\mathcal{Q}$ is said to be F-symmetric for $F : \mathcal{Q} \to \mathcal{Q}$ if its equations of motion in the continuous phase can be described by a G-symmetric vector field, where $G = (F, -\mathrm{d}F)$; alternatively, the legged robot is symmetric if its Lagrangian is invariant under G.

3.2.1 Simple Models

Many researchers have studied simple low-dimensional models of legged robots. In particular, it is common to use such simple models to generate trajectories for more complex legged robots (e.g., see (*Kajita et al.*, 2001)). Among these low-dimensional models, we can mention Inverted Pendulum (IP), LIP, Inverted Pendulum with Flywheel (IPF), SLIP, and Compass-Gait Biped (CGB). Below, we show that the governing equations of motion of all these models are represented by SVFs. Table 3.1 shows a summary of the existing symmetries in these simple models, which will be explained with more details in the following subsections.

3.2.1.1 Linear Inverted Pendulum

A 3D LIP is a 3D Inverted Pendulum (IP), where its point mass is constrained to move in a plane of constant height. Fig. 3.1 shows the schematic of a 3D LIP. A telescopic leg with an actuator constrains the motion of the point mass M to a plane

$z = z_0$.

Notation: The world coordinate frame is denoted by W. We assume that the coordinate frame I is parallel to W, but its origin is located at the support point (see Fig. 3.1).

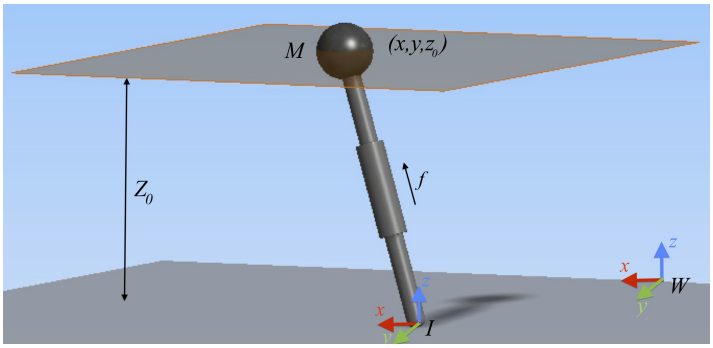

(a) 3D LIP

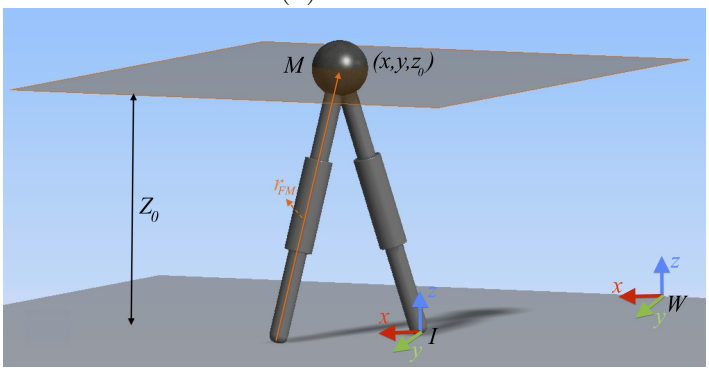

(b) 3D LIP Biped: Before Impact

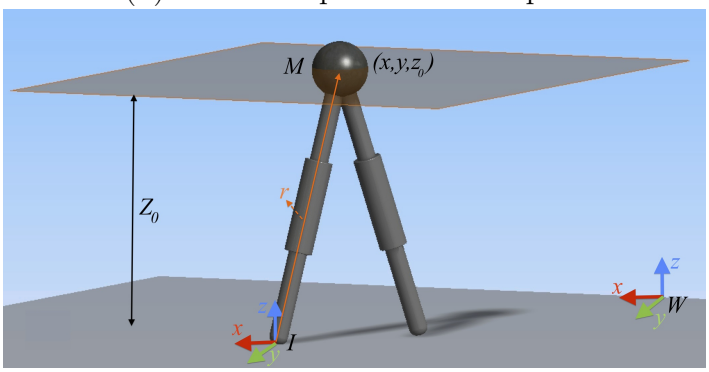

(c) 3D LIP Biped: After Impact

Figure 3.1: 3D LIP models

Let $\boldsymbol{H}$ denote the total angular momentum of the point mass M about the support point. Since the support point is stationary, the time derivative of $\boldsymbol{H}$ is equal to the

moment of external forces about the support point. Therefore, because in the LIP (as in the IP) the only external force applied to mass M is the gravitational force, we have

$$\frac{d\boldsymbol{H}}{dt} = M\boldsymbol{r} \times \boldsymbol{g},$$

where $\boldsymbol{g}$ is the vector of gravity and $\boldsymbol{r}$ is the position vector of M in I. At the same time,

$$\boldsymbol{H} = M\boldsymbol{r} \times \dot{\boldsymbol{r}}.$$

Combining the last two equations results in

$$\frac{d}{dt}(\boldsymbol{r} \times \dot{\boldsymbol{r}}) = \boldsymbol{r} \times \boldsymbol{g}.$$

Assuming a Cartesian coordinate system in I with z pointing in the opposite direction of the gravitational field, we have $\boldsymbol{g} = (0, 0, -g)$, where g is the gravitational acceleration. Therefore, denoting the coordinates of the position vector $\boldsymbol{r}$ by (x, y, z), from the equation above

$$z\ddot{x} - x\ddot{z} \;=\; gx,\; y\ddot{z} - z\ddot{y} \;=\; -gy,\; x\ddot{y} - y\ddot{x} \;=\; 0. \tag{3.2}$$

From this system, after applying the kinematic constraints, the equations of motion of the IP and LIP can be derived. In the IP $x^2 + y^2 + z^2$ is constant, while in the LIP, z is assumed to be constant. Here, we derive the equations of motion of the 3D LIP. If we set $z = z_0 > 0$ in the equations above, we obtain

$$\ddot{x} = \omega^2 x,\; \ddot{y} = \omega^2 y, \tag{3.3}$$

where $\omega^2 = g/z_0$. Equation (3.3) describes the equations of motion of the 3D LIP. Note that the third equation in (3.2) follows from (3.3).

Although for the purpose of the current paper the actuator force, $\boldsymbol{f}$, required for reinforcing the constraint $z = z_0$, need not be calculated, it is worth deriving a formula to describe this force. The actuator force (see Fig. 3.1) is always in the direction of $\boldsymbol{r}$; therefore, $\boldsymbol{f} = k\boldsymbol{r}$ for some k. In our Cartesian coordinate system, $\boldsymbol{f} = k \cdot (x, y, z)$. However, since $z = z_0$, we have $\ddot{z} = 0$. Therefore, if f_z denotes the z component of $\boldsymbol{f}$, from Newton's equations of motion, $f_z - Mg = 0$. Thus, because $f_z = kz$ and $z = z_0$, $k = \frac{Mg}{z_0}$. As a result,

$$\boldsymbol{f} = (Mg\frac{x}{z_0}, Mg\frac{y}{z_0}, Mg).$$

Note that here we assumed that the actuator can always provide the exact force above. Hence, assuming that initially $z = z_0$ and $\dot{z} = 0$, the equation $z = z_0$ holds throughout the motion. However, if the 3D LIP is used as a pattern generator for walking, then a controller is required to enforce the constraint $z = z_0$ (*Kajita et al.*, 2001).

The 3D LIP discussed above is a monoped, which, without assuming a flight phase, is incapable of providing legged locomotion. Therefore, to produce walking, the 3D LIP requires a swing leg to be able to switch the legs while walking. As shown in Fig. 3.1(b), this 3D LIP biped is, in fact, the exact same as that of the 3D LIP except for the massless swing leg that allows to switch legs one after another, enabling it to walk. It should be noted that, since the swing leg is massless, similar to the 3D LIP, the 3D LIP biped has two degrees of freedom. Below we discuss the equations of motion of the 3D LIP biped.

No matter which leg is the stance leg, the equations of motion in the coordinate

system attached to the support point remain the same:

$$\ddot{x} = \omega^2 x, \;\; \ddot{y} = \omega^2 y. \tag{3.4}$$

Since the roles of the legs will be swapped at the end of each step, we need to define a transition map.

Transition Map: To derive an expression for the transition map (also called the impact map), we make two assumptions:

1. The legs are swapped instantaneously, with the result that only one leg is the stance leg at a time.

2. During the switching of the legs, mass M remains in the plane $z = z_0$ and $\dot{z} = 0$.

By assumption (1) above, the force generated at the swing leg end at the time of impact is an impulsive force. Since this force is the only impulsive force present, the total angular momentum of the system about the swing leg end right before the impact and right after it is the same. Therefore,

$$\boldsymbol{H}_o^- = \boldsymbol{H}_o^+, \tag{3.5}$$

where $\boldsymbol{H}_o$ denotes the total angular momentum of mass M at the time of impact about the swing leg end, denoted by o. By definition of angular momentum,

$$\boldsymbol{H}_o^- = M\boldsymbol{r}_{FM}^- \times \dot{\boldsymbol{r}}^-, \;\; \boldsymbol{H}_o^+ = M(\boldsymbol{r}^+ \times \dot{\boldsymbol{r}}^+),$$

where $\boldsymbol{r}_{FM} = \boldsymbol{r} - \boldsymbol{r}_F$, and $\boldsymbol{r}_F$ is the position vector of the swing leg end in the coordinate frame I whose origin is at the stance leg's point of contact (see Fig. 3.1 (b) and (c)). Therefore, by equation (3.5)

$$\boldsymbol{r}^+ \times \dot{\boldsymbol{r}}^+ \;\; = \;\; \boldsymbol{r}_{FM}^- \times \dot{\boldsymbol{r}}^-.$$

Clearly, $\boldsymbol{r}^+ = \boldsymbol{r}^-_{FM}$, where $\boldsymbol{r}^+$ is represented in the coordinate frame attached to the support point after the transition. So, from the equation above

$$\boldsymbol{r}^-_{FM} \times (\dot{\boldsymbol{r}}^+ - \dot{\boldsymbol{r}}^-) \;=\; 0.$$

Therefore, from this equation, denoting $\boldsymbol{r} = (x, y, z)$ and $\boldsymbol{r}_F = (x_F, y_F, z_F)$,

$$\begin{aligned} y^-_{FM}(\dot{z}^+ - \dot{z}^-) - z^-_{FM}(\dot{y}^+ - \dot{y}^-) &= 0, \\ z^-_{FM}(\dot{x}^+ - \dot{x}^-) - x^-_{FM}(\dot{z}^+ - \dot{z}^-) &= 0, \\ x^-_{FM}(\dot{y}^+ - \dot{y}^-) - y^-_{FM}(\dot{x}^+ - \dot{x}^-) &= 0. \end{aligned}$$

By assumption (2), $z^+ = z^- = z_0$ and $\dot{z}^+ = \dot{z}^- = 0$. In addition, because we assume walking takes place on flat ground, $z^-_F = 0$. Substituting these equalities into the equations above gives us

$$z^-_0(\dot{y}^+ - \dot{y}^-) \;=\; 0, \qquad -z_0(\dot{x}^+ - \dot{x}^-) \;=\; 0.$$

From these equations, since $z_0 \neq 0$, $\dot{x}^+ = \dot{x}^-$, and $\dot{y}^+ = \dot{y}^-$. In sum, we obtain the following transition map:

$$x^+ \;=\; x^-_{FM}, \;\; y^+ \;=\; y^-_{FM}, \; \dot{x}^+ \;=\; \dot{x}^-, \;\; \dot{y}^+ \;=\; \dot{y}^-.$$

Next, we need to define when the transition should occur.

Transition Surface: We define a transition surface assuming the following:

1. At the time of impact, $z_F = 0$.
2. At the time of impact, the swing leg length is equal to the stance leg length.

By assumptions (1) and (2) above,

$$(x^-_{FM})^2 + (y^-_{FM})^2 + (z_0)^2 = (x^-)^2 + (y^-)^2 + (z_0)^2.$$

Canceling z_0^2,

$$(x_{FM}^-)^2 + (y_{FM}^-)^2 = (x^-)^2 + (y^-)^2.$$

Therefore, under assumptions (1) and (2) above, switching occurs when $(x, y, \dot{x}, \dot{y})$ belongs to the following surface:

$$\mathcal{S} = \left\{(x, y, \dot{x}, \dot{y}) | x^2 + y^2 = (x_{FM}^-)^2 + (y_{FM}^-)^2\right\}.$$

Based on the discussion above, the equations of motion of the 3D LIP consist of a continuous phase and a discrete phase. In the continuous phase, the equations of motion are

$$\ddot{x} = \omega^2 x, \ \ddot{y} = \omega^2 y,$$

and the discrete phase starts when $(x, y) \in \mathcal{S}$, where

$$\mathcal{S} = \left\{(x, y) | x^2 + y^2 = (x_{FM}^-)^2 + (y_{FM}^-)^2\right\},$$

and finally the transition map is

$$x^+ = x_{FM}^-, \ \ y^+ = y_{FM}^-, \ \dot{x}^+ = \dot{x}^-, \ \ \dot{y}^+ = \dot{y}^-.$$

The coordinate frame used in the equations above is I, which is attached to the support point. For later reference, we introduce an alternating coordinate system where we assume that the Cartesian coordinate system associated with I is right-handed when the right leg is the stance leg and left-handed when the left leg is the stance leg. In this left-handed coordinate system, we assume that the y-axis is in the opposite direction of the y-axis of the coordinate system associated with the world

frame. In this alternating coordinate system, the equations of the continuous phase remain unchanged but the transition map becomes:

$$x^+ = x^-_{FM}, \;\; y^+ = -y^-_{FM}, \; \dot{x}^+ = \dot{x}^-, \;\; \dot{y}^+ = -\dot{y}^-. \tag{3.6}$$

Remark III.5. As we shall see later, the importance of this coordinate system is that it enables us to study a certain class of 2-periodic motions as being 1-periodic. From now on, we assume the alternating coordinate system.

The following definition is helpful when we study stability in Chapter VI.

Defintion III.6. Let $x_0 > 0$ and $y_0 > 0$. The 3D LIP is said to be (x_0, y_0)-invariant if

$$x^-_{FM} = -x_0 \quad \text{and} \quad y^-_{FM} = -y_0$$

at the end of each step.

From the above definition, the equations of motion of the 3D LIP in the continuous phase, and by (3.6), we conclude that the equations of motion of the (x_0, y_0)-invariant 3D LIP are

$$\begin{aligned} \ddot{x} &= \omega^2 x, \\ \ddot{y} &= \omega^2 y, \\ (x^+, y^+) &= (-x_0, y_0), \\ (\dot{x}^+, \dot{y}^+) &= (\dot{x}^-, -\dot{y}^-), \\ \mathcal{S} &= \{(x, y, \dot{x}, \dot{y}) | x^2 + y^2 = x_0^2 + y_0^2\}, \end{aligned} \tag{3.7}$$

and the impact occurs when $(x, y, \dot{x}, \dot{y}) \in \mathcal{S}$. From (3.7), it is clear that the (x_0, y_0)-invariant 3D LIP biped is a G-SHS with $G(x, y, \dot{x}, \dot{y}) = (-x, y, \dot{x}, -\dot{y})$.

Although here we assumed that the swing leg is massless and hence did not assume

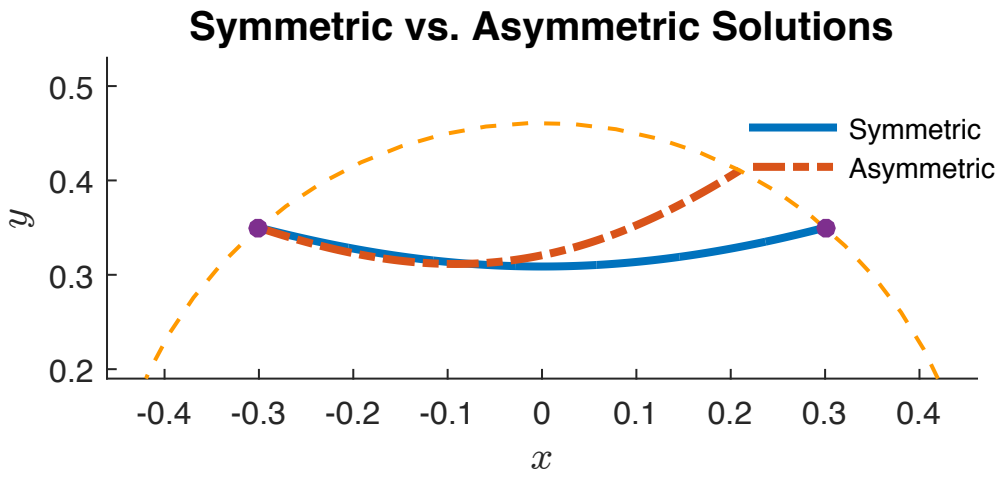

Figure 3.2: A symmetric vs. an asymmetric solution of the 3D LIP. The orange dashed line is part of the circle representing the switching surface $\mathcal{S} = \{(x, y, \dot{x}, \dot{y}) | x^2 + y^2 = x_0^2 + y_0^2\}$ projected to $x - y$ plane. In this simulation $x_0 = 0.3$ and $y_0 = 0.35$.

any dynamics for the swing leg, for an actual robot, as we will discuss later, to reach an (x_0, y_0)-invariant gait, the swing leg controllers must drive (x_{FM}, y_{FM}) to $(-x_0, -y_0)$ before the impact occurs.

Fig. 3.3 shows a few symmetric periodic solutions of a 3D LIP biped.

3.2.1.2 Inverted Pendulum

In this example, we develop the equations of motion of the 3D IP biped with massless legs similar to the 3D LIP biped discussed in Section 3.2.1.1. Let W and I be coordinate frames defined in Section 3.2.1.1. In the Cartesian coordinate system associated with I, the point mass position is denoted by (x, y, z). The equations of motion of the point mass are given in equation (3.2), that is,

$$z\ddot{x} - x\ddot{z} = gx,\ y\ddot{z} - z\ddot{y} = -gy,\ x\ddot{y} - y\ddot{x} = 0. \tag{3.8}$$

Let L denote the length of the 3D IP leg (see Fig. 3.4). We have $x^2 + y^2 + z^2 = L^2$,

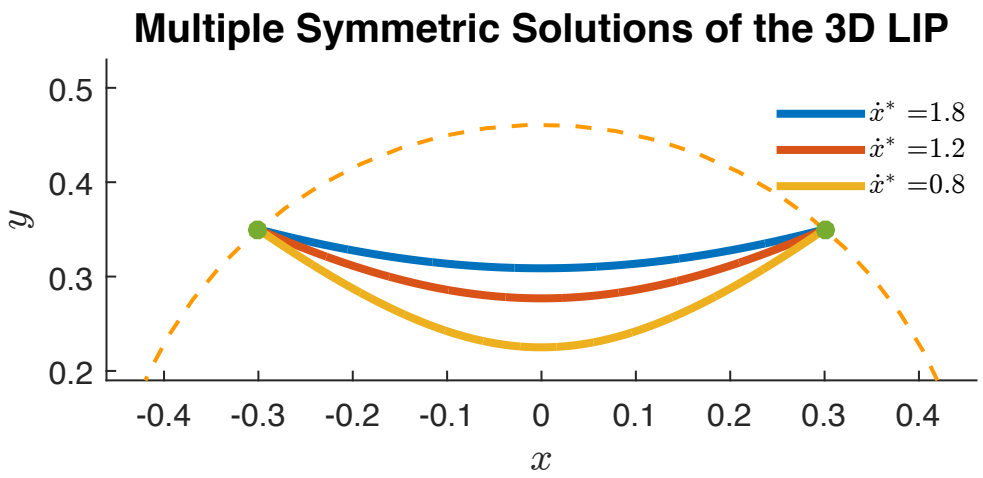

Figure 3.3: Multiple symmetric periodic solutions of the 3D LIP biped, where $\dot{x}^*$ is the time derivative of the solution at $t = 0$.

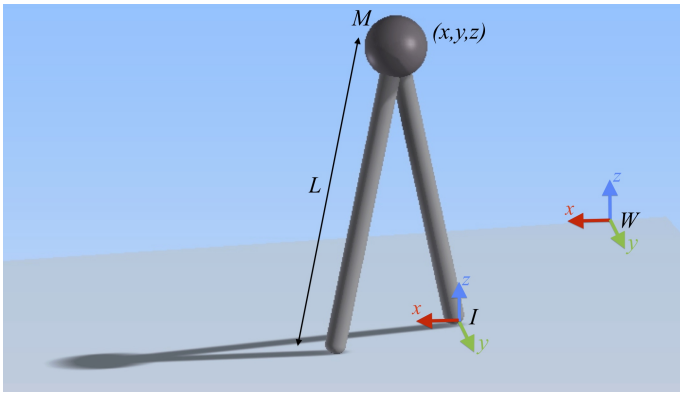

Figure 3.4: 3D Inverted Pendulum Biped with Massless Legs

which after being differentiated results in

$$x\ddot{x} + y\ddot{y} + z\ddot{z} + 2K = 0,$$

where $K = (1/2)(\dot{x}^2 + \dot{y}^2 + \dot{z}^2)$. Finding $\ddot{z}$ from the equation above and substituting it back into the system of equations (3.8), we obtain

$$\begin{aligned} z^2\ddot{x} &= -x(x\ddot{x} + y\ddot{y} + 2K) + gxz, \\ z^2\ddot{y} &= -y(y\ddot{y} + x\ddot{x} + 2K) + gyz. \end{aligned} \tag{3.9}$$

From the last equation in system (3.8), $x\ddot{y} = y\ddot{x}$. Using this equality, equation (3.9) reduces to

$$\begin{aligned} \ddot{x} &= gx\frac{z}{L^2} - \frac{2K}{L^2}x, \\ \ddot{y} &= gy\frac{z}{L^2} - \frac{2K}{L^2}y. \end{aligned}$$

This system can be written in the form $\frac{d}{dt}(x, y, \dot{x}, \dot{y}) = X(x, y, \dot{x}, \dot{y})$, where $X = (\dot{x}, \dot{y}, f(x, y), g(x, y))$ in which

$$f(x, y, \dot{x}, \dot{y}) = gx\frac{z}{L^2} - \frac{2K}{L^2}x, \quad g(x, y, \dot{x}, \dot{y}) = gy\frac{z}{L^2} - \frac{2K}{L^2}y.$$

It is easy to check that the vector field X is symmetric under the map $G : (x, y, \dot{x}, \dot{y}) \mapsto (-x, y, \dot{x}, -\dot{y})$. Similar to the 3D LIP biped introduced in Section 3.2.1.1, we can study the 3D IP biped. To this end, we can find the impact map from the conservation of angular momentum about the impact point. Although, the real impact map will not give rise to an SHS, by defining a hypothetical impact map, we can make the 3D IP an SHS. For example, if $\Delta = (\Delta_q, \Delta_{\dot{q}})$ with $\Delta_q(x^-, y^-) = (-x_0, y_0)$ for some $x_0, y_0 > 0$ and $\Delta_{\dot{q}}$ defined as

$$\Delta_{\dot{q}}(x^-, y^-, \dot{x}^-, \dot{y}^-) = (\dot{x}^-, -\dot{y}^-), \tag{3.10}$$

with the switching surface

$$\mathcal{S} = \{(x, y, \dot{x}, \dot{y}) | x^2 + y^2 = x_0^2 + y_0^2\},$$

then $(f, g, \Delta, \mathcal{Q}, \mathcal{S})$ becomes a G-SHS with $G : (x, y, \dot{x}, \dot{y}) \mapsto (-x, y, \dot{x}, -\dot{y})$.

3.2.1.3 Linear Inverted Pendulum with Flywheel

A LIPF is a LIP where the point mass is replaced with a flywheel that can rotate in the x and y directions with a torque τ_x in the x direction and τ_y in the y direction. As noted in (*Koolen et al.*, 2012), the equations of motion of the 3D LIPF are as follows:

$$\begin{aligned}
\ddot{x} &= \omega^2 x - \frac{\tau_x}{M z_0}, \\
\ddot{y} &= \omega^2 y - \frac{\tau_y}{M z_0}, \\
\ddot{\theta}_x &= \tau_x / J_{xx}, \\
\ddot{\theta}_y &= \tau_y / J_{yy},
\end{aligned}$$

where J_{xx} and J_{yy} are the moments of inertia of the flywheel in the x and y directions, respectively. Letting $q = (x, y, \theta_x, \theta_y)$, $\dot{q} = (\dot{x}, \dot{y}, \dot{\theta}_x, \dot{\theta}_y)$, $u = [\tau_x; \tau_y]$, and $X(q, \dot{q}, u) = [\omega^2 x; \omega^2 y; 0; 0] + [-\tau_x/(Mz_0); -\tau_y/(Mz_0); 0; 0]$, the equations of motion of the 3D LIPF in the continuous phase can be written as $\frac{d}{dt}(q, \dot{q}) = X(q, \dot{q}, u)$. It is easy to check that $X(q, \dot{q}, 0)$ is symmetric under the map $G = (F, -\mathrm{d}F)$ where $F(x, y, \theta_x, \theta_y) = (-x, y, -\theta_x, \theta_y)$. As we will see in Proposition IV.2, by choosing proper control law the resulting reduced-order system can still be symmetric.

3.2.1.4 Spring-Loaded Inverted Pendulum

In Example II.15, we showed that the 2D SLIP is an SHS. Here, we examine the symmetry of the 3D SLIP. We use the coordinates (x, y, z), where (x, y, z) is the position of the point mass in the inertial frame attached to the support point, to derive the equations of motion of the 3D SLIP. With this choice of coordinates the

kinetic and potential energies of the 3D SLIP can be written as follows.

$$\begin{aligned} V &= mgz + \tfrac{1}{2}k(\sqrt{x^2+y^2+z^2} - l_0)^2, \\ K &= \tfrac{1}{2}m(\dot{x}^2+\dot{y}^2+\dot{z}^2). \end{aligned}$$

If $F(x,y,z) = (-x,y,z)$, then from the two equations above it is easy to verify that the Lagrangian $L = K - V$ is invariant under the map $G = (F, -\mathrm{d}F)$. From Proposition II.3, this symmetry guarantees the existence of an infinite number of symmetric solutions $(x(t), y(t), z(t))$, where $x(t)$ is an odd function, and $y(t)$ and $z(t)$ are even functions.

3.2.1.5 3D Compass-Gait Biped

A 3D CGB is an IP biped (see Fig. 3.4) where legs have mass; thus, it has 4 degrees of freedom. We assume that the leg length is L, the point mass at the hip has a mass of M, and each leg has a mass of m. Let (x,y,z) denote the position of M in the coordinate system I (attached to the support point, as in Fig. 3.4) and let (x_{hf}, y_{hf}, z_{hf}) denote the position of the swing foot end relative to the mass M. Since the legs' lengths are constant and equal to L,

$$z = \sqrt{L^2 - x^2 - y^2}, \quad z_{hf} = \sqrt{L^2 - x_{hf}^2 - y_{hf}^2}, \tag{3.11}$$

Therefore, the map $G : (x, y, x_{hf}, y_{hf}) \mapsto (-x, y, -x_{hf}, y_{hf})$, keeps z and z_{hf} unchanged. This quick observation makes the verification of the symmetry of the Lagrangian easier. Let $\boldsymbol{r}_M$ denote the position of M, $\boldsymbol{r}_{m_{st}}$ the position of the mass m

of the stance leg, and $\boldsymbol{r}_{m_{sw}}$ the position of the point mass m in the swing leg. Then,

$$\begin{aligned}
\boldsymbol{r}_M &= (x, y, z), \\
\boldsymbol{r}_{m_{st}} &= \frac{1}{2}(x, y, z), \\
\boldsymbol{r}_{m_{sw}} &= (x - \frac{x_{hf}}{2}, y - \frac{y_{hf}}{2}, z - \frac{z_{hf}}{2}).
\end{aligned}$$

Since $K = (1/2)(M|\dot{\boldsymbol{r}}_M|^2 + m|\dot{\boldsymbol{r}}_{m_{st}}|^2 + m|\dot{\boldsymbol{r}}_{m_{sw}}|^2)$, and by definition of the potential energy, we have

$$\begin{aligned}
K &= (\frac{M}{2} + \frac{m}{4})(\dot{x}^2 + \dot{y}^2 + \dot{z}^2) + \frac{m}{2}((\dot{x} - \frac{\dot{x}_{hf}}{2})^2 + (\dot{y} - \frac{\dot{y}_{hf}}{2})^2, (\dot{z} - \frac{\dot{z}_{hf}}{2})^2), \\
V &= g(Mz + \frac{1}{2}mz + \frac{1}{2}m(z - \frac{z_{hf}}{2})).
\end{aligned}$$

From the equations for K, V and (3.11), it is easy to check that $L = K - V$ is invariant under the map $G : (x, y, x_{hf}, y_{hf}) \mapsto (-x, y, -x_{hf}, y_{hf})$.

3.2.2 More Complex Legged Robots

The symmetry in legged robots is not limited to simple models; indeed, there exist many models of complex legged robots that are symmetric.

Even though real robots are never exactly symmetric but they can be regarded as being "almost" symmetric. Sources of asymmetry in real robots could come from uneven mass distributions, friction, knees and feet. However, these sources of asymmetry with respect to the overall symmetry of the biped are "small". This fact allows us to apply the symmetry method to actual legged robots despite of the existing asymmetries. Moreover, as it will be discussed in Chapter VI, indeed, introducing asymmetries to an SHS is essential for obtaining stable limit cycles.

Consider a 3D biped robot[1] with point-feet as depicted in Fig. 3.5 for which the following assumptions hold:

[1]This 3D biped model is inspired by the bipedal robot MARLO (*Buss et al.*, 2014).

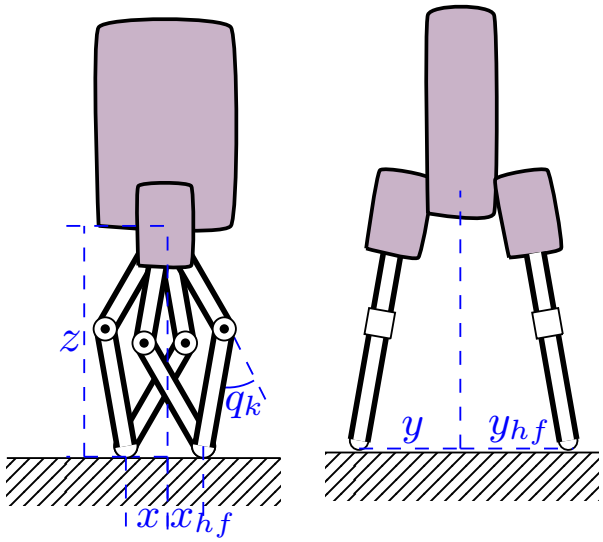

Figure 3.5: Sagittal (left) and frontal (right) view of a symmetric 3D biped.

H1. The torso and legs have uniform mass distributions.

H2. The robot has left-right symmetry, i.e., in the frontal plane the left side is a mirror image of the right side.

H3. The robot has telescopic or symmetric parallelogram legs (see Fig. 3.5).

H4. There is no friction in the actuators.

H5. Each leg has three degrees of freedom which are fully actuated. More precisely, each leg has three actuators by which one can control the leg length and the leg roll and pitch angles relative to the torso.

We note that, in Chapter VI, when we study asymptotic stability and mechanisms of stability of symmetric periodic orbits, we will see that these assumptions need to only hold approximately. For instance, in Chapter VII, we present a model of a humanoid robot without a telescopic leg or symmetric parallelogram leg and with feet, but we successfully apply the symmetry method to generate limit cycle walking gaits for this robot.

A 3D biped for which assumptions H1-H5 hold has 9-DOF and 6 actuators, hence 3 degrees of underactuation. Before presenting the symmetry map for this biped, we

briefly discuss a few possible coordinate systems that might be used to describe the robot. If $(\theta_y, \theta_r, \theta_p)$ are the yaw, roll and pitch Euler angles describing the orientation of the torso with respect to the world frame[2], (x, y, z) is the hip position and (x_{hf}, y_{hf}, z_{hf}) is the position of the swing leg end in the body frame, which is parallel to the world frame and attached to the hip, then $q = (\theta_y, \theta_r, \theta_p, x, y, z, x_{hf}, y_{hf}, z_{hf})$ is a generalized coordinate for the biped. More generally, instead of z and z_{hf} we could use ζ and ξ, respectively, where ζ and ξ could be selected to be any of the following:

$$\begin{aligned} \zeta &= z, \quad \zeta = q_k^{st}, \quad \zeta = l^{st}, \\ \xi &= z_{hf}, \quad \xi = z_f, \quad \xi = q_k^{sw}, \quad \xi = l^{sw}, \end{aligned}$$

with z_f denoting the height of the swing leg end, and q_k^{st} (q_k^{sw}) and l^{st} (l^{sw}) denoting the stance (swing) leg knee angle and stance (swing) leg length, respectively.

Proposition III.7. *A 3D biped for which assumptions H1-H5 hold is symmetric under the map* $F : (\theta_y, \theta_r, \theta_p, x, y, \zeta, x_{hf}, y_{hf}, \xi) \mapsto (-\theta_y, \theta_r, -\theta_p, -x, y, \zeta, -x_{hf}, y_{hf}, \xi)$.

Proof. The proof is done by first calculating the kinetic and potential energies as a function of $q = (q_1, q_2, \ldots, q_9)$, where q is any generalized coordinate for the configuration space $\mathcal{Q}$. In general, it is more straightforward to use joint angles and the orientation of torso as the generalized coordinate for developing the dynamic model. The proof is completed by representing F in the coordinate system q and verifying the invariance of the kinetic and potential energies under F. □

In the case that the yaw angle θ_y is constrained to zero[3], the following corollary applies.

Corollary III.8. *Consider a 3D biped for which assumptions H1-H5 hold, but the yaw angle* θ_y *is constrained to 0. Then the biped has 8-DOF and 2 degrees of under-*

[2]By convention yaw, roll and pitch denote the rotations about the z, x and y axes, respectively.

[3]For instance, this can be done by using a specific foot design (*Da et al.*, 2016) that does not allow yaw rotation.

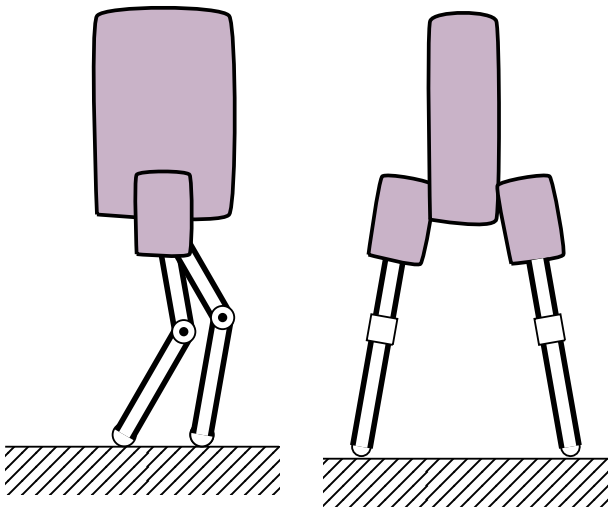

Figure 3.6: Sagittal (left) and frontal (right) view of a 3D biped with non-symmetric legs.

actuation. Moreover, it is symmetric under the map $F : (\theta_r, \theta_p, x, y, \zeta, x_{hf}, y_{hf}, \xi) \mapsto (\theta_r, -\theta_p, -x, y, \zeta, -x_{hf}, y_{hf}, \xi)$.

Remark III.9. Consider the 3D biped depicted in Fig. 3.6. If the legs have mass, this biped is no longer a symmetric biped due to the small asymmetries introduced by using non-parallelogram legs with knees. However, the same symmetry map F as that of the Proposition III.7 can be used for obtaining stable limit cycle walking gaits based on the symmetry method.

CHAPTER IV

Symmetric Zero Dynamics and Symmetric Hybrid Zero Dynamics

Even though an SHS can have an infinite number of symmetric periodic solutions, generally, for these solutions to be stable we need to use control. However, the control laws, if not chosen carefully, can destroy the natural symmetry of the system. In this chapter, we show that with an appropriate choice of control laws, the resulting zero dynamics or hybrid zero dynamics is still symmetric and hence has the properties of the SVFs or SHSs while having lower dimensions compared to the original system.

4.1 Symmetric Zero Dynamics

We first define the notion of zero dynamics briefly[1].

Definition IV.1. Let $X(x,u) = f(x) + g(x)u$ be a smooth vector field with linear control input on a manifold $\mathcal{X}$, where $u \in \mathcal{U} \subset \mathbb{R}^m$. An embedded submanifold $\mathcal{Z}$ of $\mathcal{X}$ is said to be a *zero dynamics* submanifold of $\mathcal{X}$ associated with X if there exists a smooth feedback control $u^* : \mathcal{Z} \to \mathbb{R}^m$ such that $X(z, u^*(z)) \in T_z\mathcal{Z}$ for all $z \in \mathcal{Z}$[2]. Moreover, $\dot{z} = X(z, u^*(z))$ is said to be the zero dynamics on $\mathcal{Z}$.

[1] For a detailed discussion of zero dynamics see (*Isidori*, 1995).

[2] $T_z\mathcal{Z}$ is the tangent space to $\mathcal{Z}$ at $z \in \mathcal{Z}$.

The following proposition presents conditions for the zero dynamics to be an SVF.

Proposition IV.2. *Consider the following n-dimensional control system on* $\mathcal{X} \times \mathcal{U}$

$$\dot{x} = X(x, u),$$

such that $X(x, u) = f(x) + g(x)u$*, and* $u \in \mathcal{U} \subset \mathbb{R}^m$ *is a control input with* $m < n$*. Assume that there exists a unique control law* $u(x)$ *that enforces an* $(n - m)$*-dimensional zero dynamics submanifold of* $\mathcal{X}$ *denoted by* $\mathcal{Z}$ *(thus* $X(z, u(z))$ *is tangent to* $\mathcal{Z}$ *for all* $z \in \mathcal{Z}$*). If there exists a smooth map* $G : \mathcal{X} \to \mathcal{X}$ *and an isomorphism* $H : \mathcal{U} \to \mathcal{U}$ *such that*

1. $X(x, 0)$ *is a* G*-symmetric vector field,*
2. $(g \circ G(x))H(u) = -(\mathrm{d}G \cdot g(x))u$ *for all* $x \in \mathcal{X}$ *and all* $u \in \mathcal{U}$*,*
3. $\mathcal{Z}$ *is invariant under* G*,*

then letting $X_{\mathcal{Z}}$ *and* $G_{\mathcal{Z}}$ *denote restrictions of* $X(x, u(x))$ *and* G *to* $\mathcal{Z}$*, respectively,* $X_{\mathcal{Z}}$ *is* $G_{\mathcal{Z}}$*-symmetric; that is,*

$$X_{\mathcal{Z}} \circ G_{\mathcal{Z}}(z) = -dG_{\mathcal{Z}} \cdot X_{\mathcal{Z}}(z). \tag{4.1}$$

In addition, if $x^* \in \mathcal{Z}$ *is a fixed point of* G*, then the solution* $x(t) : \mathcal{I} \to X$*, for which* $x(0) = x^*$*, lies on* $\mathcal{Z}$*, and* $G(x(t)) = x(-t)$ *for all* $t \in \mathcal{I}$*. Moreover,* $u(G(z)) = H(u(z))$ *for all* $z \in \mathcal{Z}$*.*

As we shall see later, this proposition is very useful in choosing virtual constraints for periodic walking of legged robots.

Proof. For $z \in \mathcal{Z}$,

$$X(z, u(z)) = f(z) + g(z)u(z) \in \mathcal{T}_z\mathcal{Z}, \tag{4.2}$$

where $\mathcal{T}_z\mathcal{Z}$ is the tangent space of $\mathcal{Z}$ at z. Since by the third condition $\mathcal{Z}$ is invariant under G, $G(z) \in \mathcal{Z}$. Thus, by definition of $u(z)$,

$$X(G(z), u(G(z))) = f(G(z)) + g(G(z))u(G(z)) \in \mathcal{T}_{G(z)}\mathcal{Z}. \tag{4.3}$$

Moreover, by invariance of $\mathcal{Z}$ under G, from (4.2),

$$-\mathrm{d}G \cdot f(z) - (\mathrm{d}G \cdot g(z))u(z) \in \mathcal{T}_{G(z)}\mathcal{Z}. \tag{4.4}$$

By condition 1, $-\mathrm{d}G \cdot f(z) = f(G(z))$ and by condition 2, $-(\mathrm{d}G \cdot g(z))u(z) = g(G(z))H(u(z))$; thus, (4.4) reads as

$$f(G(z)) + g(G(z))H(u(z)) \in \mathcal{T}_{G(z)}\mathcal{Z}. \tag{4.5}$$

Comparing (4.5) and (4.3), by uniqueness of $u(z)$,

$$u(G(z)) = H(u(z)). \tag{4.6}$$

Substituting (4.6) in (4.3) results in

$$X(G(z), u(G(z))) = f(G(z)) + g(G(z))H(u(z)).$$

From this equation, and by condition 1 and 2,

$$\begin{aligned} X(G(z), u(G(z))) &= -\mathrm{d}G \cdot f(z) - \mathrm{d}G \cdot g(z)u(z) \\ &= -\mathrm{d}G \cdot (f(z) + g(z)u(z)) \\ &= -dG(z) \cdot X(z, u(z)), \end{aligned}$$

which proves (4.1).

In addition, if $x^* \in \mathcal{Z}$ is a fixed point of G, then because $X(z, u(z))$ is tangent to $\mathcal{Z}$ for all $z \in \mathcal{Z}$, the solution $x(t)$, for which $x(0) = x^*$, lies on $\mathcal{Z}$. Since x^* is a fixed point of G, from Proposition II.3, $G(x(t)) = x(-t)$. □

Given a G-symmetric vector field, the key condition in the above proposition is the choice of the zero dynamics submanifold $\mathcal{Z}$. As condition 3 states, in order for the zero dynamics to remain symmetric, $\mathcal{Z}$ needs to be invariant under the symmetry map G.

Example IV.3. Consider the following control system defined on $\mathbb{R}^2$,

$$\begin{aligned} \dot{x}_1 &= x_2 \sin(x_2) + x_2 x_1^2, \\ \dot{x}_2 &= x_1^2 \sin(x_1) + 2x_1 x_2 + u(x_1, x_2). \end{aligned}$$

This system can be written as $\dot{x} = X(x, u)$ such that $X(x, 0)$ is the vector field in Example II.2 which was shown to be symmetric under the map $G : (x_1, x_2) \mapsto (-x_1, x_2)$. We can write the above system in the form $\dot{x} = f(x) + g(x)u$, with $f(x) = X(x, 0)$ and $g(x) = [0; 1]$. It can be easily checked that $g \circ G = \mathrm{d}G \cdot g$, from which it immediately follows that $(g \circ G)H(u) = -(dG \cdot g)u$ for $H(u) = -u$. Thus far, we showed that conditions 1 and 2 of Proposition IV.2 hold. To satisfy the third condition, we define the zero dynamics submanifold to be $\mathcal{Z} = \{(x_1, x_2) | x_2 = h(x_1)\}$ such that h is an even function of x_1. This choice of h renders $\mathcal{Z}$ invariant under G. The zero dynamics then will be

$$\dot{x}_1 = h(x_1) \sin(h(x_1)) + h(x_1) x_1^2,$$

which satisfies (4.1). Moreover, on $\mathcal{Z}$

$$\begin{aligned} u(x_1) &= \frac{\partial h(x_1)}{\partial x_1}(h(x_1)\sin(h(x_1)) + h(x_1)x_1^2) \\ &\quad -x_1^2\sin(x_1) - 2x_1h(x_1). \end{aligned}$$

By Proposition IV.2, we expect $u(G(z)) = H(u(z))$ for all $z \in \mathcal{Z}$, which by definition of G and H, is equivalent to the equation $u(-z) = -u(z)$. This equality, however, is clearly satisfied by $u(x_1)$ defined above. Finally, since $x^* = (0, h(0))$ is the fixed point of G on $\mathcal{Z}$, by Proposition IV.2, for the solution $x(t) = (x_1(t), x_2(t))$ with $x(0) = x^*$, we have $x(t) \in \mathcal{Z}$, and $G(x(t)) = x(-t)$; that is, $x_2(t) = h(x_1(t))$, and $x_1(-t) = -x_1(t)$.

Example IV.4. Consider the following second order hybrid system defined on $\mathbb{R}^3$:

$$\begin{aligned} \ddot{x} &= \sin(x) + x\dot{x}u_1 + x^2yu_2, \\ \ddot{y} &= \cos(x)\dot{y}^2 + x\dot{y}u_1 + xyu_2, \\ \ddot{z} &= z + zu_1 + xu_2. \end{aligned} \tag{4.7}$$

Writing this system as $X(\zeta, u) = f(\zeta) + g(\zeta)u$ with $\zeta = (x, y, z, \dot{x}, \dot{y}, \dot{z})$ yields

$$g(\zeta) = \begin{bmatrix} 0 & 0 \\ 0 & 0 \\ 0 & 0 \\ x\dot{x} & x^2y \\ x\dot{y} & xy \\ z & x \end{bmatrix}, \; f(\zeta) = \begin{bmatrix} \dot{x} \\ \dot{y} \\ \dot{z} \\ \sin(x) \\ \cos(x)\dot{y}^2 \\ z \end{bmatrix}. \tag{4.8}$$

Define $H(u = [u_1; u_2]) = [-u_1, u_2]$ and $G : (x, y, z, \dot{x}, \dot{y}, \dot{z}) \mapsto (-x, y, z, \dot{x}, -\dot{y}, -\dot{z})$. From definition of $f(\zeta)$, it immediately follows that G is the symmetry map for the above system if $u_1 = u_2 = 0$; therefore, condition 1 of Proposition IV.2 is satisfied.

To check condition 2, we note that

$$(g \circ G(\zeta))H(u) = \begin{bmatrix} 0 \\ 0 \\ 0 \\ x\dot{x}u_1 + x^2 y u_2 \\ -x\dot{y}u_1 - xyu_2 \\ -zu_1 - xu_2 \end{bmatrix}. \tag{4.9}$$

On the other hand,

$$(\mathrm{d}G(\zeta) \cdot g(\zeta))u = \begin{bmatrix} 0 \\ 0 \\ 0 \\ -x\dot{x}u_1 - x^2 y u_2 \\ x\dot{y}u_1 + xyu_2 \\ zu_1 + xu_2 \end{bmatrix}. \tag{4.10}$$

Comparing (4.9) and (4.10) yields $(g \circ G(\zeta))H(u) = -(\mathrm{d}G(\zeta) \cdot g(\zeta))u$. Thus, condition 2 of Proposition IV.2 is satisfied. For condition 3 to hold, we define the zero dynamics submanifold as

$$\mathcal{Z} = \{(x, y, z, \dot{x}, \dot{y}, \dot{z}) | y = h_1(x), z = h_2(x), \dot{y} = \frac{\partial h_1(x)}{\partial x}\dot{x}, \dot{z} = \frac{\partial h_2(x)}{\partial x}\dot{x}\},$$

where h_1 and h_2 are smooth even functions. Since h_1 and h_2 are even, $\mathcal{Z}$ is invariant under G; thus, condition 3 of Proposition IV.2 is satisfied. As a result, the zero dynamics defines a symmetric vector field under $G_{\mathcal{Z}} : (x, \dot{x}) \mapsto (-x, \dot{x})$, and any solution $\zeta(t)$ starting from $(0, \dot{x}^*)$ on $\mathcal{Z}$ with $\dot{x}^* \in \mathbb{R}$ is a symmetric solution which lies on $\mathcal{Z}$. Moreover, on $\mathcal{Z}$, $u(G_{\mathcal{Z}}(x, \dot{x})) = H(u(x, \dot{x}))$, which by definition of G and

H, results in $u_1(-x,\dot{x}) = -u_1(x,\dot{x})$ and $u_2(-x,\dot{x}) = u_2(x,\dot{x})$.

In the case of a Lagrangian system with control input, compared to Proposition IV.2, Proposition IV.6 below is easier to use.

Lemma IV.5. *Consider a Lagrangian system defined on a configuration manifold $\mathcal{Q}$ with mass matrix $A(q)$ and kinetic energy $K(q,\dot{q}) = (1/2)\dot{q}^T A(q)\dot{q}$. If $K(q,\dot{q})$ is invariant under a smooth involution $G : \mathcal{TQ} \to \mathcal{TQ}$, where $G(q,\dot{q}) = (F(q), -\mathrm{d}F(q)\cdot\dot{q})$ for $F : \mathcal{Q} \to \mathcal{Q}$, then*

$$(\mathrm{d}F(q))^T A(F(q))\mathrm{d}F(q) = A(q). \tag{4.11}$$

Proof. Since

$$K(q,\dot{q}) = (1/2)\dot{q}^T A(q)\dot{q}, \tag{4.12}$$

by definition of G,

$$\begin{array}{rcl} K(G(q,\dot{q})) & = & \frac{1}{2}(-\mathrm{d}F(q)\dot{q})^T A(F(q))(-\mathrm{d}F(q)\dot{q}), \\ & = & \frac{1}{2}\dot{q}^T(\mathrm{d}F(q))^T A(F(q))(\mathrm{d}F(q)\dot{q}. \end{array} \tag{4.13}$$

Therefore, since by assumption $K(q,\dot{q}) = K(G(q,\dot{q}))$ for all $(q,\dot{q}) \in \mathcal{TQ}$, from (4.12) and (4.13) we conclude that (4.11) holds true. □

The following proposition provides a key tool in the following chapters for obtaining periodic orbits for legged robots.

Proposition IV.6. ***(Symmetric Zero Dynamics for Lagrangian Systems)*** *Consider an n-dimensional Lagrangian system defined on the configuration space $\mathcal{Q}$ with the following equations of motion:*

$$A(q)\ddot{q} + S(q,\dot{q}) = B(q)u, \tag{4.14}$$

where $u \in \mathcal{U} \subset \mathbb{R}^m$ such that $m < n$. Suppose that there exists a smooth involution $F : \mathcal{Q} \to \mathcal{Q}$ and an isomorphism $H : \mathcal{U} \to \mathcal{U}$ such that

1. *Kinetic and potential energies are invariant under $G(q, \dot{q}) = (F(q), -\mathrm{d}F(q) \cdot \dot{q})$,*
2. *$\delta W'(q, \delta q, u) = \delta W(q, \delta q, u)$ for all $q \in \mathcal{Q}$, $u \in \mathcal{U}$, and any virtual displacement δq, where $\delta W' = \delta W(F(q), \delta F(q), H(u))$, and $\delta W(q, \delta q, u) = (B(q)u)^T \delta q$ is the virtual work done by u for a virtual displacement δq. Equivalently, $(\mathrm{d}F(q))^T B(F(q))H(u) = B(q)u$ for all $q \in \mathcal{Q}$ and all $u \in \mathcal{U}$.*

With these assumptions, if (4.14) is written in the form $\dot{x} = X(x, u) = f(x) + g(x)u$ with $x = (q, \dot{q})$, then $X(x, 0)$ and $g(x)$ satisfy conditions 1 and 2 of Proposition IV.2 for the symmetry map $G(q, \dot{q}) = (F(q), -\mathrm{d}F(q) \cdot \dot{q})$. Moreover, if $\mathcal{Z}$ is an $(n - m)$-dimensional zero dynamics submanifold enforced by a unique control law $u(x)$ such that

3. *$\mathcal{Z}$ is invariant under $G = (F, -\mathrm{d}F)$,*

then writing (4.14) in the form $\dot{x} = X(x, u)$ and letting $X_{\mathcal{Z}}$ and $G_{\mathcal{Z}}$ denote restrictions of $X(x, u(x))$ and G to $\mathcal{Z}$, respectively, $X_{\mathcal{Z}}$ is $G_{\mathcal{Z}}$-symmetric; that is,

$$X_{\mathcal{Z}} \circ G_{\mathcal{Z}}(z) = -\mathrm{d}G_{\mathcal{Z}} \cdot X_{\mathcal{Z}}(z). \tag{4.15}$$

In addition, if $x^* \in \mathcal{Z}$ is a fixed point of G, then the solution $(q_s(t), \dot{q}_s(t)) = x_s(t) : \mathcal{I} \to \mathcal{TQ}$, for which $x_s(0) = x^*$, lies on $\mathcal{Z}$, and $F(q_s(t)) = q_s(-t)$ for all $t \in \mathcal{I} = (-a, a)$, where $a > 0$. Moreover, then $u(G(z)) = H(u(z))$ for all $z \in \mathcal{Z}$. Finally, the work done by u on a symmetric solution $q_s(t)$ is zero; that is,

$$W(q_s) = \int_{-a}^{a} (g(x_s(t))u(x_s(t)))^T \dot{q}_s(t) \mathrm{d}t = 0. \tag{4.16}$$

Proof. Writing (4.14) in the form $\dot{x} = X(x,u) = f(x) + g(x)u$, yields

$$g(q,\dot{q}) = \begin{bmatrix} 0 \\ A^{-1}(q)B(q) \end{bmatrix}. \tag{4.17}$$

Condition 1 of Proposition IV.2 holds because the Lagrangian is symmetric with symmetry map F, so as noted in Proposition III.1, the vector field $X(x,0)$ is symmetric with symmetry map G. Next, we show that condition 2 of Proposition IV.2 holds. From the definition of G, $\mathrm{d}G$ is in the form

$$\mathrm{d}G(q,\dot{q}) = \begin{bmatrix} \mathrm{d}F(q) & 0 \\ \star & -\mathrm{d}F(q) \end{bmatrix}. \tag{4.18}$$

On the other hand, from (4.17),

$$g(G(q,\dot{q}))H(u) = \begin{bmatrix} 0 \\ A^{-1}(F(q))B(F(q))H(u) \end{bmatrix}. \tag{4.19}$$

By Lemma IV.5, $(\mathrm{d}F(q))^T A(F(q))\mathrm{d}F(q) = A(q)$; thus, $A^{-1}(F(q)) = (\mathrm{d}F(q))A^{-1}(q)(\mathrm{d}F(q))^T$. Substituting this into (4.19) yields

$$g(G(q,\dot{q}))H(u) = \begin{bmatrix} 0 \\ (\mathrm{d}F(q))A^{-1}(q)(\mathrm{d}F(q))^T B(F(q))H(u) \end{bmatrix}.$$

By condition 2, the equation above simplifies to

$$g(G(q,\dot{q}))H(u) = \begin{bmatrix} 0 \\ (\mathrm{d}F(q))A^{-1}(q)(B(q)u) \end{bmatrix},$$

which by (4.18) and (4.17) is equal to $\mathrm{d}G(q,\dot{q}) \cdot g(q,\dot{q})u$; this proves that condition 2

of Proposition IV.2 holds. The rest of the proof follows from Proposition IV.2, and we only need to show that work of the actuators on a symmetric solution $q_s(t)$ is zero. The work $W(q_s)$ on a symmetric solution is

$$\begin{aligned} W(q_s) = \textstyle\int_{-a}^{a}(B(q_s(t))u(x_s(t)))^T\dot{q}_s(t)\mathrm{d}t &= \textstyle\int_{-a}^{0}(B(q_s(t))u(x_s(t)))^T\dot{q}_s(t)\mathrm{d}t \\ &\quad + \textstyle\int_{0}^{a}(B(q_s(t))u(x_s(t)))^T\dot{q}_s(t)\mathrm{d}t. \end{aligned} \tag{4.20}$$

Change of variables $t \mapsto -t$ in the first integral yields

$$\begin{aligned} \int_{-a}^{0}(B(q_s(t))u(x_s(t)))^T\dot{q}_s(t)\mathrm{d} &= -\int_{a}^{0}(h(q_s(-t))u(x(-t)))^T\dot{q}_s(-t)\mathrm{d}t \\ &= \int_{0}^{a}(h(q_s(-t))u(x(-t)))^T\dot{q}_s(-t)\mathrm{d}t \\ &= -\int_{0}^{a}(B(F(q_s(t)))u(G(x_s(t)))^T\frac{\mathrm{d}}{\mathrm{d}t}(F(q_s(t)))\mathrm{d}t, \end{aligned}$$

where the second equality follows from $x_s(-t) = G(x_s(t))$ and $F(q_s(t)) = q_s(-t)$ because $x_s(t) = (q_s(t), \dot{q}_s(t))$ is a symmetric solution. Since $u(G(x)) = H(u(x))$,

$$\int_{-a}^{0}(B(q_s(t))u(x_s(t)))^T\dot{q}_s(t)\mathrm{d}t = -\int_{0}^{a}(B(F(q_s(t)))H(u(x_s(t))))^T\frac{\mathrm{d}}{\mathrm{d}t}(F(q_s(t)))\mathrm{d}t,$$

From the second condition, $B(F(q))H(u) = (\mathrm{d}F(q))^{-T}\cdot B(q)u$. Thus, since $\frac{\mathrm{d}}{\mathrm{d}t}(F(q_s(t))) = \mathrm{d}F(q_s(t))\dot{q}_s(t)$, we have

$$\int_{-a}^{0}(B(q_s(t))u(x_s(t)))^T\dot{q}_s(t)\mathrm{d}t = -\int_{0}^{a}(\mathrm{d}F(q_s(t))^{-T}B(q_s(t))u(x_s(t)))^T\mathrm{d}F(q_s(t))\dot{q}_s(t)\mathrm{d}t,$$

Simplifying the right-hand side yields

$$\int_{-a}^{0} (B(q_s(t))u(x_s(t)))^T \dot{q}_s(t)\mathrm{d}t \;=\; -\int_{0}^{a} (B(q_s(t))u(x_s(t))^T \dot{q}_s(t)\mathrm{d}t.$$

Substituting this back into (4.20) proves (4.16). □

Example IV.7. (2D DIP Zero Dynamics) Consider the 2D DIP in Example III.2. If u is an actuator that controls the angle between the two links, the equations of motion are

$$\begin{aligned} (m_1+m_2)l_1^2\ddot{\theta}_1 + m_2 l_1 l_2 \ddot{\theta}_2 - (m_1+m_2)l_1 \sin(\theta_1) &= -u, \\ m_2 l_2^2 \ddot{\theta}_2 + m_2 l_1 l_2 \ddot{\theta}_1 - m_2 l_2 \sin(\theta_2) &= u. \end{aligned} \tag{4.21}$$

We show that conditions 1, 2 and 3 of Proposition IV.6 hold. Recall that in Example III.2 we showed that the 2D DIP kinetic and potential energies are invariant under the map $F(\theta_1, \theta_2) = (-\theta_1, -\theta_2)$. Thus, condition 1 of Proposition IV.6 is satisfied for $G = (F, -\mathrm{d}F)$. For condition 2, we note that the virtual work done by u for a virtual displacement $\delta q = (\delta\theta_1, \delta\theta_2)$ is $\delta W = -u\delta\theta_1 + u\delta\theta_2$. Now we calculate $\delta W' = \delta W(F(q), \delta F(q), H(u))$ for $q = (\theta_1, \theta_2)$ and $H(u) = -u$. Since $\delta F(\theta_1, \theta_2) = -(\delta\theta_1, \delta\theta_2)$, $\delta W' = u(-\delta\theta_1) - u(-\delta\theta_2)$; so, $\delta W' = \delta W$, and as a result, condition 2 of Proposition IV.6 is satisfied for $H(u) = -u$.

For condition 3 of Proposition IV.6 to hold, define the zero dynamics manifold as

$$\mathcal{Z} = \{(\theta_1, \theta_2, \dot{\theta}_1, \dot{\theta}_2) | \theta_2 = h(\theta_1), \dot{\theta}_2 = \frac{\partial h}{\partial \theta_1}\dot{\theta}_1\},$$

where h is an odd function of θ_1. Note that $\mathcal{Z}$ is invariant under $G = (F, -\mathrm{d}F)$, which maps $(\theta_1, \theta_2, \dot{\theta}_1, \dot{\theta}_2)$ to $(-\theta_1, -\theta_2, \dot{\theta}_1, \dot{\theta}_2)$. The restriction of G to $\mathcal{Z}$ is $G_{\mathcal{Z}}(\theta_1, \dot{\theta}_1) = (-\theta_1, \dot{\theta}_1)$, whose fixed points are of the form $(0, \dot{\theta}_1^*)$. Therefore, by Proposition IV.6, any symmetric solution $(\theta_1(t), \theta_2(t))$ starting from a fixed point of G on $\mathcal{Z}$ lies on $\mathcal{Z}$

and is invariant under G. That is, $\theta_2(t) = h(\theta_1(t))$ and $\theta_1(-t) = -\theta_1(t)$. Moreover, by Proposition IV.6, the torque $u(\theta_1, \dot{\theta}_1)$ on $\mathcal{Z}$, satisfies the following equality:

$$u(G_{\mathcal{Z}}(\theta_1, \dot{\theta}_1)) = H(u(\theta_1, \dot{\theta}_1)),$$

which by definition of H and G, equivalently reads as

$$u(-\theta_1, \dot{\theta}_1) = -u(\theta_1, \dot{\theta}_1).$$

That is, u on $\mathcal{Z}$ is an odd function of θ_1. Finally, as predicted by Proposition IV.6, the work done by u on a symmetric solution, $x_s(t)$, on $\mathcal{Z}$ is zero because $u(x_s(t))$ is an odd function of t, while $(\dot{\theta}_1(t), \dot{\theta}_2(t))$ is even; thus,

$$\int_{-a}^{a} -u(x_s(t))\dot{\theta}_1(t) + u(x_s(t))\dot{\theta}_2(t) = 0$$

for any a in the domain of $x_s(t)$.

Remark IV.8. In many cases of second order hybrid systems with a coordinate system $(q, \dot{q})$, such as Example IV.7, the symmetry map G simply reverses the signs of a number of q_is. In these cases, q can be written as $q = (\phi, \psi)$ and $G : (\phi, \psi, \dot{\phi}, \dot{\psi}) \mapsto (-\phi, \psi, \dot{\phi}, -\dot{\psi})$. In such case, the first two conditions of Proposition IV.6 can be easily checked; it suffices to check that equations of motion are invariant under the map $(\phi, \psi, \dot{\phi}, \dot{\psi}, \ddot{\phi}, \ddot{\psi}) \mapsto (-\phi, \psi, \dot{\phi}, -\dot{\psi}, -\ddot{\phi}, \ddot{\psi})$ with appropriate mapping of u_is. For instance, it immediately follows that (4.21) is invariant under the map $(\theta_1, \theta_2, \dot{\theta}_1, \dot{\theta}_2, \ddot{\theta}_1, \ddot{\theta}_2) \mapsto (-\theta_1, -\theta_2, \dot{\theta}_1, \dot{\theta}_2, -\ddot{\theta}_1, -\ddot{\theta}_2)$ and $u \mapsto -u$. Similarly, it is easy to check that (4.7) is invariant under the map $(x, y, z, \dot{x}, \dot{y}, \dot{z}, \ddot{x}, \ddot{y}, \ddot{z}) \mapsto (-x, y, z, \dot{x}, -\dot{y}, -\dot{z}, -\ddot{x}, \ddot{y}, \ddot{z})$ and $(u_1, u_2) \mapsto (-u_1, u_2)$.

4.2 Symmetric Hybrid Zero Dynamics

First, we briefly discuss the notion of a hybrid system with control and Hybrid Zero Dynamics (HZD)[3].

Definition IV.9. (**Hybrid System with Control Input**) Let $X(x,u)$ be a smooth vector field defined on an n-dimensional manifold $\mathcal{X}$, where u is a control input in $\mathcal{U} \subset \mathbb{R}^m$ such that $m \leq n$. Suppose that $\mathcal{S}$ is an embedded submanifold of $\mathcal{X}$ with co-dimension one. Moreover, assume that $\Delta : \mathcal{S} \to \mathcal{X}$ is a smooth map such that $\Delta(\mathcal{S}) \cap \mathcal{S} = \emptyset$. A hybrid system with control, denoted by $\Sigma = (X, \Delta, \mathcal{X}, \mathcal{S}, \mathcal{U})$, is defined as

$$\begin{cases} \dot{x} = X(x,u), & x^- \notin \mathcal{S}, \\ x^+ = \Delta(x^-), & x^- \in \mathcal{S}, \end{cases} \tag{4.22}$$

where $X(x,u)$ is in the form of $f(x) + g(x)u$. Since $\mathcal{X}$ has a dimension n, Σ is said to be an n-dimensional hybrid system with control input.

Definition IV.10. (**Hybrid Zero Dynamics**) Consider the n-dimensional hybrid system with control $\Sigma = (X, \Delta, \mathcal{X}, \mathcal{S}, \mathcal{U})$, and let $\mathcal{Z}$ be a zero dynamics submanifold associated with X enforced by the control law $u(x)$. Then $\mathcal{Z}$ is said to be hybrid invariant if $\Delta(\mathcal{Z} \cap \mathcal{S}) \subset \mathcal{Z}$. Moreover, $\Sigma_{\mathcal{Z}} = (X_{\mathcal{Z}}, \Delta_{\mathcal{Z}}, \mathcal{Z}, \mathcal{S} \cap \mathcal{Z})$, with the dynamic equations

$$\begin{cases} \dot{z} &= X_{\mathcal{Z}}(z, u(z)), & z^- \notin \mathcal{S} \cap \mathcal{Z}, \\ z^+ &= \Delta_{\mathcal{Z}}(z^-), & z^- \in \mathcal{S} \cap \mathcal{Z}, \end{cases}$$

where $X_{\mathcal{Z}}$ and $\Delta_{\mathcal{Z}}$ are the restrictions of X and Δ to $\mathcal{Z}$, is the hybrid zero dynamics on $\mathcal{Z}$ associated with Σ.

[3]For a detailed discussion of HZD see (*Westervelt et al.*, 2007).

The following proposition presents the conditions that a given hybrid system needs to fulfill in order to become a reduced dimension SHS, also called Symmetric HZD.

Proposition IV.11. *(**Symmetric Hybrid Zero Dynamics**) Let* $\Sigma = (X, \Delta, \mathcal{X}, \mathcal{S}, \mathcal{U})$ *be an* n*-dimensional hybrid system with* m*-dimensional linear control input, where* $m < n$*; that is,* X *can be written in the form* $X(x,u) = f(x) + g(x)u$*. Assume that there exists a unique control law* $u(x)$ *that enforces* $\mathcal{Z}$ *as an* $(n-m)$*-dimensional HZD submanifold of* $\mathcal{X}$*. If there exists a smooth map* $G : \mathcal{X} \to \mathcal{X}$ *and an isomorphism* $H : \mathcal{U} \to \mathcal{U}$ *such that*

1. $X(x,0)$ *is a* G*-symmetric vector field,*
2. $(g \circ G(x))H(u) = -(\mathrm{d}G \cdot g)u$ *for all* $x \in \mathcal{X}$ *and all* $u \in \mathcal{U}$*,*
3. $\mathcal{Z}$ *is invariant under* G*,*

then by Proposition IV.2, $\mathcal{X}_{\mathcal{Z}} = f(z) + g(z)u(z)$ *is* $G_{\mathcal{Z}}$*-symmetric and any symmetric solution,* $x_s(t)$*, starting from a fixed point of* G *on* $\mathcal{Z}$*, stays on* $\mathcal{Z}$*. If for any such* $x_s(t)$ *which is a feasible*[4] *solution that crosses the switching surface* $\mathcal{S} \cap \mathcal{Z}$ *at, say* $t = t_I$*, we have*

4. $\Delta(x_s(t_I)) = G(x_s(t_I))$,

then $\Sigma_{\mathcal{Z}} = (X_{\mathcal{Z}}, \Delta_{\mathcal{Z}}, \mathcal{Z}, \mathcal{S} \cap \mathcal{Z})$ *is a* $G_{\mathcal{Z}}$*-SHS, and* $x_s(t)$ *is a periodic orbit on* $\mathcal{Z}$*. In addition,* $u \circ G(z) = H(u(z))$ *on* $\mathcal{Z}$*.*

Proof. The proof quickly follows from Proposition IV.2 and definition of an SHS. □

Note that condition 4 only needs to hold for solutions $x_s(t)$ that lie on $\mathcal{Z}$, are feasible, and cross the switching surface (not all symmetric solutions that cross the switching surface). The following corollary concerns the case where condition 4 is satisfied for all symmetric solutions that cross the switching surface.

[4] See Definition II.8.

Corollary IV.12. *In Proposition IV.11, if* $\Sigma = (X(x, u(x)), \Delta, \mathcal{X}, \mathcal{S})$ *is an* n*-dimensional G-SHS for a symmetry map* G*, then* $\Sigma_{\mathcal{Z}}$ *is an* $(n-m)$*-dimensional* $G_{\mathcal{Z}}$*-SHS.*

In the following example, given a 3-DOF biped, the zero dynamics submanifold is defined such that the conditions of Proposition IV.11 are satisfied; as a consequence, without any numerical searches, we obtain periodic orbits of the system which correspond to periodic walking of the biped. In Section 5.4, Proposition IV.11 is applied to a 5-DOF 2D Biped to obtain symmetric periodic orbits.

Example IV.13. (3-DOF Biped Symmetric HZD) Consider the 2D biped in Fig. 4.1, which is a simple 2D model of the bipedal robot MARLO (*Buss et al.*, 2014). Assuming that the legs are massless, this biped has 3 DOF. Suppose that the torso has a mass of m and a moment of inertia I about the center of mass (COM), and let l be the distance from the hip joint to the COM. Let (x, z) denote the hip position and let θ_p denote the pitch angle of the torso. The actuators include a motor at the hip which applies a torque u_θ to control the angle between the thigh and torso and an actuator which controls the knee angle. Without loss of generality (for non-zero knee angles), we can replace the torque at the knee by a force f_l along the line connecting the support point to the hip. This line may be referred to as a virtual leg. Then, f_l controls the length of this virtual leg. The kinetic energy and potential energies of the biped are

$$\begin{aligned} K &= \frac{1}{2}(I + ml^2)\dot{\theta}_p^2 + \frac{1}{2}m(\dot{x}^2 + \dot{z}^2 + 2l\dot{x}\dot{\theta}_p\cos(\theta_p) - \\ &\quad 2l\dot{z}\dot{\theta}_p\sin(\theta_p)), \\ V &= mg(z + l\cos(\theta_p)). \end{aligned}$$

To simplify the equations of motion, we non-dimensionalize the equations of motion by replacing x/l with x, z/l with z, f_l/ml with f_l, and u_θ/ml^2 with u_θ. With these

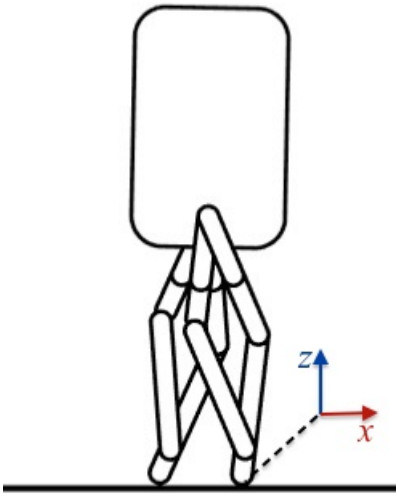

Figure 4.1: A simple 2D model of the bipedal robot MARLO (*Buss et al.*, 2014).

assignments, the equations of motion of this biped are:

$$\begin{aligned}
&\ddot{x} + \ddot{\theta}_p \cos(\theta_p) - \dot{\theta}_p \sin(\theta_p) && = F_1, \\
&\ddot{z} - \ddot{\theta}_p \sin(\theta_p) - \dot{\theta}_p^2 \cos(\theta_p) + \tfrac{g}{l} && = F_2, \\
&(\tfrac{I}{ml^2} + 1)\ddot{\theta}_p + \cos(\theta_p)\ddot{x} - \sin(\theta_p)\ddot{z} - \\
&\dot{x}\dot{\theta}_p \sin(\theta_p) - \dot{z}\dot{\theta}_p \cos(\theta_p) - \tfrac{g}{l}\sin(\theta_p) && = -u_\theta,
\end{aligned} \tag{4.23}$$

where

$$F_1 = \frac{f_l x}{\sqrt{x^2+z^2}} + \frac{u_\theta z}{x^2+z^2}, \; F_2 = \frac{f_l z}{\sqrt{x^2+z^2}} - \frac{u_\theta x}{x^2+z^2}.$$

Suppose that the biped is taking constant swing leg end to hip strides, that is, if $q = (x, z, \theta_p)$ and $\dot{q} = (\dot{x}, \dot{z}, \dot{\theta}_p)$, then the switching surface is $\mathcal{S} = \{(q, \dot{q}) | x = x_0\}$, and $x^+ = -x_0$ for some $x_0 > 0$. With this assumption, the impact map is $\Delta = (\Delta_q, \Delta_{\dot{q}})$,

where

$$\begin{aligned}\Delta_q(x^-, z^-, \theta_p^-) &= (-x_0, z^-, \theta_p^-),\\ \Delta_{\dot{q}}(q^-, \dot{q}^-) &= \dot{q}^+,\end{aligned}$$

and $\dot{q}^+$ can be found by conservation of angular momentum about the swing leg end and swing knee joint before and after impact (*McGeer*, 1990). Our goal is to choose the virtual constraints that define the zero dynamics such that the zero dynamics is hybrid invariant and an SHS with symmetric periodic orbits. From the equations of kinetic and potential energies, the Lagrangian is invariant under the map

$$F(x, z, \theta_p) = (-x, z, -\theta_p), \tag{4.24}$$

which proves condition 1 of Proposition IV.6. As explained in Remark IV.8, condition 1 and 2 of Proposition IV.6 can be immediately checked by verifying the invariance of the equations of motion under the map $(x, z, \theta_p, \dot{x}, \dot{z}, \dot{\theta}_p, \ddot{x}, \ddot{z}, \ddot{\theta}_p) \mapsto (-x, z, -\theta_p, \dot{x}, -\dot{z}, \dot{\theta}_p, -\ddot{x}, \ddot{z}, -\ddot{\theta}_p)$ and $(f_l, u_\theta) \mapsto (f_l, -u_\theta)$. Alternatively, we could directly verify condition 2 of Proposition IV.6 in which case

$$\delta W = (\frac{f_l x}{\sqrt{x^2+z^2}} + \frac{u_\theta z}{x^2+z^2})\delta x + (\frac{f_l z}{\sqrt{x^2+z^2}} - \frac{u_\theta x}{x^2+z^2})\delta z - u_\theta \delta\theta_p.$$

With $H(f_l, u_\theta) = (f_l, -u_\theta)$, and by definition of $\delta W'$ in Proposition IV.6,

$$\delta W' = (\frac{(f_l)(-x)}{\sqrt{x^2+z^2}} + \frac{-u_\theta z}{x^2+z^2})(-\delta x) + (\frac{f_l z}{\sqrt{x^2+z^2}} - \frac{(-u_\theta)(-x)}{x^2+z^2}\delta z - (-u_\theta)\delta(-\theta_p).$$

Clearly $\delta W' = \delta W$, which proves condition 2 of Proposition IV.6.

So far we showed that conditions 1 and 2 of Proposition IV.6 hold, thus by Proposition IV.6, conditions 1 and 2 of Proposition IV.11 hold. To satisfy the third condition

of Proposition IV.11, define the submanifold $\mathcal{Z}$ as follows:

$$\mathcal{Z} = \{(q, \dot{q}) | z = h_1(x), \theta_p = h_2(x), \dot{z} = \frac{\partial h_1}{\partial x}\dot{x}, \dot{\theta}_p = \frac{\partial h_2}{\partial x}\dot{x}\}.$$

where h_1 and h_2 are are even and odd smooth functions, respectively. Since h_1 is even and h_2 is odd, $\mathcal{Z}$ is invariant under the symmetry map $G = (F, -\mathrm{d}F)$. However, more conditions on h_1 and h_2 need to be imposed to ensure $\mathcal{Z}$ is hybrid invariant and condition 4 holds. Here, we present two sets of (h_1, h_2) that render $\mathcal{Z}$ hybrid invariant while satisfying condition 4. In the next chapter general conditions on virtual constraints in order for them to render $\mathcal{Z}$ hybrid invariant and at the same time to preserve the symmetry of the system shall be discussed.

Example A: If $h_1(x) = z_0$ and $h_2(x) = 0$, then $\mathcal{Z}$ is invariant under $G = (F, -\mathrm{d}F)$. In this case, the fixed points of G lying on $\mathcal{Z}$ are $(q^*, \dot{q}^*)$, where

$$q^* = (0, z_0, 0), \dot{q}^* = (\dot{x}^*, 0, 0), \tag{4.25}$$

and the zero dynamics equation is simply that of the 2D LIP:

$$\ddot{x} = \frac{g/l}{1 + z_0} x,$$

with $\dot{x}^+ = \dot{x}^-$ and $x^+ = -x_0$; therefore, condition 4 of Proposition IV.11 is also satisfied because $G_Z(x, \dot{x}) = (-x, \dot{x})$ and $\Delta(x^-, \dot{x}^-) = G(x_0, \dot{x}^-)$. Consequently, the HZD is a $G_{\mathcal{Z}}$-SHS and has an infinite number of symmetric periodic orbits (*Razavi et al.*, 2016) as predicted by Proposition IV.11 as well.

Example B: Another set of holonomic constraints that can render $\mathcal{Z}$ invariant under G is defined by $h_1(x) = z_0 - a\cos((\pi/x_0)x)$ and $h_2(x) = 0$, for which the HZD

is

$$\ddot{x} = \frac{(g/l)x + ax(\frac{\pi}{x_0})^2 \cos((\frac{\pi}{x_0})x)\dot{x}^2}{1 + z_0 - a\cos((\frac{\pi}{x_0})x) - ax\frac{\pi}{x_0}\sin((\frac{\pi}{x_0})x)}, \tag{4.26}$$

with $\dot{x}^+ = \dot{x}^-$ and $x^+ = -x_0$. Letting $x_1 = x$ and $x_2 = \dot{x}$, one can write (4.26) in the state-space form:

$$\begin{bmatrix} \dot{x}_1 \\ \dot{x}_2 \end{bmatrix} = \begin{bmatrix} x_2 \\ \frac{(g/l)x_1 + ax_1(\frac{\pi}{x_0})^2 \cos((\frac{\pi}{x_0})x_1)x_2^2}{1+z_0-a\cos((\frac{\pi}{x_0})x_1)-ax\frac{\pi}{x_0}\sin((\frac{\pi}{x_0})x_1)} \end{bmatrix}.$$

Denoting the right-hand side of the equation above by $X(x_1, x_2)$, it is easy to see that X is $G_{\mathcal{Z}}$-symmetric, where $G_{\mathcal{Z}}(x, \dot{x}) := (-x, \dot{x})$ is the restriction of $G = (F, -\mathrm{d}F)$ to $\mathcal{Z}$ with F defined in (4.24). By Proposition IV.11, since $(x^+, \dot{x}^+) = G_{\mathcal{Z}}(x_0, x^-)$, this HZD is a $G_{\mathcal{Z}}$-SHS. Fig. 4.2 shows a symmetric periodic orbit of this SHS together with z as a function of x. Fig. 4.3 shows multiple periodic solutions lying on the HZD. Indeed, the HZD has an infinite number of periodic solutions because the symmetry map $G_{\mathcal{Z}}$ has an infinite number of fixed points in the form $(0, \dot{x}^*)$.

The two sets of virtual constraints defined above preserve the symmetry of the system on its HZD. More general virtual constraints which can preserve the symmetry of the system will be discussed in the next chapter.

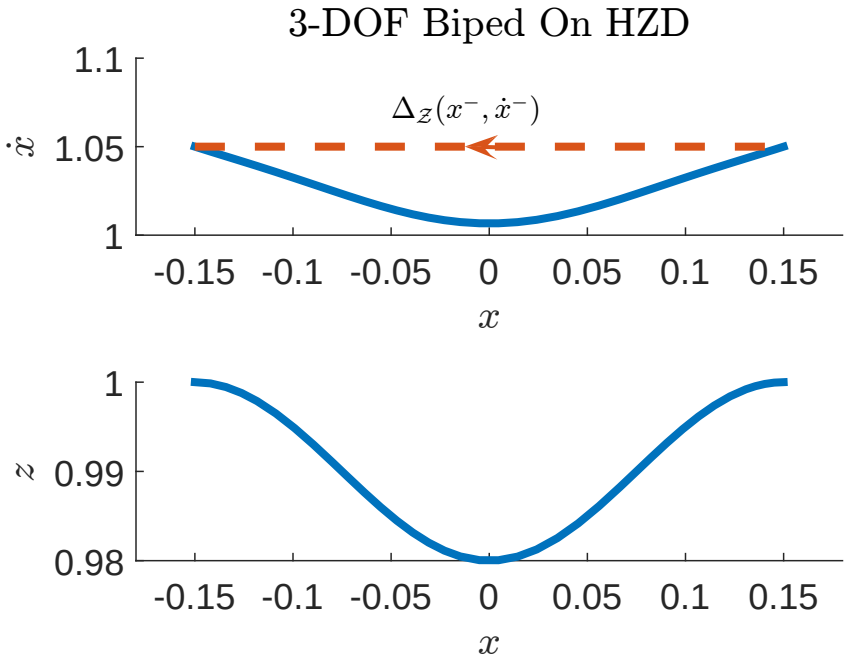

Figure 4.2: A symmetric periodic solutions of the 3-DOF biped on the HZD defined by $h_1(x) = z_0 - a\cos((\pi/x_0)x)$ and $h_2(x) = 0$. Note that $\dot{x}$ and z are both even functions of x.

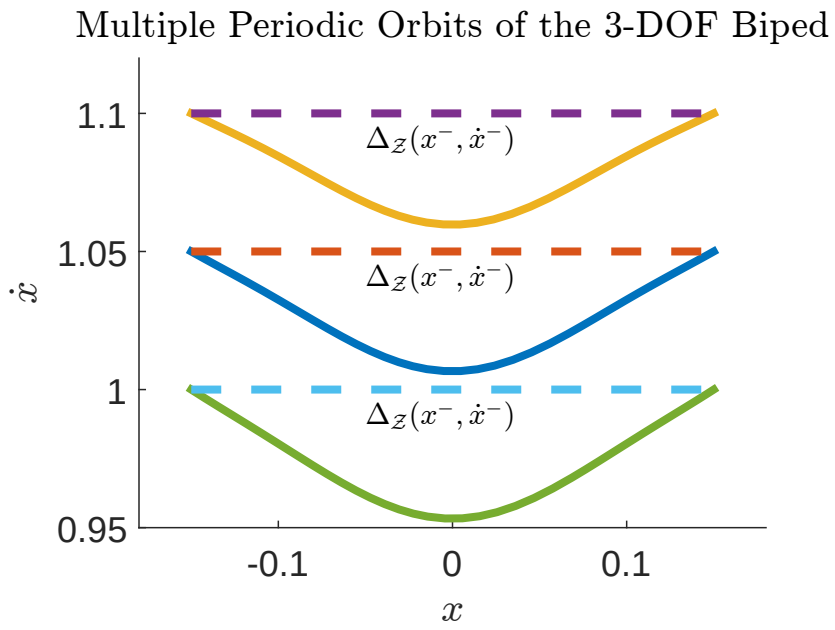

Figure 4.3: Multiple symmetric periodic solutions of the 3-DOF biped on the HZD defined by $h_1(x) = z_0 - a\cos((\pi/x_0)x)$ and $h_2(x) = 0$. There are an infinite number of symmetric periodic solutions on this HZD which can be identified by fixed points of the symmetry map $G_{\mathcal{Z}}$, which are in the form $(0, \dot{x}^*)$.

CHAPTER V

Symmetric Virtual Constraints and Symmetric Periodic Orbits

In Proposition IV.2 of Chapter IV, we saw that for a vector field with linear control input $X(x,u) = f(x) + g(x)u$ that satisfies certain symmetry conditions (conditions 1 and 2) under a map G if the zero dynamics submanifold $\mathcal{Z}$ is G-invariant, the resulting zero dynamics is a lower dimensional SVF and hence, has symmetric solutions as many as fixed points of the restriction of G to $\mathcal{Z}$. Moreover, based on Proposition II.13, in case of a hybrid system, these solutions can become symmetric periodic orbits. To build such G-invariant zero dynamics submaniolds, in this chapter, we introduce the notion of Symmetric Virtual Constraints (SVCs). SVCs directly result in realizing feedback controllers that render $\mathcal{Z}$ invariant under G; hence, in the case of a hybrid system existence of symmetric periodic orbits can be guaranteed without any need for searching for periodic orbits. The results of this chapter will be used in Chapter VII to obtain limit cycle walking gaits for a 12-DOF 3D Biped.

5.1 Symmetric Virtual Constraints

First, we briefly discuss the notion of virtual constraints. In a Lagrangian system with control input, a functional relation between the generalized coordinates in the

form

$$y = h(q, \dot{q}),$$

for a smooth real-valued function h, which is asymptotically zeroed by a feedback control law is said to be a *virtual constraint*. If h is only a function of configuration variables q, then the virtual constraint is a *holonomic* constraint, and if h is a non-integrable function of $\dot{q}$, then the virtual constraint is said to be *nonholonomic* (*Bloch et al.*, 2003). While the notion of symmetry for virtual constraints, which will be discussed in the following sections, is applicable to both holonomic and nonholonomic virtual constraints, we only will discuss holonomic constraints. Nonholonomic virtual constraints for dynamic walking of bipedal robots have been discussed in (*Griffin and Grizzle*, 2015).

In the following subsections, we first discuss the notion of SVCs for achieving a symmetric zero dynamics and then will discuss SVCs for symmetric hybrid zero dynamics.

5.1.1 Symmetric Virtual Constraints for Symmetric Zero Dynamics

Defintion V.1. (**SVCs for Symmetric Zero Dynamics)** Let X be a G-symmetric vector field with linear control input on a manifold $\mathcal{X}$, that is, $X(x, u) = f(x)+g(x)u$, where X satisfies conditions 1 and 2 of Proposition IV.2 for a symmetry map G on $\mathcal{X}$. A set of virtual constraints $y = h(x)$ for $h : \mathcal{X} \to \mathbb{R}^k$ is said to be symmetric if $h \circ G = h$, and h has a constant rank k such that

$$\mathcal{Z} = \{x \in \mathcal{X} | h(x) = 0\}$$

is a zero dynamics submanifold of $\mathcal{X}$ for X with dimension $m = n-k$. In this case, the virtual constraints defined by $y = h(x)$ are said to be *Symmetric Virtual Constraints*

for X.

In this definition, $\mathcal{Z}$ is G-invariant because $h \circ G = h$. The zero dynamics submanifolds defined in Example IV.3, IV.4 and IV.7 are examples of G-invariant submanifolds defined by SVCs.

In case of a Lagrangian system on an n-dimensional configuration manifold $\mathcal{Q}$, if the Lagrangian L is symmetric under a map $F : \mathcal{Q} \to \mathcal{Q}$, $h : \mathcal{Q} \to \mathbb{R}^k$ and its Jacobian $\mathrm{d}h$ has a rank k, and $h \circ F = h$, then

$$\mathcal{Z} = \{(q, \dot{q}) \in \mathcal{X} | h(q) = 0, \frac{\partial h(q)}{\partial q} \dot{q} = 0\}$$

has a dimension $2(n-k)$ and is G-invariant, where $G = (F, -\mathrm{d}F)$. Hence, h together with its derivative are SVCs for this Lagrangian system. Such SVCs are used in Example IV.7 to define the zero dynamics submanifold $\mathcal{Z}$.

5.1.2 Symmetric Virtual Constraints for Symmetric Hybrid Zero Dynamics

Based on Proposition IV.11, in the case of a hybrid system, in order for the HZD to become an SHS, the zero dynamics submanifold $\mathcal{Z}$ needs to be invariant under the symmetry map as well as the transition map, and moreover, as noted in condition 4 of Proposition IV.11, if a symmetric solution $x(t)$ on $\mathcal{Z}$ crosses the switching surface at a point $x(t_I)$, then the transition map needs to map this solution to $G(x(t_I))$, where G is the symmetry map. In order for $\mathcal{Z}$ to satisfy these conditions, compared to the Definition V.1, the SVCs need to satisfy more conditions as described in the following definition.

Defintion V.2. (**SVCs for Symmetric Hybrid Zero Dynamics**) Let $\Sigma = (X, \Delta, \mathcal{X}, \mathcal{S}, \mathcal{U})$ be a hybrid system with linear control input on a manifold $\mathcal{X}$, where X satisfies conditions 1 and 2 of Proposition IV.11 for a symmetry map G on $\mathcal{X}$. A

set of virtual constraints $y = h(x)$ for $h : \mathcal{X} \to \mathbb{R}^k$ is said to be symmetric for the hybrid system Σ if

1. $h \circ G = h$ and h has a constant rank k,
2. $h(\Delta(z)) = 0$ for all $z \in \mathcal{Z} \cap \mathcal{S}$ (i.e., $\mathcal{Z}$ is invariant under the impact map),
3. If $x_s(t)$ is a feasible symmetric solution of X lying on $\mathcal{Z}$ which crosses $\mathcal{S}$ at $t = t_I$, then $\Delta(x_s(t_I)) = G(x_s(t_I))$.

In this case, the virtual constraints defined by $y = h(x)$ are said to be *Symmetric Virtual Constraints* for the hybrid system Σ.

According to the above definition and Proposition IV.11, the HZD generated by SVCs is a $G_{\mathcal{Z}}$-SHS; hence, it can possess as many symmetric periodic solutions as the number of fixed points of $G_{\mathcal{Z}}$. Example IV.13 shows two sets of SVCs which lead to symmetric HZDs.

5.2 SVCs for a 5-DOF Biped

Consider the planar biped with point feet as depicted in Fig. 5.1. Assuming that the legs have mass, this biped has five DOFs and four actuators (two in each leg to control the leg length and the angle between the leg and torso), hence, has one degree of underactuation. We denote the control input vector by $u = [u_1; u_2; u_3; u_4]$, where u_1 controls the knee angle q_1, u_2 controls the angle between the stance leg and torso q_2, u_3 controls the angle between the torso and swing leg thigh q_3, and finally, u_4 controls the swing knee angle q_4. We assume that when all these angles are zero the configuration of the biped is as in Fig. 5.2.

Proposition V.3. *If the equations of motion of the 5-DOF bipedal robot in Fig. 5.1 are written in the form*

$$A(q)\ddot{q} + S(q, \dot{q}) = B(q)u,$$

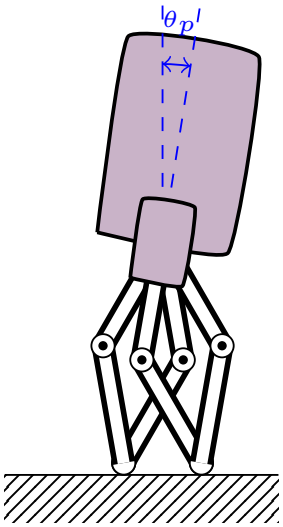

Figure 5.1: 5-DOF 2D Symmetric Biped.

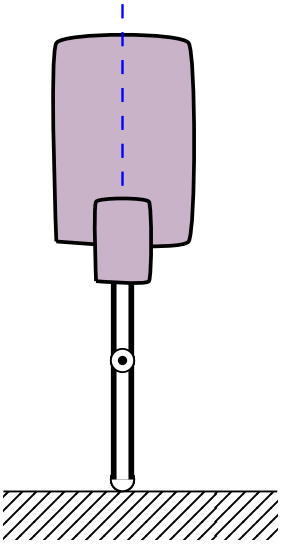

Figure 5.2: 5-DOF 2D Symmetric Biped Zero Pose.

for $q = (q_1, q_2, \theta_p, q_3, q_4)$, and $F(q_1, q_2, \theta_p, q_3, q_4) = (q_1, -q_2, -\theta_p, -q_3, q_4)$, then conditions 1 and 2 of Proposition IV.6 are satisfied; that is,

1. *Kinetic and potential energies are invariant under $G(q, \dot{q}) = (F(q), -\mathrm{d}F(q) \cdot \dot{q})$,*
2. *$\delta W'(q, \delta q, u) = \delta W(q, \delta q, u)$, or equivalently $B(F(q))H(u) = (\mathrm{d}F(q))^T B(q)u$,*

where $H(u = [u_1; u_2; u_3; u_4]) = [u_1; -u_2; -u_3; u_4]$.

Proof. The first condition of Proposition IV.6 follows simply by writing the kinetic and potential energies and verifying their invariance under the map G. To show the second condition, we look at the virtual work δW done by actuators for a virtual displacement $\delta q = (\delta q_1, \delta q_2, \delta\theta_p, \delta q_3, \delta q_4)$. By definition,

$$\delta W = u_1 \delta q_1 + u_2 \delta q_2 + u_3 \delta q_3 + u_4 \delta q_4.$$

Let $\delta W'$ be as in Proposition IV.6. From the definition of F and H,

$$\begin{aligned} \delta W' &= u_1 \delta q_1 + (-u_2)\delta(-q_2) + (-u_3)\delta(-q_3) + u_4 \delta q_4 \\ &= u_1 \delta q_1 + u_2 \delta q_2 + u_3 \delta q_3 + u_4 \delta q_4. \end{aligned}$$

From this equation and definition of δW, we have $\delta W' = \delta W$. □

Even though for simplicity we used the joint angles together with torso pitch angle as the generalized coordinates in the proposition above, since the symmetry properties are all coordinate-independent, we can use any other generalized coordinates if they are more convenient for design of virtual constraints. For instance, to present the SVCs, we use the generalized coordinate $q = (x, z, \theta_p, x_{hf}, z_f)$, where (x, z) is the position of the hip, θ_p is the torso pitch angle as shown in Fig 5.1, z_f is the height of the swing leg, and (x_{hf}, z_{hf}) is the position of the swing leg foot relative to the hip; that is, if (x_f, z_f) is the coordinate of the swing leg end in the inertial frame attached

to the support point (i.e., stance leg end point), then $(x_{hf}, z_{hf}) = (x_f - x, z_f - z)$. The symmetry map F sends $(x, z, \theta_p, x_{hf}, z_f)$ to $(-x, z, -\theta_p, -x_{hf}, z_f)$.

By Proposition V.3, the 5-DOF 2D biped satisfies the first two conditions of Proposition IV.6. For the third condition of Proposition IV.6 to hold, as explained in the following proposition, based on the symmetry map in Proposition V.3, SVCs are chosen such that the HZD of the 5-DOF biped is invariant under G. Moreover, condition 4 of Proposition IV.6 should hold so that the HZD becomes an SHS, which can have infinitely many symmetric periodic orbits. We note that naturally, it is assumed that the transition occurs when the swing leg hits the ground. That is, the switching surface is assumed to be $\mathcal{S} = \{(q, \dot{q}) | z_f(q) = 0\}$.

Proposition V.4. *(**SVCs for the 5-DOF Biped**) In the 5-DOF biped, define the zero dynamics submanifold $\mathcal{Z}$ by the virtual constraints $z = h_1(x), \theta_p = h_2(x), x_{hf} = h_3(x)$, $z_f = h_4(x)$ and their derivatives. These virtual constraints are SVCs if*

$$
\begin{aligned}
&h_1(-x) = h(x), \frac{\mathrm{d}h_1}{\mathrm{d}x}|_{x=x_0} = 0, \\
&h_2(-x), = -h_2(x), h_2(x_0) = 0, \\
&h_3(-x) = -h_3(x), h_3(x_0) = x_0, \frac{\mathrm{d}h_3}{\mathrm{d}x}|_{x=x_0} = -1, \\
&h_4(-x) = h(x), h_4(x_0) = 0, \frac{\mathrm{d}h_4}{\mathrm{d}x}|_{x=x_0} = 0, \\
&h_4(x) > 0, \text{if } x \in (-x_0, x_0),
\end{aligned}
$$

for some $x_0 > 0$. Thus, $\mathcal{Z}$ is hybrid invariant, and the resulting HZD is a $G_{\mathcal{Z}}$-SHS with $G_{\mathcal{Z}}(x, \dot{x}) = (-x, \dot{x})$, where G is defined in Proposition V.3. Consequently, the continuous phase of equations on the HZD can be written as $\ddot{x} = f(x, \dot{x})$, where $f(-x, \dot{x}) = -f(x, \dot{x})$. Moreover, the impact map restricted to $\mathcal{S} \cap \mathcal{Z}$ and its switching surface are

$$
(x^+, \dot{x}^+) = (-x_0, \dot{x}^-), \ \mathcal{S} \cap \mathcal{Z} = \{(x, \dot{x}) | x = x_0\}, \tag{5.1}
$$

Proof. By the choice of virtual constraints right before the impact the velocity of the COM of the biped is parallel to the ground, and the swing leg end hits the ground with zero velocity at a position x_0 relative to the hip. As a result, there is no impact loss and the impact map is as in (5.1). With this impact map, and by the odd-even symmetries of the virtual constraints, it is easy to check that $\Delta(\mathcal{S} \cap \mathcal{Z}) \subset \mathcal{Z}$. Thus, $\mathcal{Z}$ is hybrid invariant.

By Proposition V.3 and Proposition IV.11, to show that the HZD is an SHS it suffices to show that (i) $\mathcal{Z}$ is invariant under G (ii) Condition 4 of Proposition IV.11 holds. However, invariance of $\mathcal{Z}$ under G immediately follows by odd-even symmetries of the virtual constraints and definition of the symmetry map F. Also, condition 4 of Proposition IV.6 holds true because $\Delta(x^-, \dot{x}^-) = \Delta(x_0, \dot{x}^-) = (-x_0, \dot{x}^-) = G(x_0, \dot{x}^-)$; thus, $\Delta = G$ on $\mathcal{S} \cap \mathcal{Z}$. □

Note that as long as the virtual constraints satisfy conditions of Definition V.2, it is guaranteed that the HZD is an SHS and hence, can have many symmetric periodic orbits without any need for numerical search.

Remark V.5. While the outputs in Proposition V.4 were chosen to be functions of x, with appropriate change of variables one can use any other variable which is an odd function of x and monotonically increasing or decreasing. For example, if $\theta = h_\theta(x)$, where h_θ is an odd function and monotonic, then the outputs h_1 through h_5 can be written as functions of θ, and they must satisfy the same odd-even conditions as that of x. The other conditions of Proposition V.4, such as the ones involving the derivatives of h_is, need to be modified by appropriate use of chain rule.

Example V.6. Based on Proposition V.4 the following holonomic constraints to-

gether with their derivatives are SVCs for the 5-DOF biped:

$$\begin{aligned} z &= z_0 - a_1 \cos(\frac{\pi x}{x_0}), \\ \theta_p &= b_1 \sin(\frac{\pi x}{x_0}), \\ x_{hf} &= x + \frac{2x_0}{\pi} \sin(\frac{\pi x}{x_0}), \\ z_f &= a_2(x_0^4 - 2x_0^2 x^2 + x^4) \end{aligned}$$

It should be noted that the conditions on virtual constraints in Proposition V.4 can all be satisfied by just using polynomials, and in particular, by the so-called Symmetric Bézier polynomials, which will be discussed in Section 5.4.

5.3 SVCs for an 8-DOF 3D biped

To show how SVCs can lead to periodic gait design in 3D legged locomotion, here we discuss an 8-DOF 3D biped as depicted in Fig. 5.3. As discussed in Section 3.2.2 this biped has 6 actuators, 3 in each leg to control the knee angle, the hip pitch angle and the hip roll angle.

This biped is assumed to have uniform mass distribution and left-right symmetry, hence it satisfies the assumptions H1-H5 in Section 3.2.2. Consequently, it is a symmetric legged robot. We assume that the yaw angle θ_y is constrained to be zero[1]. By Proposition III.7 and Corollary III.8, F defined by

$$(\theta_r, \theta_p, x, y, \zeta, x_{hf}, y_{hf}, \xi) \mapsto (\theta_r, -\theta_p, -x, y, \zeta, -x_{hf}, y_{hf}, \xi)$$

is a symmetry map for this biped, where ζ could be any of the following

a. $\zeta = z$, where z is the height of the hip (i.e., the z-coordinate of the hip in the inertial frame attached to the support point)

[1]This can be achieved, for instance, by using a foot that prevents rotation in the yaw direction.

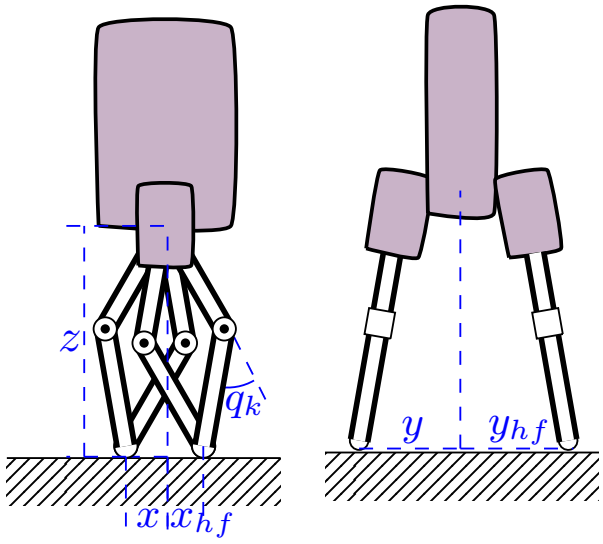

Figure 5.3: Sagittal (left) and Frontal (right) View of a Symmetric 3D Biped.

b. $\zeta = l^{st}$, where l^{st} is the length of the stance leg[2],

c. $\zeta = q_k^{st}$, where q_k^{st} is the stance knee angle,

and ξ could be any of the following,

d. $\xi = z_{hf}$, where z_{hf} is $z_f - z$ with z_f being the height of the swing leg end,

e. $\xi = l^{sw}$, where l^{sw} is the length of the swing leg,

f. $\xi = q_k^{sw}$, where q_k^{sw} is the swing leg knee angle,

g. $\xi = z_f$, where z_f is the height of the swing leg end.

Any combinations of $\{a, b, c\}$ and $\{d, e, f, g\}$ can be selected for (ζ, ξ). For example, (ad) is the case where ζ is selected to be z and ξ is selected to be z_{hf}. For future reference, let $q = (\theta_r, \theta_p, x, y, \zeta, x_{hf}, y_{hf}, \xi)$, and denote the configuration space of this biped by $\mathcal{Q}$.

Now, based on this symmetry map, we define SVCs so that the resulting zero dynamics is an SHS with symmetric periodic orbits. Since the biped has only 6

[2]By length of the leg we mean length of the line connecting the right (left) foot to the right (left) hip joint. This line is referred to as the virtual leg.

actuators, we choose 6 virtual constraints as follows

$$\begin{array}{rclrclrcl} \theta_r & = & h_1(x), & \theta_p & = & h_2(x), & \zeta & = & h_3(x), \\ x_{hf} & = & h_4(x), & y_{hf} & = & h_5(x), & \xi & = & h_6(x). \end{array} \tag{5.2}$$

The constraints are chosen as functions of x, which we call the *phase variable*, however, the phase variable can be chosen to be any odd function of x which is monotonically increasing or decreasing. Clearly, since there are 8 DOFs and 6 virtual constraints the zero dynamics is 2-dimensional (4-dimensional in the state-space representation).

We impose appropriate conditions on $h = (\theta_r - h_1; \theta_p - h_2; \cdots; \xi - h_6)$ so that the conditions of Definition V.2 are satisfied; thus, $h = 0$ defines SVCs for a symmetric HZD. The zero dynamics manifold corresponding to these virtual constraints is

$$\mathcal{Z} = \{(q, \dot{q}) | h(q) = 0, \frac{\partial h}{\partial q}\dot{q} = 0\}.$$

With virtual constraints (5.2), $(x, y, \dot{x}, \dot{y})$ can be thought of as a coordinate system on $\mathcal{Z}$. In order for $\mathcal{Z}$ to be invariant under the symmetry map F, we need to have $h \circ F = h$. To this end, it suffices that the following conditions are being satisfied.

1. $h_1(-x) = h_1(x)$,
2. $h_2(-x) = -h_2(x)$,
3. $h_3(-x) = h_3(x)$,
4. $h_4(-x) = -h_4(x)$,
5. $h_5(-x) = h_5(x)$,
6. $h_6(-x) = h_6(x)$,

In the following, we impose more conditions on h_is to ensure that the zero dynamics is hybrid invariant and an SHS with symmetric periodic orbits. To this end, we study two cases, named Case A and Case B. In Case A, the height of the hip z and

swing leg height z_f are the chosen for ζ and ξ, and a number of conditions are imposed on the virtual constraints so that the upper body moves parallel to the ground to minimize the impact losses so that the impact map is closer to a trivial impact map where there is no energy losses due to impact. In Case B, the stance leg length and swing leg length are chosen for ζ and ξ. In either case, a trivial impact map is assumed so that the zero dynamics become hybrid invariant and the HZD becomes an SHS. In Chapter VI, where asymmetries such as impact losses are included, we will see that the choice of a trivial impact map for a preliminary analysis will not cause any issues in obtaining asymptotically stable limit cycles at the end.

5.3.1 SVCs for the 8-DOF 3D Biped: Case A

By selecting $\zeta = z = h_3(x)$ and $\xi = z_f = h_6(x)$, we impose the following conditions. For some $x_0 > 0$,

7a. $h_1(x_0) = 0$,

8a. $h_2(x_0) = 0$,

9a. $(\mathrm{d}h_3/\mathrm{d}x)(x_0) = 0$,

10a. $h_4(x_0) = x_0$, $(\mathrm{d}h_4/\mathrm{d}x)(x_0) = 0$,

11a. $h_5(x_0) = y_0$, $(\mathrm{d}h_5/\mathrm{d}x)(x_0) = 0$,

12a. $h_6(x_0) = 0$, and $h_6(x) > 0$ if $x \neq \pm x_0$.

Conditions 7a-9a guarantee that the upper body is moving parallel to the ground right before the impact to minimize the impact losses, conditions 10a to 12a ensure that the swing leg end is at the position (x_0, y_0) with respect to the hip. However, because the swing leg end hits the ground with nonzero velocity there exist small impact losses that we ignore. Finally, condition 12a guarantees that impact does not occur until $x = x_0$. Therefore, by conditions 7a-12a and the assumption of no-loss

impact, the impact surface and impact map on the zero dynamics are

$$\begin{aligned} \mathcal{S} \cap \mathcal{Z} &= \{(q, \dot{q}) | x = x_0\}, \\ (x^+, y^+) &= (-x_0, y_0), \\ (\dot{x}^+, \dot{y}^+) &= (\dot{x}^-, -\dot{y}^-), \end{aligned}$$

We note that the reason that sign of $\dot{y}$ is changed after impact is that for simplicity even after impact when the stance leg becomes the swing leg and vice versa, with appropriate swapping of coordinates, we assume that the right leg remains the stance leg. So $\dot{y} > 0$ means that the hip is moving away from the support point (this occurs before impact) and $\dot{y} < 0$ means that the hip is moving toward the support point (this occurs at the beginning of the step). Therefore, since there is no impact loss, $\dot{y}^+ = -\dot{y}^-$.

Next, we verify condition 3 of Definition V.2. By definition of the symmetry map and the virtual constraints, it immediately follows that the symmetry map on $\mathcal{Z}$ is

$$G_{\mathcal{Z}}(x, y, \dot{x}^-, \dot{y}^-) = (-x, y, \dot{x}^-, -\dot{y}^-).$$

From this equation and the transition map on the HZD, $\Delta_{\mathcal{Z}}(x_0, y_0, \dot{x}^-, \dot{y}^-) = G_{\mathcal{Z}}(x_0, y_0, \dot{x}^-, \dot{y}^-)$, which means that $\Delta_{\mathcal{Z}} = G_{\mathcal{Z}}$ on $S \cap \mathcal{Z}$. Therefore, by Proposition II.10, we conclude that Condition 3 of Definition V.2 is also satisfied. Thus h satisfying conditions 1-12 defines SVCs for the 8-DOF 3D biped.

Remark V.7. The SVCs satisfying conditions 7a-12a have a disadvantage; namely, the impact occurs when $x = x_0$ with no dependence on y. As we will discuss the notion of synchronization in Section 6.2 (and as discussed in Corollary 3), such impact surface will not lead to self-synchronization of periodic orbits. In Case B, assuming a trivial impact map, the SVCs are chosen such that this issue is resolved.

5.3.2 SVCs for the 8-DOF 3D Biped: Case B

With $\zeta = l^{st} = h_3(x)$ and $\xi = l^{sw} = h_6(x)$, we impose the following conditions. For some $x_0, l_0 > 0$,

7b. $h_1(x_0) = 0$,

8b. $h_2(x_0) = 0$,

9b. $h_3(x_0) = l_0$ and $(\mathrm{d}h_3/\mathrm{d}x)(x_0) = 0$,

10b. $h_4(x_0) = x_0$ and $(\mathrm{d}h_4/\mathrm{d}x)(x_0) = 0$,

11b. $h_5(x_0) = y_0$ and $(\mathrm{d}h_5/\mathrm{d}x)(x_0) = 0$,

12b. $h_6(x_0) = l_0$, $(\mathrm{d}h_6/\mathrm{d}x)(x_0) = 0$, and for ground clearance, h_6 is chosen such that $z_f > 0$ when $h_6(x) \neq l_0$,

13b. $h(x) = h(x_0)$ for $x \geq x_0$.

With these constraints, the swing leg length h_6 starts from l_0 then retracts (for ground clearance) until it extends to l_0 again. Then, it remains at l_0 until impact occurs.

From 9b, 12b, and 13b, at impact, where $z_f = 0$, stance leg length and swing leg length are l_0, so $x^2 + y^2 + z^2 = l_0^2$ and $x_{hf}^2 + y_{hf}^2 + z_{hf}^2 = l_0^2$. Therefore, from these equations, noting that $z_{hf} = z_f - z$, at impact $z_{hf} = -z$. Thus, at impact,

$$x^2 + y^2 = x_{hf}^2 + y_{hf}^2.$$

Also, by 10b, 11b and 13b, at impact, $x_{hf} = x_0$ and $y_{hf} = y_0$; thus, from the equation above, the impact surface on the zero dynamics is

$$\mathcal{S} \cap \mathcal{Z} \;\; = \;\; \{(q, \dot{q}) | x^2 + y^2 = x_0^2 + y_0^2\}.$$

However, with assumptions 7b-13b the real impact map is no longer lossless; thus, with the real impact map the zero dynamics is not an SHS. To be able to still exploit

the properties of SHSs, we assume that there is no loss at the impact, and $\dot{x}^+ = \dot{x}^-$ and $\dot{y}^+ = -\dot{y}^-$. We refer to this impact map as the trivial impact map. With 7b-13b, and the assumption of lossless impact map, the transition map is

$$\begin{aligned} \mathcal{S} \cap \mathcal{Z} &= \{(q, \dot{q}) | x^2 + y^2 = x_0^2 + y_0^2\}, \\ (x^+, y^+) &= (-x_0, y_0), \\ (\dot{x}^+, \dot{y}^+) &= (\dot{x}^-, -\dot{y}^-). \end{aligned}$$

The assumption of the trivial map will be removed when we study stability of symmetric periodic orbits and their stabilization by introducing asymmetries in Chapter VI. Similar to Case A, with the above transition map, from the odd-even symmetries of the SVCs, the zero dynamics together with the trivial impact map becomes a $G_{\mathcal{Z}}$-SHS with

$$G_{\mathcal{Z}}(x, y, \dot{x}^-, \dot{y}^-) = (-x, y, \dot{x}^-, -\dot{y}^-).$$

Compared to Case A, the impact surface $\mathcal{S} \cap \mathcal{Z}$ depends on y as well as x. As we will see in Section 6.2, this impact surface can lead to self-synchronization of the periodic orbits and in general is easier to stabilize compared to Case A.

5.4 Symmetric Bézier Polynomials

In this section, first we briefly discuss the Bézier Polynomials in general and their application in generating virtual constraints. Then, we will discuss the notion of Symmetric Bézier Polynomials for generating SVCs.

As noted in (*Westervelt et al.*, 2007), a one-dimensional Bézier polynomial of

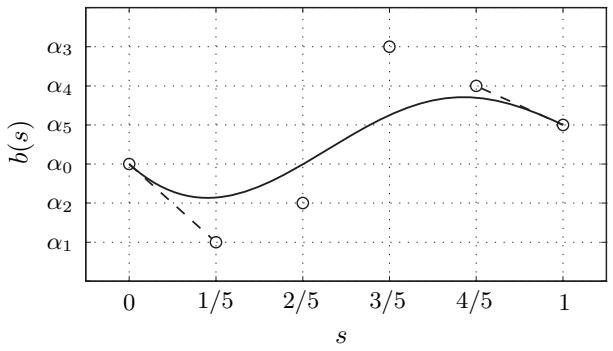

Figure 5.4: (figure and caption from (*Westervelt et al.*, 2007)) An example of a Bézier degree five ($M = 5$) polynomial curve. Note that (i) the curve is contained within the convex hull of the 6 coefficients (as viewed as points in R2, $\{(0, \alpha_0), (1/5, \alpha_1), ..., (1, \alpha_5)\}$), (ii) the curve begins at $(0; \alpha_0)$ and ends at $(1, \alpha_5)$, and (iii) the curve is tangent to the line segments connecting $(0, \alpha_0)$ and $(1/5, \alpha_1)$, and $(4/5, \alpha_4)$ and $(1, \alpha_5)$ at the start and end points, respectively.

degree M is a polynomial, $b : [0, 1] \to \mathbb{R}$, defined by $M + 1$ coefficients, α_k, per

$$b(s) = \sum_{k=0}^{M} \alpha_k \frac{M!}{k!(M-k)!} s^k (1-s)^{M-k}.$$

Bézier polynomials have very useful properties some of which are listed below (*Westervelt et al.*, 2007):

1. The graph of the Bézier polynomial is contained in the convex hull of the $M+1$ coefficients (as viewed in $\mathbb{R}^2$, $\{(0, \alpha_0), (1/M, \alpha_1), \cdots (1, \alpha_M)\}$).

2. $b(0) = \alpha_0$ and $b(1) = \alpha_M$.

3. The line segment that connects $(0, \alpha_0)$ to $(1/M, \alpha_1)$, and the line segment that connects $((M-1)/M, \alpha_{M-1})$ to $(1, \alpha_M)$ are tangent to the polynomial at $s = 0$ and $s = 1$, respectively. That is, $b'(0) = M(\alpha_1 - \alpha_0), b'(1) = M(\alpha_M - \alpha_{M-1})$ (see Fig. 5.4).

For later use, if $b(s)$ is a Bézier polynomial defined on $[0, 1]$, we define the shifted Bézier polynomial on the interval $[-1/2, 1/2]$ by $\hat{b}(s) = b(s + 1/2)$; thus,

$$\hat{b}(s) = \sum_{k=0}^{M} \alpha_k \frac{M!}{k!(M-k)!}(s+1/2)^k(1/2-s)^{M-k}.$$

Hereafter, we only shall work with shifted Bézier polynomials; thus, we denote a shifted Bézier polynomial simply by $b(s)$ instead of $\hat{b}(s)$.

A *Symmetric Bézier Polynomial (SBP)* is a Bézier polynomial defined on $[-1/2, 1/2]$ that is either an odd or an even function. A Bézier polynomial of degree M with coefficients α_k is **even** if

$$\alpha_k = \alpha_{M-k},$$

and is **odd** if

$$\alpha_k = -\alpha_{M-k},$$

for $k = 0, 1, \ldots, M$. Fig. 5.5 shows examples of SBPs.

In the following, we present a numerical examples to show how SBPs can be used to generate symmetric periodic orbits of legged robots.

Example V.8. (**SBPs to Generate Symmetric Periodic Walking for the Symmetric 5-DOF 2D Biped**)

In section 5.2, a symmetric 5-DOF 2D biped was introduced and in Proposition V.4 the conditions on SVCs for this biped were given so that the resulting HZD becomes an SHS. Hence, it has symmetric periodic orbits that can be identified easily (i.e., without any searches). In this section, we present a numerical example to show how SBPs can be used to obtain symmetric periodic orbits for the 5-DOF 2D biped. The numerical values of the masses and dimensions of the biped match those of MARLO (*Buss et al.*, 2014).

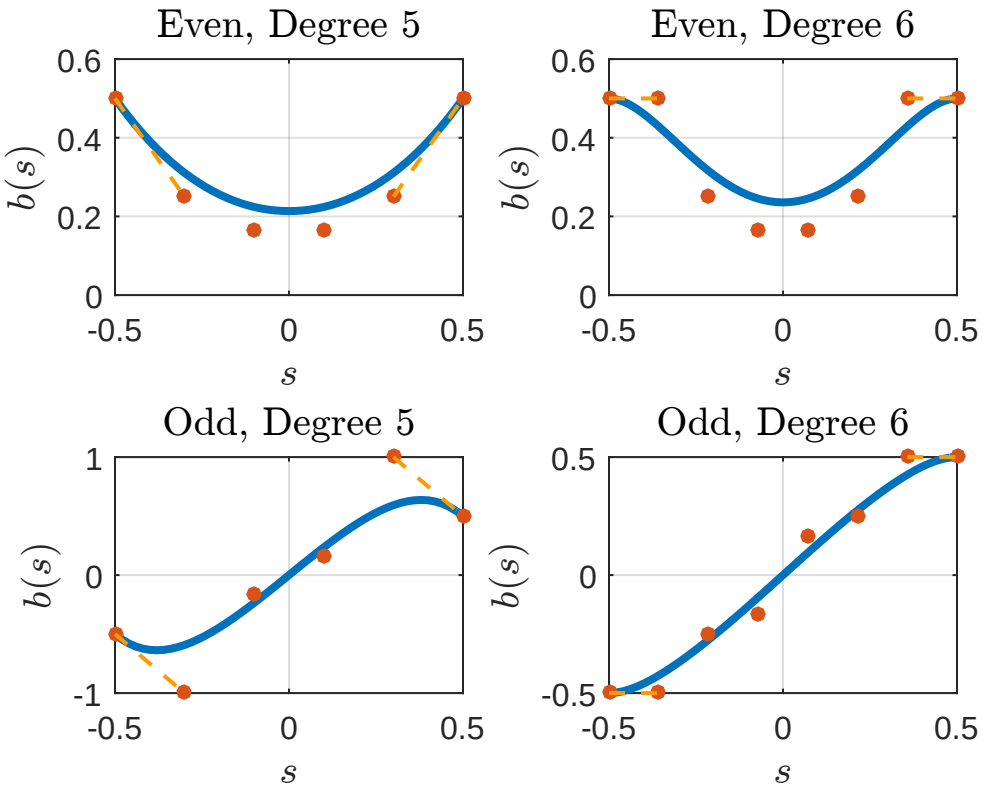

Figure 5.5: Examples of SBPs.

According to Proposition V.4, we need $z = h_1(x)$ to be an even function for which $\mathrm{d}h_1/\mathrm{d}x = 0$ when $x = x_0$. Since in SBPs, $s \in [-1/2, 1/2]$, given x, we define $s = x/(2x_0)$ which will be in $[-1/2, 1/2]$ as x varies in $[-x_0, x_0]$. With this definition of s, conditions of Proposition V.4 as a function of s are as follows:

1. $z = h_1(s), h_1(-s) = h_1(s), (\mathrm{d}h_1/\mathrm{d}s)|_{s=1/2} = 0,$
2. $\theta_p = h_2(s), h_2(-s) = -h_2(s), h_2(1/2) = 0,$
3. $x_{hf} = h_3(s), h_3(-s) = -h_3(s), h_3(1/2) = x_0, (\mathrm{d}h_3/\mathrm{d}s)|_{s=1/2} = -2x_0,$
4. $z_f = h_4(s), h_4(-s) = h_4(s), h_4(1/2) = 0, (\mathrm{d}h_4/\mathrm{d}s)|_{s=1/2} = 0,$
5. $h_4(s) > 0$ if $s \in (-1/2, 1/2)$.

We show how an SBP can be used for h_1 such that h_1 satisfies condition 1. SBPs for other h_is can be determined similarly. Based on the discussion in Section 5.4, for h_1, we can use an even SBP of degree $M_1 = 5$ with coefficients:

$$\boldsymbol{\alpha}_1 = [\alpha_1, \alpha_1, \alpha_3, \alpha_1, \alpha_1].$$

Note that since $\boldsymbol{\alpha}_1(1) = \boldsymbol{\alpha}_1(2)$ and $\boldsymbol{\alpha}_1(3) = \boldsymbol{\alpha}_1(4)$ by the third property of Bézier Polynomials in Section 5.4, we necessarily have $\mathrm{d}h_1/\mathrm{d}s = 0$ at $s = 1/2$, which based on the discussion in Section 5.4 guarantees that h_1 is an even function and $\mathrm{d}h_1/\mathrm{d}s = 0$ at $s = 1/2$.

Fig. 5.6 shows a few numerical examples of SBPs for h_is that satisfy conditions 1-5. Fig. 5.7 shows three different symmetric periodic solutions (out of infinitely many of them) on the HZD of the 5-DOF biped for a given set of SVCs. In these simulations, the torque limits of the MARLO are respected.

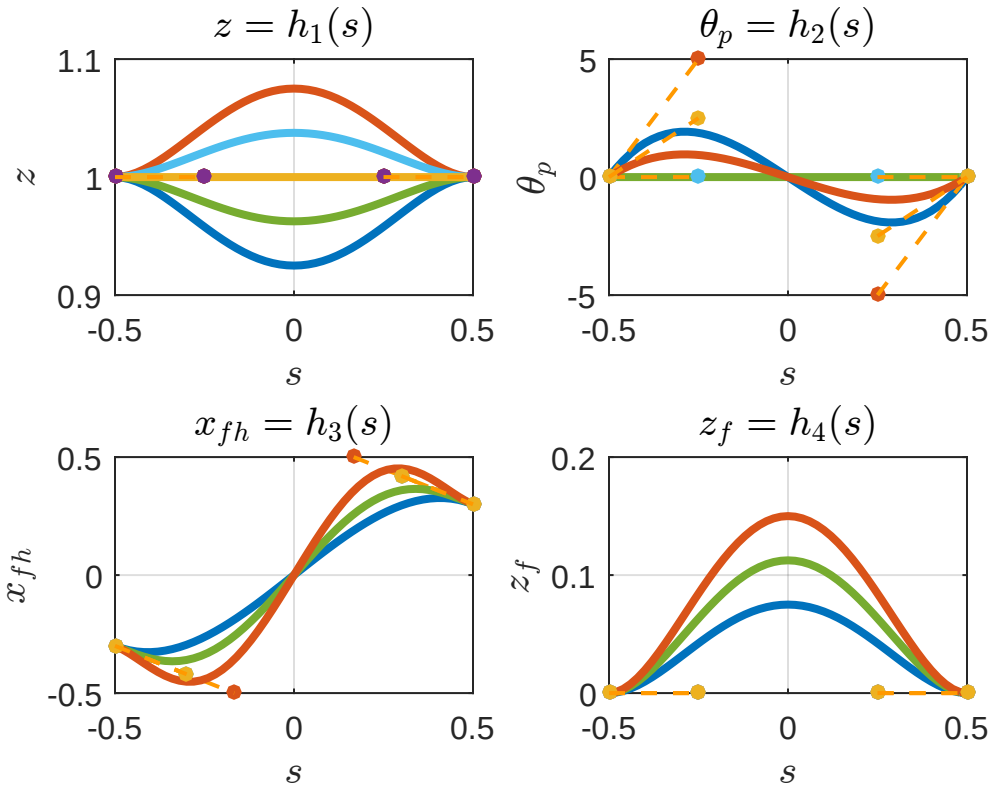

Figure 5.6: Examples of SBPs for the 5-DOF 2D Biped Satisfying Conditions 1-5.

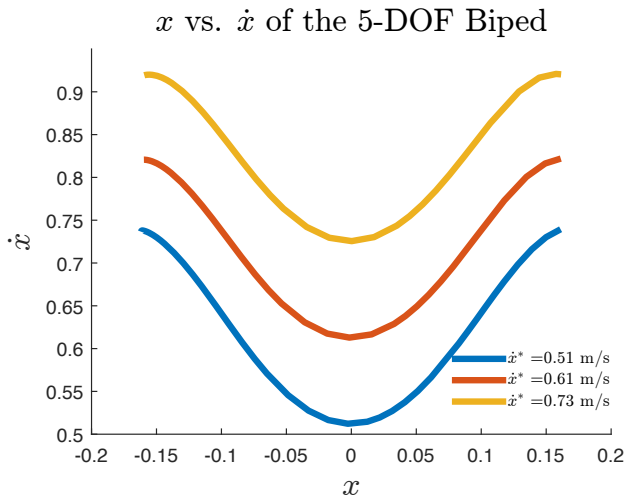

Figure 5.7: Multiple symmetric periodic orbits of the 5-DOF biped for a set of SVCs. The impact map sends the end point of these symmetric solutions to the starting points making them periodic orbits.

CHAPTER VI

Stability of Symmetric Periodic Orbits and the Notion of Synchronization

In Chapter II the notion of SHS was introduced, and it was shown that an SHS can have as many symmetric periodic orbits as the fixed points of the symmetry map. In this chapter, we study the stability of such periodic orbits. In particular, it is shown that symmetric periodic orbits at best are neutrally stable. However, we show that by appropriate introduction of asymmetries to an SHS, neutrally stable symmetric periodic orbits turn into a stable limit cycle. In the case of legged robots, these asymmetries are either so-called energy injecting or energy dissipating asymmetries. Many numerical examples are presented to show how adding such asymmetries can lead to stable limit cycle walking of legged robots. Moreover, we present a simple foot placement algorithm which can render unstable or neutrally stable symmetric periodic orbits of an SHS stable.

6.1 Stability Analysis of Symmetric Periodic Orbits

For stability analysis of the periodic orbits of a hybrid system we use the method of Poincaré sections[1].

[1]For a detailed discussion on the method of Poincaré sections for stability analysis of the periodic orbits of a hybrid system see (*Westervelt et al.*, 2007).

Let $\Sigma = (X, \Delta, \mathcal{X}, \mathcal{S})$ be a G-SHS for a symmetry map $G : \mathcal{X} \to \mathcal{X}$. Let x^* be a fixed point of G. By Proposition II.3, the solution $x_s(t)$ of Σ that starts from x^*, is symmetric, that is,

$$G(x_s(t)) = x_s(-t).$$

Moreover, by Proposition II.13, if $x_s(t)$ crosses the switching surface at $t_I > 0$, where

$$t_I = \inf\{t > 0 | x_s(t) \in \mathcal{S}\},$$

then $x_s(t)$ is a symmetric periodic solution of Σ with period $T = 2t_I$.

Let P denote the Poincaré map corresponding to $x_s(t)$ defined on a hyperplane[2] including x^*. Since $x_s(t)$ is periodic and $x_s(0) = x^*$, $P(x^*) = x^*$. The Poincaré criterion states that $x_s(t)$ is asymptotically stable if the discrete system $x_{n+1} = P(x_n)$ is asymptotically stable at x^*; equivalently, if the eigenvalues of the Jacobian of P, denoted by $\mathrm{d}P$, lie within the unit circle, then $x_s(t)$ is asymptotically stable.

Let $G : \mathcal{X} \to \mathcal{X}$ be a symmetry map for an SHS $\Sigma = (X, \Delta, \mathcal{X}, \mathcal{S})$. A fixed point x^* of G is said to be feasible if the solution starting from x^* is feasible (see Definition II.8). Denote the set of feasible fixed points of a G by S_G, that is,

$$S_G = \{x \in \mathcal{X} | G(x) = x, \text{ and } x \text{ is feasible}\}.$$

For the rest of this chapter, we assume that S_G is an embedded submanifold of $\mathcal{X}$ with a constant dimension. For instance, in Example II.11, where $\mathcal{X} = \mathbb{R}^2$ and $G(x_1, x_2) = (-x_1, x_2)$, $S_G = \{(0, x_2) | x_2 \in \mathbb{R}\}$, which is a one-dimensional submanifold of $\mathbb{R}^2$.

Lemma VI.1. *If $x_s(t)$ is a symmetric solution of a G-SHS Σ starting from x^* and*

[2] An embedded submanifold with co-dimension one.

crossing the switching surface at $t_I > 0$*, where* $t_I = \inf\{t > 0 | x_s(t) \in \mathcal{S}\}$*, then* $\dot{x}_s(0) \neq 0$*. Moreover, there exists a hypersurface* $\mathcal{S}_{x^*}$ *at* x^* *to which* $x_s(t)$ *is transversal and* $T_{x^*} S_G \subset T_{x^*} \mathcal{S}_{x^*}$*.*

Proof. The proof is given in the appendix. □

Proposition VI.2. *Suppose that the periodic solution* $x_s(t)$ *of the G-SHS* Σ *crosses the switching surface transversally*[3]*. Assuming that* $\dim(S_G) < \dim(\mathcal{X})$*, the Jacobian of the Poincaré map* P *associated with* $x_s(t)$ *has unit eigenvalues at least as many as* $\dim(S_G)$*. Moreover, the Jacobian of* P*, denoted by* $\mathrm{d}P$ *can be written in the form*

$$\mathrm{d}P = \begin{bmatrix} 1 & 0 & 0 & \cdots & 0 & \mathrm{d}P_{1,k+1} & \cdots & \mathrm{d}P_{1,n} \\ 0 & 1 & 0 & \cdots & 0 & \mathrm{d}P_{2,k+1} & \cdots & \mathrm{d}P_{2,n} \\ 0 & 0 & 1 & \cdots & 0 & \mathrm{d}P_{3,k+1} & \cdots & \mathrm{d}P_{3,n} \\ \vdots & \vdots & \vdots & \cdots & \vdots & \vdots & \cdots & \vdots \\ 0 & 0 & 0 & \cdots & 1 & \mathrm{d}P_{n,k+1} & \cdots & \mathrm{d}P_{n,n} \end{bmatrix}, \tag{6.1}$$

where $k = \dim(S_G)$.

Proof. First, note that since S_G is an embedded submanifold of $\mathcal{X}$, there exists a coordinate system (ξ, η) of $\mathcal{X}$ defined on an open neigborhood $\mathcal{O}$ of x^* such that $\xi = (\xi_1, \xi_2, \ldots, \xi_k)$ is a coordinate system of S_G, where $k = \dim(S_G)$. By Lemma VI.1, there exists a hypersurface $\mathcal{S}_{x^*}$ at x^* which is transverse to $x_s(t)$ at $t = 0$, and $T_{x^*} S_G \subset T_{x^*} \mathcal{S}_{x^*}$. Since $x_s(t)$ crosses the switching surface $\mathcal{S}$ transversally, there exists an open neigborhood $\mathcal{N} \subset \mathcal{X}$ of x^* such that every solution $x_s(t)$ starting from $\mathcal{N}$ crosses $\mathcal{S}$. Hence, the Poincaré map of $x_s(t)$ is well-defined. For simplicity, without loss of generality, we assume that $S_{x^*} \subset \mathcal{N} \subset \mathcal{O}$. Let P be the Poincaré map defined on $\mathcal{S}_{x^*}$. We show that the Jacobian of P at x^*, denoted by $\mathrm{d}P(x^*)$, has at least as many unit eigenvalues as $k = \dim(S_G)$. Let $P = [P_1; P_2; \ldots; P_n]$ in the

[3]That is if $x_I = x_s(t_I) \in \mathcal{S}$, then $\dot{x}_s(t_I) \notin T_{x_I} \mathcal{S}$. In other words, $x_s(t)$ does not "bounce off" the surface $\mathcal{S}$.

coordinate system (ξ, η), where $n = \dim \mathcal{X}$. By definition of the coordinate system (ξ, η), since $x^* \in S_G$, x^* can be written in the form $x^* = (\xi_1^*, \ldots, \xi_k^*, 0, \ldots, 0)$. Because $(\xi, 0) \in S_G \cap \mathcal{O}$, every solution starting from $(\xi, 0)$ crosses the switching surface and by Proposition II.13 is a periodic orbit. Therefore, we conclude that $P(\xi, 0) = \xi$. Thus, if $\mathrm{d}P_{ij}(x^*)$ is the ijth component of the matrix $\mathrm{d}P(x^*)$, then

$$\begin{aligned} \mathrm{d}P_{11}(x^*) &= \lim_{\epsilon=0} \frac{P_1(\xi_1^* + \epsilon, \xi_2^*, \ldots, \xi_k^*, 0, \ldots, 0) - P_1(x^*)}{\epsilon} \\ &= \lim_{\epsilon=0} \frac{(\xi_1^* + \epsilon) - \xi_1^*}{\epsilon} \\ &= 1. \end{aligned}$$

Also,

$$\begin{aligned} \mathrm{d}P_{21}(x^*) &= \lim_{\epsilon=0} \frac{P_2(\xi_1^* + \epsilon, \xi_2^*, \ldots, \xi_k^*, 0, \ldots, 0) - P_2(x^*)}{\epsilon} \\ &= \lim_{\epsilon=0} \frac{\xi_2^* - \xi_2^*}{\epsilon} \\ &= 0. \end{aligned}$$

Similarly, $\mathrm{d}P_{ij} = \delta_{ij}$ for $i = 1, \ldots, n$ and $j = 1, \ldots, k$, where $\delta_{ij} = 1$ if $i = j$ and $\delta_{ij} = 0$ if $i \neq j$. This proves that $\mathrm{d}P$ is in the form (6.1); and, hence, has at least k unit eigenvalues. □

Intuitively, the above proposition states that there are many directions (as many as $\dim(S_G)$) in which one can move infinitesimally from one symmetric solution to another one. Consequently, the symmetric periodic orbits are not isolated.

In general, in a hybrid system $\Sigma = (X, \Delta, \mathcal{X}, \mathcal{S})$, Δ which maps $\mathcal{S}$ to $\Delta(\mathcal{S})$ might have a smaller rank than $\dim(\mathcal{S}) = n - 1$ in which case the following proposition will be helpful.

Proposition VI.3. *Suppose that $x_s(t)$ is a periodic solution of the n-dimensional hybrid system $\Sigma = (X, \Delta, \mathcal{X}, \mathcal{S})$, and let P be a Poincaré map corresponding to $x_s(t)$.*

If Δ has a constant rank r, then $\mathrm{d}P$ *has at least* $n-r-1$ *zero eigenvalues.*

Proof. Let P be a Poincaré map defined at the switching surface, that is, $P : \mathcal{S} \to \mathcal{S}$. Let $\phi(t,x)$ be the flow map and $T_I : \mathcal{X} \to \mathbb{R} \cup \{\infty\}$ be the time-to-impact function defined as follows (*Grizzle et al.*, 2001):

$$T_I(x_0) = \begin{cases} \inf\{t \geq 0 | \phi(t,x_0) \in \mathcal{S}\} & \text{if } \exists\ t \text{ such that } \phi(t,x_0) \in \mathcal{S}, \\ \infty. \end{cases}$$

Define the function $H : \Delta(\mathcal{S}) \to \mathcal{S}$ by $H(x) = \phi(T_I(x), x)$. With this definition $P(x) = H(\Delta(x))$, hence, $\mathrm{d}P = \mathrm{d}H \cdot \mathrm{d}\Delta$. Consequently, $\mathrm{rank}(\mathrm{d}P) \leq \mathrm{rank}(\Delta) = r$. As a result, since $\dim(\mathcal{S}) = n-1$ (note that $\mathcal{S}$ by definition has co-dimension one) $\mathrm{d}P$ has at least $(n-1)-r$ zero eigenvalues. □

Example VI.4. In the 3D LIP biped, as noted in (3.7), $\Delta(x, y, \dot{x}, \dot{y}) = (-x_0, y_0, \dot{x}^-, \dot{y}^-)$. Therefore, noting that x_0 and y_0 are constant, $\mathrm{rank}(\Delta) = 2$. On the other hand, $n = 4$ (note that 3D LIP has two degrees of freedom and is a second order system). Consequently, $\mathrm{d}P$ has at least one zero eigenvalue.

Example VI.5. (**Stability Analysis of the 3D LIP Symmetric Periodic Orbits**) In Chapter III, it was shown that the 3D LIP biped is an SHS with the following equations:

$$\begin{aligned} \ddot{x} &= \omega^2 x, \\ \ddot{y} &= \omega^2 y, \\ (x^+, y^+) &= (-x_0, y_0), \\ (\dot{x}^+, \dot{y}^+) &= (\dot{x}^-, -\dot{y}^-), \\ \mathcal{S} &= \{(x, y, \dot{x}, \dot{y}) | x^2 + y^2 = x_0^2 + y_0^2\}, \end{aligned}$$

which is a 4-dimensional G-SHS with $G : (x, y, \dot{x}, \dot{y}) \mapsto (-x, y, \dot{x}, -\dot{y})$. The fixed points of this symmetry map are in the form $(0, y^*, \dot{x}^*, 0)$ for any $y^* \in \mathbb{R}$ and $\dot{x}^* \in \mathbb{R}$;

thus, the space of fixed points of G is 2-dimensional. However, not all of these fixed points are feasible; in fact, only the ones starting from $x = -x_0$, $y = y_0$ are feasible, which makes the space of feasible fixed points of G, S_G, one-dimensional[4]. Therefore, by Proposition VI.2 the Jacobian of Poincré map, $\mathrm{d}P$, of a symmetric periodic orbit of this SHS is in the form:

$$\mathrm{d}P = \begin{bmatrix} 1 & \star & \star \\ 0 & \star & \star \\ 0 & \star & \star \end{bmatrix}.$$

On the other hand, as noted in Example VI.4, $\mathrm{d}P$ has at least one zero eigenvalue. Thus, with a proper choice of coordinates, $\mathrm{d}P$ can be written in the form

$$\mathrm{d}P = \begin{bmatrix} 1 & \star & 0 \\ 0 & \star & 0 \\ 0 & \star & 0 \end{bmatrix}.$$

Therefore, eigenvalues of $\mathrm{d}P$ are $\{1, \lambda, 0\}$ for some $\lambda \in \mathbb{R}$. If P_r is the restriction of the Poincaré map to $\Delta(S)$, which has a dimension 2, then

$$\mathrm{d}P_r = \begin{bmatrix} 1 & \star \\ 0 & \lambda \end{bmatrix}.$$

Therefore, if $|\lambda| < 1$ the symmetric periodic orbit is neutrally (marginally) stable. In the next section, we will show that for the 3D LIP, λ represents how well the motion in the x-direction will be coordinated with the motion in the y-direction.

[4]This will be shown in Section 6.2.

6.2 Synchronization

The symmetric HZD of many examples of 3D legged robots are second order hybrid systems of dimension two which can be described by the (x, y) position of the hip of COM (see Section VI.5 and all 3D examples in Chapter III). The general form of such symmetric HZD is

$$\ddot{x} = f(x, y, \dot{x}, \dot{y}),$$
$$\ddot{y} = g(x, y, \dot{x}, \dot{y}),$$

such that

$$\begin{aligned} f(-x, y, \dot{x}, -\dot{y}) &= -f(x, y, \dot{x}, \dot{y}), \\ g(-x, y, \dot{x}, -\dot{y}) &= g(x, y, \dot{x}, \dot{y}), \end{aligned}$$

with the impact surface $\mathcal{S} = \{(x, y, \dot{x}, \dot{y}) | x^2 + y^2 = x_0^2 + y_0^2\}$ for some $x_0, y_0 > 0$ and

$$\Delta(x^-, y^-, \dot{x}^-, \dot{y}^-) = (-x_0, y_0, \dot{x}^-, -\dot{y}^-).$$

Writing this HZD in the from $\dot{\zeta} = X(\zeta)$, it is easy to check that this hybrid system is a G-SHS with $G : (x, y, \dot{x}, \dot{y}) \mapsto (-x, y, \dot{x}, -\dot{y})$. Since (x^+, y^+) is fixed to $(-x_0, y_0)$, in the following, this G-SHS is referred to as (x_0, y_0)-invariant (to imply invariance of (x^+, y^+)).

Below, we discuss the 3D LIP as an example of such G-SHS through which we introduce the notion of self-synchronization.

Example VI.6. (3D LIP Self-Synchronization) The equations of motion of the 3D LIP biped in the continuous phase of motion are

$$\ddot{x} = \omega^2 x, \;\; \ddot{y} = \omega^2 y, \tag{6.2}$$

where the symmetry map is $G(x, y, \dot{x}, \dot{y}) = (-x, y, \dot{x}, -\dot{y})$. With the initial conditions

$$x(0) = -x_0,\ y(0) = y_0,\ \dot{x}(0) = \dot{x}_0,\ \dot{y}(0) = \dot{y}_0, \tag{6.3}$$

the solution of system (6.2) is

$$x(t) = -x_0 \cosh(\omega t) + \frac{\dot{x}_0}{\omega} \sinh(\omega t), \tag{6.4}$$

$$y(t) = y_0 \cosh(\omega t) + \frac{\dot{y}_0}{\omega} \sinh(\omega t). \tag{6.5}$$

We want to find $(\dot{x}_0, \dot{y}_0)$ such that the solution that starts from $(-x_0, y_0)$ is symmetric (a.k.a. synchronized). Such a solution passes through one of the fixed points of G, which are in the from $(x^*, y^*, \dot{x}^*, \dot{y}^*) = (0, y^*, \dot{x}^*, 0)$. That is, when $x(t) = 0$, we should have $\dot{y}(t) = 0$. Therefore, if we set the derivative of the derivative of the second equation above to zero, we find the time, t_y, that it takes for $\dot{y}$ to become zero:

$$\tanh(\omega t_y) = -\frac{\dot{y}_0}{y_0 \omega}. \tag{6.6}$$

Similarly, from equation (6.4), the time t_x at which $x = 0$ is found from the following equation:

$$\tanh(\omega t_x) = \frac{x_0 \omega}{\dot{x}_0}. \tag{6.7}$$

In order for the solution to be synchronized t_x must be equal to t_y. Therefore, from equations (6.6) and (6.7), this solution is synchronized if and only if

$$\dot{x}_0 \dot{y}_0 + \omega^2 x_0 y_0 = 0.$$

Thus, if we define $L : \mathcal{T}_{(-x_0,y_0)}\mathcal{Q} \to \mathbb{R}$ by

$$L(\dot{x}_0, \dot{y}_0) = \dot{x}_0\dot{y}_0 + \omega^2 x_0 y_0, \tag{6.8}$$

the solution starting from $(-x_0, y_0)$ with initial velocity $(\dot{x}_0, \dot{y}_0)$ is synchronized if $L(\dot{x}_0, \dot{y}_0) = 0$.

Function L defined in equation (6.8) is called the *synchronization measure* of the (x_0, y_0)-invariant 3D LIP. In fact, $L(\dot{x}_0, \dot{y}_0) = 0$ defines a one-dimensional submanifold, $\mathcal{K}$, of $\mathcal{T}_{(-x_0,y_0)}\mathcal{Q}$; any solution starting from this submanifold is synchronized and leads to periodic motion.

By Proposition 1 in the appendix, for a general 2-dimensional (x_0, y_0)-invariant second order SHS, under some conditions, there exists a function $L : \mathcal{T}_{(-x_0,y_0)}\mathcal{Q} \to \mathbb{R}$ with rank 1 such that if $L(\dot{x}_0, \dot{y}_0) = 0$, then the solution starting from $(-x_0, y_0)$ with initial velocity $(\dot{y}_0, \dot{y}_0)$ is synchronized. Function L is called the *synchronization measure* of the (x_0, y_0)-invariant SHS. If

$$\mathcal{K} = \{(q, \dot{q}) \in \mathcal{T}_{(-x_0,y_0)}\mathcal{Q} | L(\dot{q}) = 0\},$$

then $\mathcal{K}$ is a one-dimensional submanifold of $\mathcal{T}_{(-x_0,y_0)}\mathcal{Q}$ and is called the *synchronization submanifold* of the SHS at $(-x_0, y_0)$. Any solution starting from the synchronization manifold is synchronized. Since $\mathcal{K}$ is an embedded submanifold of $\mathcal{T}_{(-x_0,y_0)}\mathcal{Q}$, we can define a local coordinate system (K, L) such that $(K, 0)$ is a local coordinate system on $\mathcal{K}$. Hereafter, we assume that such a coordinate system exists.

Corresponding to a 2-dimensional (x_0, y_0)-invariant second order SHS, there exists an 2-dimensional restricted Poincaré map $P : \mathcal{T}_{(-x_0,y_0)}\mathcal{Q} \to \mathcal{T}_{(-x_0,y_0)}\mathcal{Q}$ that maps $(\dot{x}, \dot{y})$ at the beginning of a step to its value at the beginning of the next step. In the coordinate system (K, L), P is denoted by (P_K, P_L).

If $L = 0$, the solution is symmetric; therefore, in the coordinate system (K, L), P

has fixed points of the form $(K_*, 0)$ for some $K_* \in \mathbb{R}$. In the following proposition, a general form for the Jacobian of P at $(K_*, 0)$ is derived.

Proposition VI.7. *Let $P : \mathcal{T}_{(-x_0,y_0)}\mathcal{Q} \to \mathcal{T}_{(-x_0,y_0)}\mathcal{Q}$ denote the restricted Poincaré map corresponding to an $(x_0, y_0)-$invariant SHS. Let $(K_*, 0)$ be a fixed point of P. In the coordinate system (K, L) of $\mathcal{T}_{(-x_0,y_0)}\mathcal{Q}$, we have*

$$DP(K_*, 0) = \begin{pmatrix} 1 & \partial P_K/\partial L(K_*, 0) \\ 0 & \partial P_L/\partial L(K_*, 0) \end{pmatrix}. \tag{6.9}$$

Proof. By definition of Jacobian,

$$\begin{aligned} DP_{2,1}(K_*, 0) &= \tfrac{\partial P_L}{\partial K}(K_*, 0) \\ &= \lim_{\delta K_0 \to 0} \tfrac{P_L(K_* + \delta K_0, 0) - P_L(K_*, 0)}{\delta K_0}. \end{aligned}$$

However, for small enough δK_0, when $L = 0$ the solution is periodic; therefore,

$$P_L(K_* + \delta K_0, 0) = 0,\ P_L(K_*, 0) = 0.$$

From the above equation for $DP_{1,1}(K_*, 0)$, we have

$$DP_{2,1}(K_*, 0) = 0,$$

as desired. Similarly,

$$P_K(K_* + \delta K_0, 0) = K_* + \delta K_0,\ P_K(K_*, 0) = K_*.$$

Therefore,

$$\begin{aligned} DP_{1,1}(K_*, 0) &= \tfrac{\partial P_K}{\partial K}(K_*, 0) \\ &= \lim_{\delta K_0 \to 0} \tfrac{P_K(K_* + \delta K_0, 0) - P_K(0, K_*)}{\delta K_0} \\ &= \lim_{\delta K_0 \to 0} \tfrac{K_* + \delta K_0 - K_*}{\delta K_0} \\ &= 1. \end{aligned}$$

Thus, the first column of the matrix $DP(K_*, 0)$ is $[1, 0]^T$ as desired. □

Equation (6.9), as expected, is consistent with Proposition VI.2 and shows that the Jacobian of the restricted Poincaré map P at $(K_*, 0)$ necessarily has an eigenvalue of 1.

In (6.9), letting $\lambda = \partial P_L / \partial L(K_*, 0)$,

$$DP(K_*, 0) = \begin{pmatrix} 1 & \star \\ 0 & \lambda \end{pmatrix}. \tag{6.10}$$

Thus, the eigenvalues of $DP(K_*, 0)$ are $\{\lambda, 1\}$ with $\lambda = \partial P_L / \partial L(K_*, 0)$. In general, even for 2-dimensional SHSs, we cannot find a closed-form formula for λ. However, in the 3D LIP, as the following proposition states, we can find a closed-form formula for λ (see (*Razavi et al.*, 2015)).

Proposition VI.8. *Suppose that a symmetric periodic orbit of an (x_0, y_0)-invariant 3D LIP biped model has velocities $\dot{x} = \dot{x}_0 > 0$ and $\dot{y} = \dot{y}_0 < 0$ when $x = -x_0$. Suppose that K_0 is the kinetic energy of the periodic orbit at $x = -x_0$ and $K_0 - \omega^2 x_0 y_0 > 0$. Then*

$$\lambda = -1 + \frac{2\omega^2(y_0^2 - x_0^2)}{\omega^2(y_0^2 - x_0^2) + 2\sqrt{K_0^2 - \omega^4 x_0^2 y_0^2}}. \tag{6.11}$$

According to equation (6.11) for the 3D LIP, $|\lambda| < 1$ if $y_0 > x_0$.

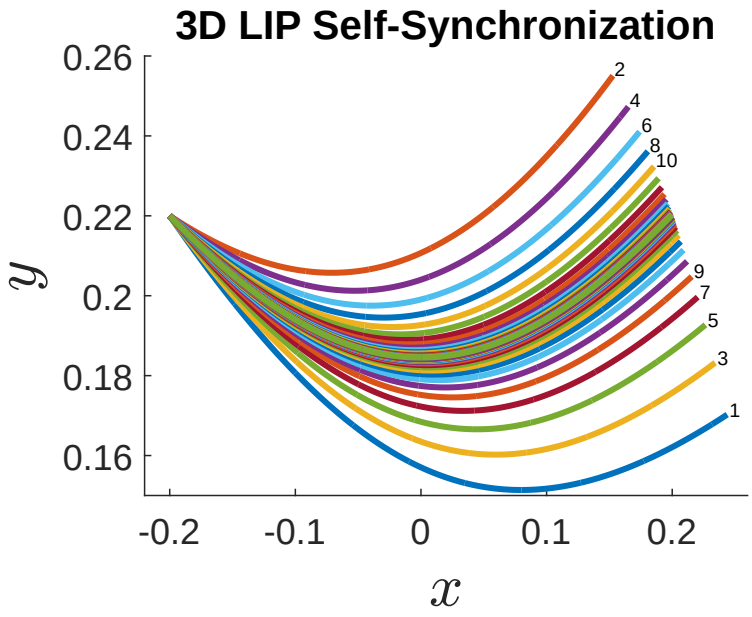

Figure 6.1: Self-synchronization of the 3D LIP for $x_0 = 0.2$ and $y_0 = 0.22$. The numbers on the graph refer to the step number.

Proposition 2 in the appendix generalizes this proposition to a class of switching surfaces. In particular, it is shown that by modifying the switching surface, $|\lambda|$ can become smaller than 1 for values of x_0 and y_0, where y_0 is not necessarily greater than x_0.

Definition VI.9. A periodic orbit of a 2-dimensional second order (x_0, y_0)-invariant SHS, with DP in the form (6.11), is said to be *self-synchronized* at K_* if $|\lambda| < 1$.

Fig. 6.2 shows a simulation of the 3D LIP, demonstrating its self-synchronization property under an (x_0, y_0)-invariant gait, where $x_0 = 0.2$ and $y_0 = 0.22$. In this simulation, the initial velocities $(\dot{x}_0, \dot{y}_0)$ are such that $L(\dot{x}_0, \dot{y}_0) \neq 0$, but eventually L converges to zero, and the solution approaches a symmetric periodic orbit.

Remark VI.10. In the case of a planar robot, if the zero dynamics is a one-dimensional second order system, with obvious modification of the proof of Proposition VI.7, it immediately follows that $DP(K_*) = 1$. That is, the only eigenvalue of the Jacobian of the Poincaré map associated with the symmetric periodic orbit is 1.

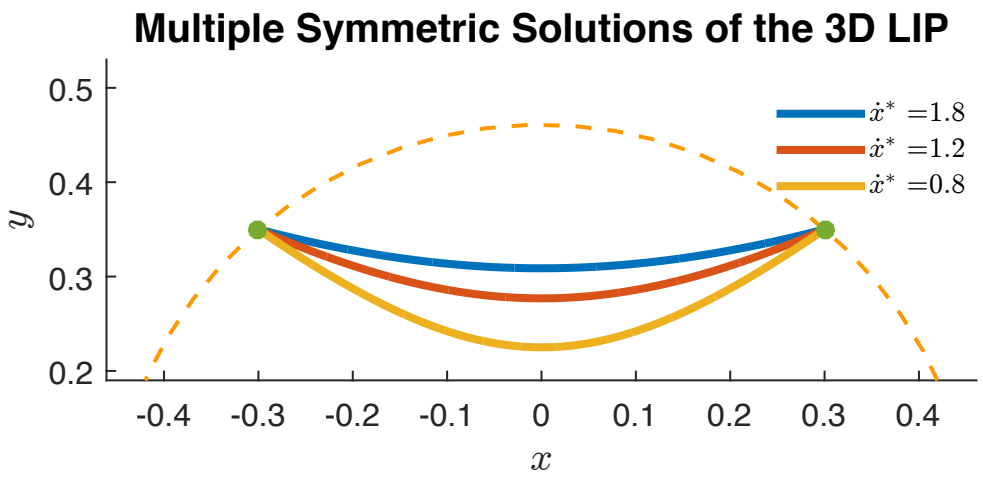

Figure 6.2: Multiple symmetric periodic solutions of the 3D LIP biped, where $\dot{x}^*$ is the time derivative of the solution at the mid-step. The top curve corresponds to a higher kinetic energy.

Remark VI.11. (Synchronization and Kinetic Energy) For the 3D LIP it was shown that the eigenvalues of the Poincaré map at the fixed points $(K_*, 0)$ are $\{\lambda, 1\}$, and if $|\lambda| < 1$, then the symmetric periodic orbits are self-synchronized. This means that the period of oscillations in the x direction eventually matches that in the y direction, and the 3D LIP biped follows a periodic orbit. The other eigenvalue, which is 1, corresponds to neutral stability in kinetic energy. That is, if a small perturbation is applied to the 3D LIP, it will still become synchronized but will eventually follow a periodic orbit with a different level of kinetic energy. For instance, Fig. 6.2 shows three periodic orbits of a 3D LIP with three different levels of kinetic energy. In Section 6.3, we illustrate how judiciously chosen asymmetries, such as loss of energy at impact in combination with energy gain over a step, can move the eigenvalues within the unit circle. With this approach, the stability problem in 3D legged locomotion is viewed as synchronization plus the convergence of the kinetic energy. Of course, in 2D legged locomotion, synchronization is not an issue.

6.3 Mechanisms of Stability

Based on the stability analysis in Section 6.1 and 6.2, a symmetric periodic orbit of an SHS is at best neutrally (marginally) stable. In this section, we discuss two methods for stabilization of symmetric periodic orbits of an SHS: (i) introducing asymmetries and (ii) foot placement.

Asymmetries include *energy injecting asymmetries* and *energy dissipating* asymmetries. As it will be discussed in Section 6.3.1, appropriate choice of such asymmetries will cause the neutrally stable symmetric periodic orbits of the SHS to converge to a single stable limit cycle. While introduction of energy injecting and energy dissipating asymmetries can asymptotically stabilize neutrally stable symmetric periodic orbits (i.e., the symmetric periodic orbits which are self-synchronized), for unstable symmetric periodic orbits, and in general, to increase the basin of attraction of the symmetric periodic orbits, foot placement is essential. In Section 6.3.2, we show that a simple foot placement strategy can render a symmetric periodic orbit asymptotically stable. In Chapter VII, symmetry method with introduction of asymmetries and foot placement is successfully tested on a 12-DOF 3D model of a humanoid.

6.3.1 Introducing Asymmetries

By introducing small asymmetries to an SHS, the system is no longer symmetric, but is close to an SHS. That is why according to the following definition we refer to such a system as a perturbed SHS.

Definition VI.12. *Let $\Sigma_\epsilon = (X_\epsilon, Q, \Delta_\epsilon, \mathcal{S})$ be a class of second order hybrid systems systems indexed by $\epsilon \in O \subset \mathbb{R}^k$ such that $\Sigma_s := \Sigma_0$ is an SHS, and O is an open set containing $\epsilon = 0$. Then Σ_ϵ is said to be a Perturbed Symmetric Hybrid System (PSHS) with perturbation ϵ.*

We assume that Σ_ϵ is smooth, that is, $X_\epsilon(x) = X(\epsilon, x)$ and $\Delta_\epsilon(x) = \Delta(\epsilon, x)$ for

some smooth functions X and Δ.

Below we present three examples to show how adding asymmetries, which according to the above definition are quantified by ϵ, can turn infinitely many periodic orbits of an SHS into an isolated stable limit cycle. If the asymmetries are appropriately introduced, for each set of asymmetries there is a stable limit cycle. Therefore, we end up having a family of stable limit cycles, which can be classified based on the amount of asymmetry. Moreover, by changing the asymmetries (for instance, the average pitch angle) during walking, the legged system can move from one periodic orbit to another. The effect of introducing asymmetries to symmetric walking gaits for a spring-leg biped is also studied in (*Merker et al.*, 2011) and (*Merker et al.*, 2015), and it is shown that an appropriate choice of asymmetries can result in stability.

6.3.1.1 Planar Examples

We first discuss planar examples in which clearly, synchronization is not relevant. Indeed, in 2D legged locomotion at a fixed point K_* as noted in Remark VI.10, $DP(K_*) = 1$; thus, the only eigenvalue of the Jacobian of the Poincaré map associated with a symmetric periodic orbit is 1. Consequently, the symmetric periodic orbits are neutrally stable. In the following examples, we show that with appropriate introduction of asymmetries, all symmetric periodic orbits turn into one single stable limit cycle.

Example VI.13. (2D LIP with External Force and Impact Loss) For the first example, we discuss a 2D LIP biped. As discussed in Example II.12, the 2D LIP biped is an SHS. In a 2D LIP, the synchronization measure L is always 0 simply because the problem is planar (thus, synchronization is not an issue). The equations of motion of an x_0-invariant 2D LIP are

$$\ddot{x} = \omega^2 x,$$

where $\omega^2 = g/M$ with M being the point mass, and

$$x^+ = -x_0,\ \dot{x}^+ = \dot{x}^-,$$

with the switching surface

$$\mathcal{S} = \{(x, \dot{x}) | x = x_0\},$$

for some $x_0 > 0$. The symmetry map for this SHS is $G : (x, \dot{x}) \mapsto (-x, \dot{x})$. By Proposition II.13, this SHS possesses infinitely many symmetric periodic orbits corresponding to fixed points of G which are in the form $(0, \dot{x}^*)$. Thus, for these periodic orbits, according to Proposition VI.7, the derivative of the Poincaré map is 1. We now add energy injecting and energy dissipating asymmetries and investigate the stability of the periodic orbits. The energy injecting asymmetry we add is a positive external force applied to mass M, and the energy dissipating asymmetry added is the kinetic energy loss at impact. We model such asymmetries as follows. In the continuous phase,

$$\ddot{x} = \omega^2 x + \frac{c_1}{M} F_0(x), \tag{6.12}$$

for a constant $c_1 > 0$ and a smooth function $F_0(x) > 0$, and in the discrete phase,

$$x^+ = -x_0,\ \dot{x}^+ = c_2 \dot{x}^-, \tag{6.13}$$

for a constant $0 < c_2 < 1$ with the switching surface

$$\mathcal{S} = \{(x, \dot{x}) | x = x_0\}.$$

Then the above hybrid system is an x_0-invariant PSHS with $\epsilon = (c_1, 1 - c_2)$. Since

the problem is planar, to study stability, all we need to check is whether the kinetic energy is stable, that is, if after adding the above asymmetries, the eigenvalue 1 moves within the unit circle. If we multiply both sides of equation (6.12) by $\dot{x}$ and integrate with respect to time from $t = 0$, where $x = -x_0$, to $t = T$, where $x = x_0$, we obtain

$$\int_0^T \ddot{x}\dot{x}dt = \omega^2 \int_0^T x\dot{x}dt + \int_0^T \frac{c_1}{M} F_0(x)\dot{x}dt.$$

From this equation,

$$\int_0^T \ddot{x}\dot{x}dt = \omega^2 \int_{-x_0}^{x_0} xdx + \int_{-x_0}^{x_0} \frac{c_1}{M} F_0(x)dx.$$

Simplifying this equation results in

$$\frac{1}{2}((\dot{x}^-)^2 - (\dot{x}^+)^2) = 0 + \frac{c_1}{M} W_0, \tag{6.14}$$

where

$$W_0 = \int_{-x_0}^{x_0} F_0(x)dx,$$

and $c_1 W_0$ is the work done by the external force $c_1 F_0(x)$ in one step. Since by assumption $F_0(x) > 0$, we have $W_0 > 0$. Moreover, from equation (6.14), we have

$$K_0^- - K_0^+ = c_1 W_0, \tag{6.15}$$

where K_0^+ is the kinetic energy at the beginning of the step and K_0^- is the kinetic energy at the end of the step. From equation (6.13), if K_1^+ is the kinetic energy at

the beginning of the next step, we have

$$K_1^+ = c_2^2 K_0^- .$$

Combining this equation with equation (6.15),

$$K_1^+ = c_2^2 K_0^+ + c_2^2 c_1 W_0. \tag{6.16}$$

This equation is, in fact, the equation for the Poincaré map in terms of kinetic energy. If we set $K_1^+ = K_0^+$, for $c = (c_1, c_2)$ we find the unique fixed point K_*^c of the Poincaré map of the PSHS:

$$K_*^c = \frac{c_2^2 c_1 W_0}{1 - c_2^2}. \tag{6.17}$$

From equation (6.16), the eigenvalue of the linearized Poincaré map is $\lambda = c_2^2$, which is clearly in the unit circle, since $0 < c_2 < 1$.

In the above example, before adding asymmetries, the Poincaré map has infinitely many fixed points that are neutrally stable; whereas after adding appropriate asymmetries, the system has one single asymptotically stable limit cycle. In fact, based on equation (6.17), each value of c_1 and c_2 results in a different limit cycle. That is, we obtain a family of stable limit cycles that can be indexed by (c_1, c_2).

We note that a general criterion for stability of hybrid systems with one degree of underactuation is given in (*Chevallereau et al.*, 2003), which for this example will yield the same results as above.

It is immediate to generalize the above example to the following proposition.

Proposition VI.14. *Consider the PSHS*

$$\ddot{x} = f_s(x) + c_1 F(x),$$

where $F(x)$ is a smooth function, $f_s(x)$ is a smooth odd function, and $c_1 > 0$, with the impact map

$$x^+ = -x_0,\ \dot{x}^+ = c_2\dot{x}^-,$$

and the switching surface

$$\mathcal{S} = \{(x, \dot{x}) | x = x_0\},$$

where $0 < c_2 < 1$. Let $W_0 = \int_{-x_0}^{x_0} F(x)dx$ and define $K = (1/2)\dot{x}^2$. If $W_0 > 0$, then the system has an asymptotically stable periodic orbit such that

$$K_* = \frac{c_2^2 c_1 W_0}{1 - c_2^2}$$

is a fixed point of the Poincaré map and

$$\lambda = c_2^2$$

is its derivative at K_*.

Example VI.15. (2D Inverted Pendulum on Slope) Another example in 2D that illustrates the introduction of asymmetries to an SHS is the IP biped on a slope, as described in Fig. 6.3. If we assume that the slope is zero and the impact map is trivial, that is, $\dot{\theta}^+ = \dot{\theta}^-$, the system is a G-SHS with $G : (\theta, \dot{\theta}) \mapsto (-\theta, \dot{\theta})$ and has infinitely many periodic orbits with neutrally stable kinetic energy. With slope $\alpha > 0$, which is acting as a perturbation to this SHS, the equation of motion in the continuous phase is

$$\ddot{\theta} = \omega^2 \cos(\alpha) \sin(\theta) + \omega^2 \sin(\alpha) \cos(\theta),$$

where $\omega^2 = g/l$. Using the conservation of angular momentum at impact, the impact map is found to be

$$\dot{\theta}^+ = \cos(2\theta_0)\dot{\theta}^-,$$

where $-\theta_0$ is the initial value of θ in each step. The step length will then be $d = 2l\sin(\theta_0)$. Using the terminology of Proposition VI.14, $f_s(\theta) = \omega^2\cos(\alpha)\sin(\theta)$, $F(\theta) = \cos(\theta)$, $c_1 = \omega^2\sin(\alpha)$ and $c_2 = \cos(2\theta_0)$. Therefore, the PSHS is described by the following equations:

$$\ddot{\theta} = f_s(\theta) + c_1 F(\theta), \tag{6.18}$$

where f_s is an odd function of θ, and

$$\theta^+ = -\theta_0,\ \dot{\theta}^+ = c_2\dot{\theta}^-. \tag{6.19}$$

Define

$$\begin{aligned} W_0 &= \int_{-\theta_0}^{\theta_0} f_a(\theta)d\theta \\ &= \omega^2\sin(\alpha)\int_{-\theta_0}^{\theta_0}\cos(\theta)d\theta \\ &= 2\omega^2\sin(\alpha)\sin(\theta_0). \end{aligned} \tag{6.20}$$

From Proposition VI.14, the fixed point of the Poincaré map in terms of $K = (1/2)\dot{\theta}^2$ is

$$K_* = \frac{2\omega^2\cos^2(2\theta_0)\sin(\theta_0)\sin(\alpha)}{1-\cos^2(2\theta_0)},$$

and the derivative of the Poincaré map at this point is $\lambda = \cos^2(2\theta_0)$, which has an absolute value of less than one for $0 < \theta_0 < \pi/4$; hence, the periodic orbit is stable.

We note that in contrast to the passive compass gait models such as (*Garcia et al.*, 1998) and (*Goswami et al.*, 1997), we assume that the initial configuration of the biped at the beginning of each step is fixed. This condition in an actual biped can be achieved by swing leg control.

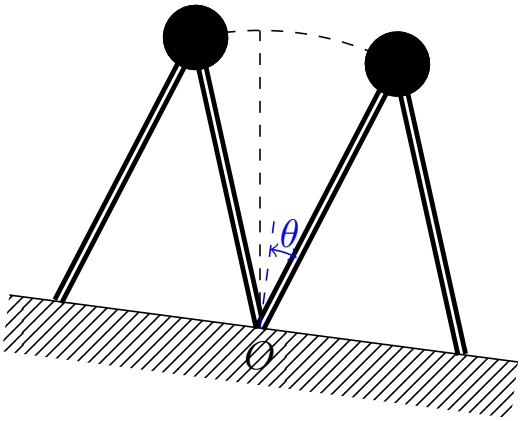

Figure 6.3: Simple Planar Biped on Slope. The time that center of mass spends before the support point (i.e., the deceleration period) is less than the time it spends after the support point (i.e., acceleration period)

6.3.1.2 A 3D Example

Example VI.16. (3D LIP with External Force) Consider the (x_0, y_0)-invariant 3D LIP biped with a constant positive external force $F_0 > 0$ in the x-direction. The equations of motion are

$$\ddot{x} = \omega^2 x + F_0,\ \ddot{y} = \omega^2 y, \tag{6.21}$$

with the impact map

$$x^+ = -x_0, y^+ = y_0,\ \dot{x}^+ = c_1\dot{x}^-,\ \dot{y}^+ = -c_2\dot{y}^-, \tag{6.22}$$

for $0 < c_1 < 1$ and $0 < c_2 < 1$. Also, the switching surface is assumed to be

$$\mathcal{S} = \{(x, y, \dot{x}, \dot{y}) | x^2 + y^2 = x_0^2 + y_0^2\}.$$

for $x_0 > 0$ and $y_0 > 0$. Clearly, this is a PSHS with $\epsilon = (F_0, 1 - c_1, 1 - c_2)$; that is, if $\epsilon = 0$, the system becomes an SHS. To study the existence and stability of the periodic orbits of this PSHS, we find the fixed points of the restricted Poincaré map $P : \mathcal{T}_{(-x_0,y_0)}\mathcal{Q} \to \mathcal{T}_{(-x_0,y_0)}\mathcal{Q}$ and the eigenvalues of its Jacobian. One can check that the above system has the following integrals:

$$\begin{aligned} \dot{x}^2 - \omega^2 x^2 - 2F_0 x &= C_1, \\ \dot{y}^2 - \omega^2 y^2 &= C_2, \\ \dot{x}\dot{y} - \omega^2 xy - F_0 y &= C_3. \end{aligned}$$

Let $(-x_0, y_0, \dot{x}_0, \dot{y}_0)$ be the state at the beginning of the current step and $(x_1, y_1, \dot{x}_1^-, \dot{y}_1^-)$ be the state at the end of the step. By the equations above,

$$\begin{aligned} \dot{x}_0^2 - \omega^2 x_0^2 + 2F_0 x_0 &= (\dot{x}_1^-)^2 - \omega^2 x_1^2 - 2F_0 x_1, \\ \dot{y}_0^2 - \omega^2 y_0^2 &= (\dot{y}_1^-)^2 - \omega^2 y_1^2, \\ \dot{x}_0\dot{y}_0 + \omega^2 x_0 y_0 - F_0 y_0 &= \dot{x}_1^-\dot{y}_1^- - \omega^2 x_1 y_1 - F_0 y_1. \end{aligned}$$

Based on the definition of the impact map, we have $\dot{x}_1^+ = c_1\dot{x}_1^-$ and $\dot{y}_1^+ = -c_2\dot{y}_1^-$. If we substitute these into the equations above, then

$$\begin{aligned} \dot{x}_0^2 - \omega^2 x_0^2 + 2F_0 x_0 &= d_1(\dot{x}_1^+)^2 - \omega^2 x_1^2 - 2F_0 x_1, \\ \dot{y}_0^2 - \omega^2 y_0^2 &= d_2(\dot{y}_1^+)^2 - \omega^2 y_1^2, \\ \dot{x}_0\dot{y}_0 + \omega^2 x_0 y_0 - F_0 y_0 &= d_3\dot{x}_1^+\dot{y}_1^+ - \omega^2 x_1 y_1 - F_0 y_1, \end{aligned}$$

where $d_1 = \frac{1}{c_1^2}, d_2 = \frac{1}{c_2^2}$ and $d_3 = \frac{-1}{c_1 c_2}$. Also, according to the definition of the switching surface,

$$x_1^2 + y_1^2 = x_0^2 + y_0^2.$$

The last four equations implicitly define the restricted Poincaré map $(\dot{x}_0, \dot{y}_0) \mapsto (\dot{x}_1^+, \dot{y}_1^+)$. Setting $\dot{x}_* = \dot{x}_0 = \dot{x}_1^+$ and $\dot{y}_* = \dot{y}_0 = \dot{y}_1^+$ in these equations, we can find the fixed point, $(\dot{x}_*, \dot{y}_*)$, of the Poincaré map. Let x_1^* and y_1^* be the values of the x_1 and y_1 on this periodic orbit. If we linearize the equations above around $(\dot{x}_*, \dot{y}_*)$, we can find the Jacobian of the restricted Poincaré map. Let $(-x_0, y_0, \dot{x}_* + \delta\dot{x}_0, \dot{y}_* + \delta\dot{y}_0)$ be the perturbed initial state and let $x_1 = x_1^* + \delta x_1$, $y_1 = y_1^* + \delta y_1$ and $(\dot{x}_1^+, \dot{y}_1^+) = (\dot{x}_* + \delta\dot{x}_1, \dot{y}_* + \delta\dot{y}_1)$. From the equations above,

$$\begin{aligned}
2\dot{x}_*\delta\dot{x}_0 &= 2d_1\dot{x}_*\delta\dot{x}_1 - (2\omega^2 x_1^* + 2F_0)\delta x_1, \\
2\dot{y}_*\delta\dot{y}_0 &= 2d_2\dot{y}_*\delta\dot{y}_1 - 2\omega^2 y_1^*\delta y_1, \\
\dot{y}_*\delta\dot{x}_0 + \dot{x}_*\delta\dot{y}_0 &= d_3(\dot{y}_*\delta\dot{x}_1 + \dot{x}_*\delta\dot{y}_1), \\
&\quad -\omega^2 y_1^*\delta x_1 - (\omega^2 x_1^* + F_0)\delta y_1, \\
0 &= x_1^*\delta x_1 + y_1^*\delta y_1.
\end{aligned}$$

These equations implicitly define the Jacobian of the Poincaré map. For simplicity, we write them in matrix form. Define

$$A = \begin{pmatrix} 2\dot{x}_* & 0 \\ 0 & 2\dot{y}_* \\ \dot{y}_* & \dot{x}_* \\ 0 & 0 \end{pmatrix},$$

and

$B =$

$$\begin{pmatrix} 2d_1\dot{x}_* & 0 & -(2\omega^2 x_1^* + 2F_0) & 0 \\ 0 & 2d_2\dot{y}_* & 0 & -2\omega^2 y_1^* \\ d_3\dot{y}_* & d_3\dot{x}_* & -\omega^2 y_1^* & -(\omega^2 x_1^* + F_0) \\ 0 & 0 & x_1^* & y_1^* \end{pmatrix}.$$

Then

$$A \begin{bmatrix} \delta\dot{x}_0 \\ \delta\dot{y}_0 \end{bmatrix} = B \begin{bmatrix} \delta\dot{x}_1 \\ \delta\dot{y}_1 \\ \delta x_1 \\ \delta y_1 \end{bmatrix}.$$

From this equation,

$$\begin{bmatrix} \delta\dot{x}_1 \\ \delta\dot{y}_1 \\ \delta x_1 \\ \delta y_1 \end{bmatrix} = B^{-1}A \begin{bmatrix} \delta\dot{x}_0 \\ \delta\dot{y}_0 \end{bmatrix}.$$

The first two rows of the equation above define the linearized Poincaré map at $(\dot{x}_*, \dot{y}_*)$; thus, if $C = B^{-1}A$, then

$$DP(\dot{x}_*, \dot{y}_*) = \begin{pmatrix} C_{1,1} & C_{1,2} \\ C_{2,1} & C_{2,2} \end{pmatrix}.$$

These results are used below to numerically study the (x_0, y_0)-invariant PSHS described in equations (6.21) and (6.22) with

$$x_0 = 0.3,\ y_0 = 0.4,\ \omega^2 = 9.$$

The fixed points are found in the (K, L) coordinates, where L is the synchronization measure of the 3D LIP, that is, $L = \dot{x}\dot{y} + \omega^2 x_0 y_0$ and $K = (1/2)(\dot{x}^2 + \dot{y}^2)$. The fixed points of the restricted Poincaré map are denoted by (K_*, L_*). We know that for the associated SHS, that is, when the perturbation is zero, $L_* = 0$; however, for the PSHS, as it can be seen in Table 6.2, L_* is nonzero, but as long as asymmetries (i.e., F_0, $1 - c_1$ and $1 - c_2$) are small, L_* remains small.

Fig. 6.4 illustrates how the eigenvalues change with the addition of asymmetries. The bottom graph shows how asymmetries turn the neutrally stable periodic orbits into asymptotically stable limit cycles. Again, we end up with a family of limit cycles, which can be indexed by (F_0, c_1, c_2).

$Case$	F_0	c_1	c_2
1	0.5	0.95	0.92
2	1	0.90	0.90
3	2	0.90	0.85

Table 6.1: Different Numerical Cases of the PSHS with $\epsilon = (F_0, 1 - c_1, 1 - c_2)$.

$Case$	L_*	K_*	λ_1	λ_{1_s}	λ_2	λ_{2_s}
1	0.078	2.680	0.905	1	-0.705	-0.772
2	0.117	2.522	0.810	1	-0.680	-0.757
3	0.145	5.037	0.811	1	-0.750	-0.880

Table 6.2: The cases are defined in Table 6.1. λ_s denotes the eigenvalue of the corresponding SHS evaluated at $K_* = 0.5((\dot{x}_*)^2 + (\dot{y}_*)^2)$. As seen in the table, the eigenvalue 1 of the SHS becomes smaller than 1 once the asymmetries are added.

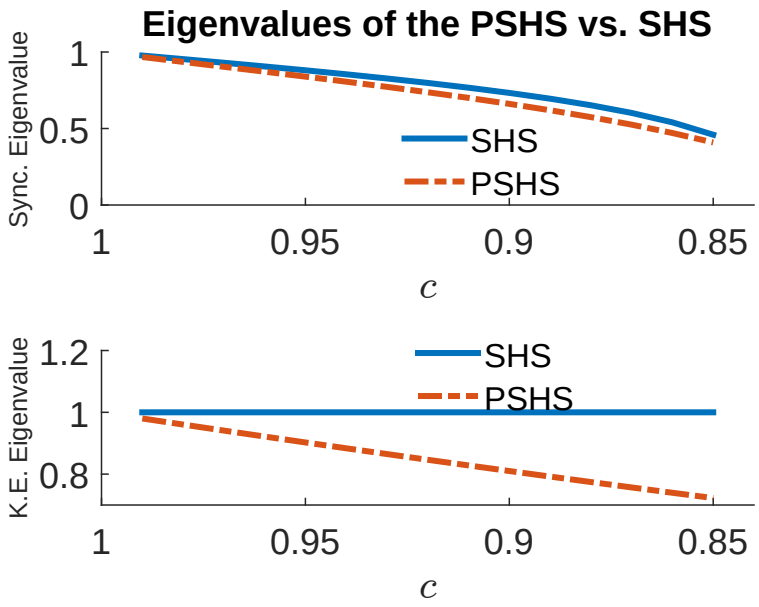

Figure 6.4: Synchronization and Kinetic Energy (K.E.) Eigenvalues of the PSHS vs. SHS when $F_0 = 1$ and $c_1 = c_2 = c$ is changing from 0.99 to 0.85. In these graphs, for each value of c there exists a fixed point $(\dot{x}_*, \dot{y}_*)$ for the PSHS. At this fixed point, the eigenvalues of the corresponding SHS is found from equation (6.11) with $K_0 = (1/2)(\dot{x}_*^2 + \dot{y}_*^2)$. From the bottom graph it is clear that after adding asymmetries the neutral stability of kinetic energy is turned into asymptotic stability.

6.3.2 Foot Placement

In the previous section, we showed that by introducing appropriate asymmetries, the symmetric periodic orbits of an SHS can turn into asymptotically stable limit cycles.

In this section, we show that it is possible to turn the symmetric periodic orbits of a symmetric legged robot into asymptotically stable limit cycles by merely using an event-based foot placement algorithm.

First, we discuss a simple foot placement algorithm for the 2D LIP, and then we present a foot placement algorithm for the 3D LIP. In Chapter VII, we verify the effectiveness of this algorithm on a 12-DOF 3D biped.

6.3.2.1 A Foot Placement Algorithm for the 2D LIP Biped

Recall the equations of motion of the x_0-invariant 2D LIP:

$$\begin{aligned} \ddot{x} &= \omega^2 x, \\ x^+ &= -x_0, \\ \dot{x}^+ &= \dot{x}^-, \\ \mathcal{S} &= \{(x, \dot{x}) | x = x_0\}, \end{aligned} \tag{6.23}$$

where $x_0 > 0$. To implement the foot placement algorithm, we modify the 3D LIP equations as follows

$$\begin{aligned} \ddot{x} &= \omega^2 x, \\ x^+ &= -(x_0 + \delta), \\ \dot{x}^+ &= \dot{x}^-, \\ \mathcal{S} &= \{(x, \dot{x}) | x = x_0\}, \end{aligned} \tag{6.24}$$

where δ is to be determined. Suppose that $x_s(t)$ is a symmetric solution of the 2D LIP that we wish to stabilize with foot placement. Suppose that $\dot{x}_m^*$ is the value of $\dot{x}(t)$ at the mid-step (i.e., when $x = 0$). Let

$$\delta = c(\dot{x}_m - \dot{x}_m^*), \tag{6.25}$$

for some $c > 0$, where $\dot{x}_m$ is $\dot{x}$ calculated at mid-step. With this definition, when $\dot{x}_m = x_m^*$ the solution is periodic (in fact, it is exactly $x_s(t)$). Substituting δ from equation (6.25) to the second equation of (6.24) results in the following event-based foot placement algorithm

$$x_{n+1}^+ = -x_0 + c(\dot{x}_{m_n} - \dot{x}^*), \tag{6.26}$$

where $\dot{x}_{m_n}$ is the velocity at the mid-step of step n and x_{n+1}^+ is the initial position at the beginning of step $n + 1$. In an actual robot, (6.26) can be achieved by swing leg foot placement. From (6.26) and the definition of orbital energy (see (*Kajita et al.*, 2001; *Razavi et al.*, 2015)),

$$\dot{x}_{m_{n+1}}^2 = \dot{x}_{m_n}^2 - \omega^2((x_0 + \delta_n)^2 - x_0^2), \tag{6.27}$$

where $\delta_n = c(\dot{x}_{m_n} - \dot{x}^*)$. Equation (6.27) can be written in the form $\dot{x}_{m_{n+1}} = g(\dot{x}_{m_n})$ with

$$g(\dot{x}_{m_n}) = (\dot{x}_{m_n}^2 - \omega^2((x_0 + \delta_n)^2 - x_0^2))^{\frac{1}{2}}. \tag{6.28}$$

It is easy to check that $\dot{x}_m^*$ is a fixed point of this function; moreover,

$$\frac{\mathrm{d}g}{\mathrm{d}\dot{x}_m}(\dot{x}_m^*) = 1 - \frac{c\omega^2 x_0}{\dot{x}^*}. \tag{6.29}$$

Clearly, for small enough $c > 0$,

$$\left| \frac{\mathrm{d}g}{\mathrm{d}\dot{x}_m}(\dot{x}_m^*) \right| < 1, \tag{6.30}$$

which guarantees that the fixed point $\dot{x}_m^*$ is asymptotically stable.

The above foot placement algorithm can be explained in terms of energy as well; with the above choice of δ, the input energy per unit mass to the system at each step is

$$\begin{aligned} E_{in} &= \int_{-x_0-\delta}^{x_0} \omega^2 x \, \mathrm{d}x \\ &= \frac{1}{2}\omega^2(x_0^2 - (x_0+\delta)^2). \end{aligned} \tag{6.31}$$

If the perturbation is in form of an injection of energy, then by (6.25), $\delta > 0$, hence, from (6.31), $E_{in} < 0$, and if the perturbation is in form of a reduction of energy, then by (6.25), $\delta < 0$, hence, from (6.31), $E_{in} > 0$.

Remark VI.17. Note that even though we did not include any impact losses in this example, the stability mechanisms of foot placement is in principle similar to that of the introducing asymmetries with impact losses as in Example VI.13. Based on this principle, if there is an injection of energy to the system due to a perturbation, then to cancel this perturbation the input energy to the system by actuators or from the impact has to be negative (i.e., either by negative work of actuators or impact losses), and if there is a reduction of energy due to a perturbation, then the input energy to the system has to be positive either by more positive work of actuators or less negative energy loss due to impact.

Since in practice there always will be impact and friction losses, a practical mechanism for stabilization of symmetric periodic orbits of a legged robot would be a combination of passivity-based method (i.e., introducing energy-injecting and energy-

dissipating asymmetries) and foot placement algorithm.

6.3.2.2 A Foot Placement Algorithm for the 3D LIP

The equations of motion of the 3D LIP with foot placement can be written as follows:

$$\begin{aligned} \ddot{x} &= \omega^2 x, \\ \ddot{y} &= \omega^2 y, \\ (x^+, y^+) &= (-(x_0 + \delta_x), y_0 + \delta_y), \\ (\dot{x}^+, \dot{y}^+) &= (\dot{x}^-, -\dot{y}^-), \\ \mathcal{S} &= \{(x, y, \dot{x}, \dot{y}) | x^2 + y^2 = x_0^2 + y_0^2\}, \end{aligned}$$

where δ_x and δ_y are set at the mid-step (i.e., when $x = 0$) as follows:

$$\begin{aligned} \delta_x &= c_x(\dot{x}_m - \dot{x}_m^*), \\ \delta_y &= \max\{0, c_y \dot{y}_m\}, \end{aligned}$$

where, $\dot{x}_m$ and $\dot{y}_m$ are the velocities in the x and y directions, respectively, and $\dot{x}_m^* > 0$ is the target velocity in the x-direction. Based on the equation of δ_y, y^+ is always greater than or equal to y_0; in other words, in the lateral plane, the swing foot is only allowed to be placed farther than y_0.

By (6.10) and Proposition VI.8 the symmetric periodic orbits of the 3D LIP are at best neutrally stable (if $y_0 > x_0$). Below, we present a numerical example to show that with the above foot placement algorithm, symmetric periodic orbits of the 3D LIP turn into asymptotically stable limit cycles.

Fig. 6.5 and 6.6 show the results of the numerical simulations for $x_0 = 0.15$ and $y_0 = 0.09$. Since $y_0 < x_0$, by (6.11), $|\lambda| > 1$, thus, the symmetric orbits of the 3D LIP with these x_0 and y_0 are not stable. However, as it can be seen in Fig. 6.5 with the

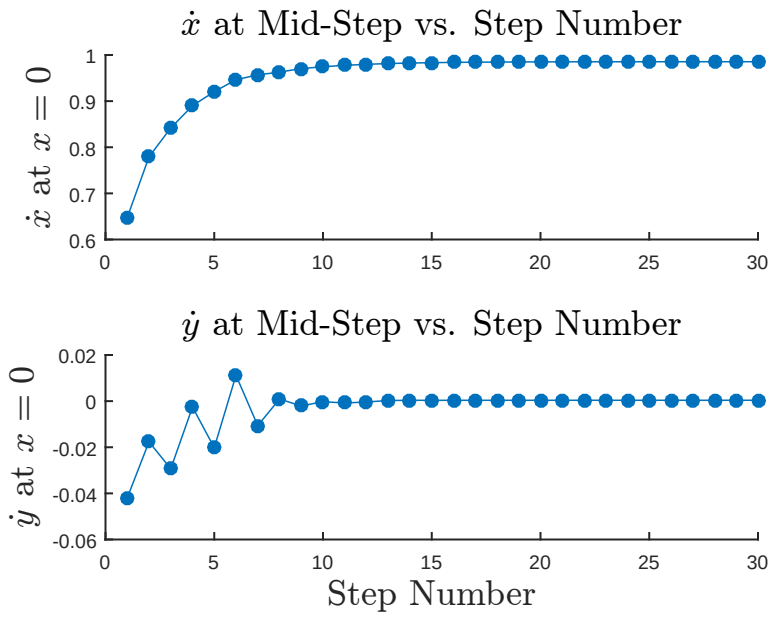

Figure 6.5: $\dot{x}$ and $\dot{y}$ at mid-step vs. step Number for $x_0 = 0.15$ and $y_0 = 0.09$. Convergence of $\dot{x}$ and of $\dot{y}_{COM}$ at the mid-step confirms stability of kinetic energy, and synchronization, respectively.

above foot placement algorithm an asymptotically stable limit cycle is achieved. Fig. 6.6 shows the resulting trajectory of y vs. x which as expected is an even function.

6.4 Perturbed Symmetric Bézier Polynomials

In Example V.8, we showed that by using appropriate SBPs the HZD of the 5-DOF 2D biped becomes an SHS with one degree of freedom which has an infinite number of symmetric periodic orbits (Fig. 5.7 shows a few of them). By Proposition VI.2, these periodic orbits are all neutrally stable (the only eigenvalue of the Jacobain Poincaré map on the HZD is one). In this section, we show that by slight modification of the SBPs we can obtain asymptotically stable limit cycles. By this modification of SBPs both introduction of asymmetries and foot placement can be achieved systematically.

Suppose that $y = \boldsymbol{h}(x)$ defines a set of SVCs for a hybrid system. A set of *perturbed SVCs* is defined as $y = \boldsymbol{h}(x) + \boldsymbol{h}_p(\boldsymbol{\epsilon}, x)$ such that $\boldsymbol{h}_p$ is a smooth function

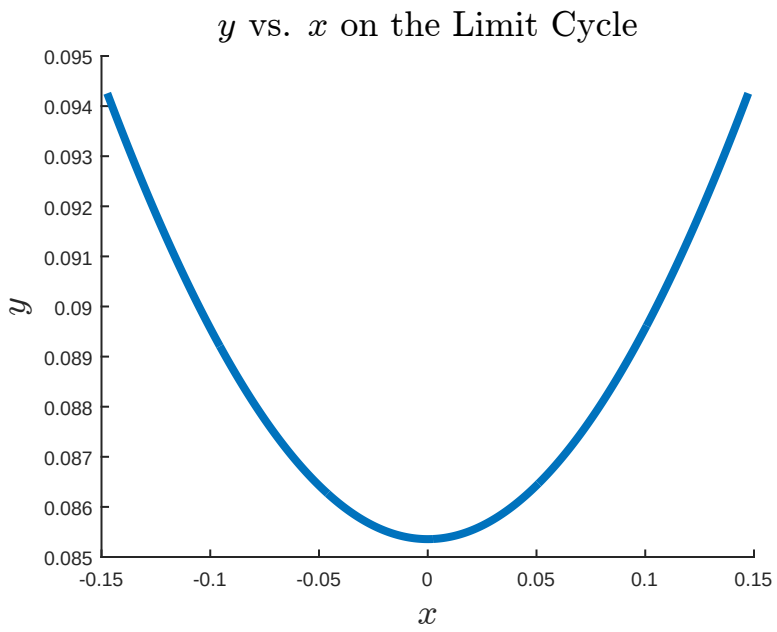

Figure 6.6: y vs. x on the limit cycle for $x_0 = 0.15$ and $y_0 = 0.08$ without foot placement. y_{COM} is an almost symmetric (even) function of x as expected.

and $\lim_{\boldsymbol{\epsilon}\to 0} \boldsymbol{h}_p(\epsilon, x) = 0$

Similarly, if α_k for $k = 0, 1, \ldots, M$ are the coefficients of an SBP of degree M. A *Perturbed Symmetric Bézier Polynomial (PSBP)* is an SBP with coefficients $\alpha_k + \epsilon_k$ with small $\epsilon_k \in \mathbb{R}$. Figs. 6.7 and 6.8 show two examples of PSBPs vs. SBPs for the 5-DOF 2D biped.

Example VI.18. (**PSBPs for the 5-DOF Biped and Limit Cycle Walking**) Fig. 5.7 in Chapter V shows a few of the symmetric periodic orbits obtained by using SBPs. In order to obtain a limit cycle walking gait, we modify a few of the SBPs as depicted in Fig. 6.7 and Fig. 6.8. Based on the PSBP in Fig. 6.7, the COM of the biped will have a non-zero component in the z-direction which causes impact loss. On the other hand, as depicted in Fig. 6.8, by modifying h_2, the biped is leaning forward during each step; as a result, the robot's COM spends more time in front of the support point (thus, generating energy input to cancel the impact loss). Fig. 6.9 shows the asymptotic stability of the resulting limit cycle. By modifying h_1 or

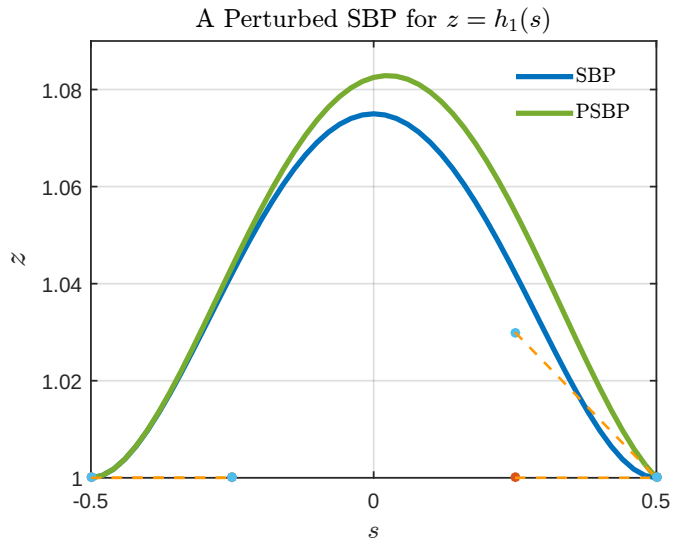

Figure 6.7: An SBP vs. a Perturbed SBP for $z = h_1(s)$. For the SBP $\boldsymbol{\alpha}_s = (1, 1, 1.2, 1, 1)$ and for the PSBP $\boldsymbol{\alpha}_{ps} = (1, 1, 1.2, 1.03, 1)$. That is, $\boldsymbol{\alpha}_{ps} = \boldsymbol{\alpha}_s + \boldsymbol{\epsilon}_1$, where $\boldsymbol{\epsilon}_1 = (0, 0, 0, 0.03, 0)$. With this skewed output, right before the impact the biped's COM velocity is pointing toward the ground and hence, causes impact loss.

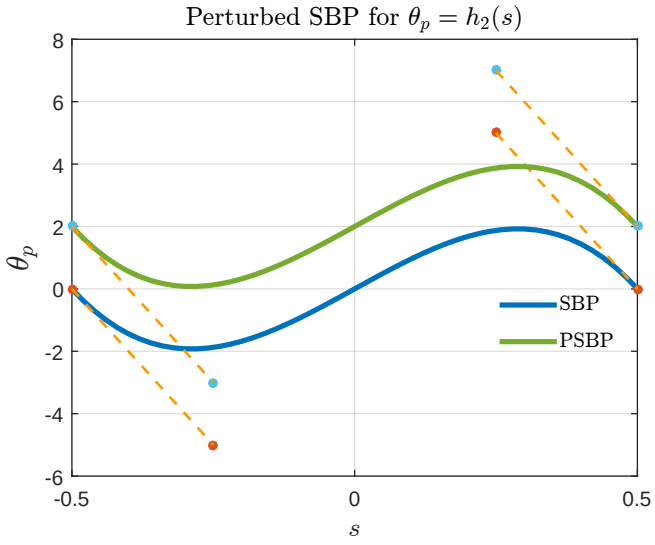

Figure 6.8: An SBP vs. a PSBP for $\theta_p = h_2(s)$. For the SBP, $\boldsymbol{\alpha}_s = (0, 5, 0, -5, 0)$ (in degrees) and for the PSBP $\alpha_{ps} = (2, 7, 2, 3, 2)$. That is, $\boldsymbol{\alpha}_{ps} = \boldsymbol{\alpha}_s + \boldsymbol{\epsilon}_2$, where $\boldsymbol{\epsilon}_2 = (2, 2, 2, 2, 2)$. With this skewed output, the pitch angle of the torso is on average greater than zero; which results in a positive average position of the COM.

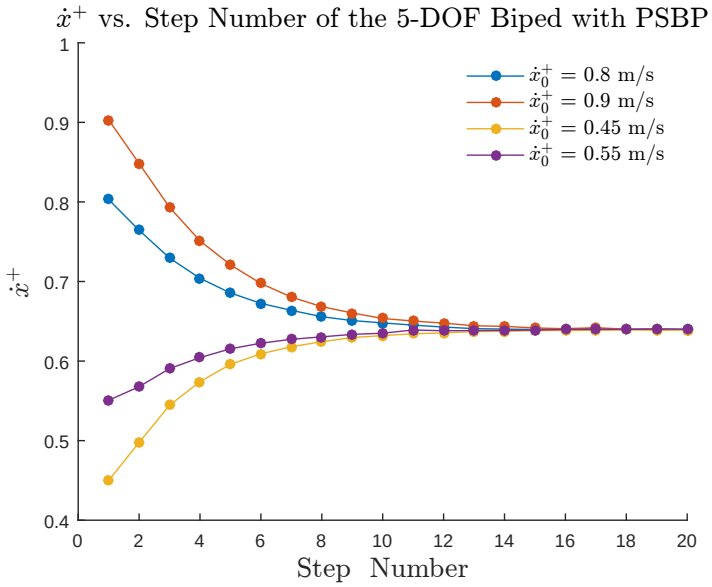

Figure 6.9: The resulting limit cycle using PSBPs as in Fig. 6.8 and 6.7. For a large range of initial velocities the solutions asymptotically approach a limit cycle.

h_2 differently different limit cycle walking gaits (for instance, with different average speeds) can be achieved easily. This can lead to a library of stable gaits which are functions of $\boldsymbol{\epsilon}_1$ and $\boldsymbol{\epsilon}_2$. For instance, Fig. 6.10 shows the steady-state velocity (right after impact) vs. the amount of the modification of θ_p, ϵ_p. As expected, by increasing the average pitch angle (i.e., the more the torso is leaned forward) the steady-state speed increases.

In the next chapter, the PSBPs are used for a 12-DOF 3D biped to achieve stable limit cycle walking gaits.

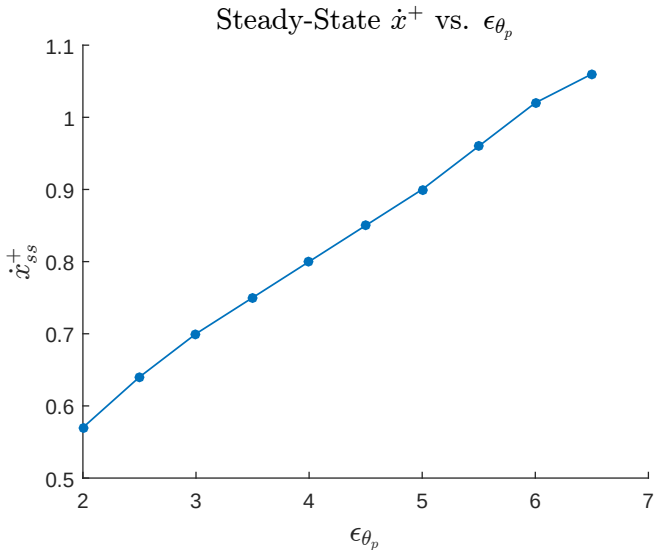

Figure 6.10: In this simulation SBP of θ_p has the coefficients $(0, 0, -5, 0, 5, 0, 0)$ and the perturbation is $(\epsilon_{\theta_p}, \epsilon_{\theta_p}, \epsilon_{\theta_p}, \epsilon_{\theta_p}, \epsilon_{\theta_p}, \epsilon_{\theta_p})$ where ϵ_{θ_p} varies from 2 degrees to 6.5 degrees.

CHAPTER VII

Symmetry Method Applied to the Bipedal Robot Romeo

Romeo is a humanoid robot built by Aldebaran Robotics© with the ultimate goal of serving as a personal assistant. In this chapter, first, we briefly explain the model of the robot, and then we apply the symmetry method to develop stable walking gaits for this robot.

7.1 Romeo's Model

Fig. 7.1 shows the humanoid robot Romeo. Romeo weighs about 42 kg and its height is 1.2 m. When standing upright, the COM height is 0.67 m. Excluding the eyes, fingers, and passive toes this robot has 31 joints each with one DOF. By convention, rotation about the z-axis is called yaw, rotation about x-axis is called roll and rotation about y-axis is called pitch. In our study, we assume that the upper body is fixed (by setting all upper body angles to fixed values). This simplified model has 12 DOF; 6 DOF in each leg. Figs. 7.2 through 7.4 describe the joints and their limits for this 12-DOF model.

The joint and link information such as link masses and axes of rotations of joints are provided in a so-called *Unified Robot Description Format (URDF)* file. After

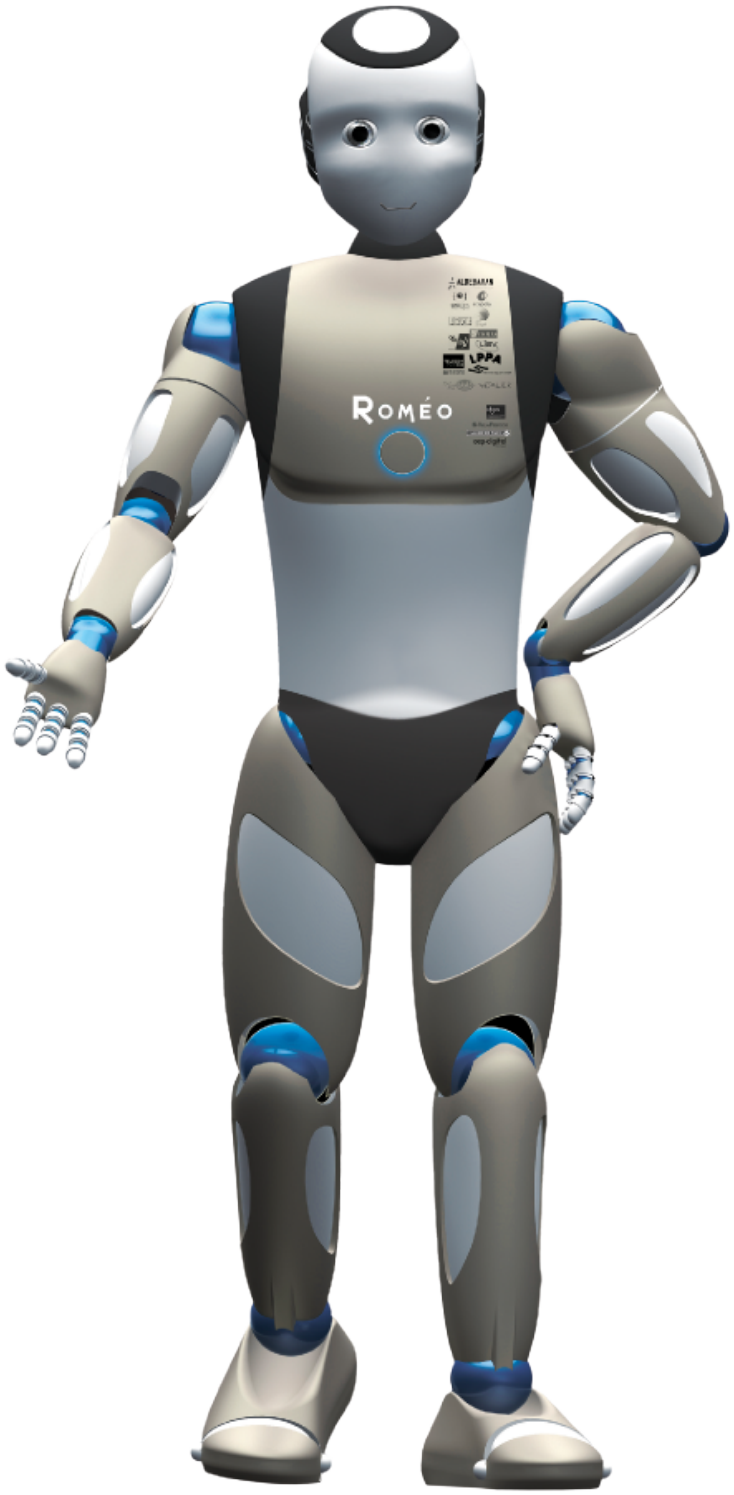

Figure 7.1: Romeo (from www.projetromeo.com)

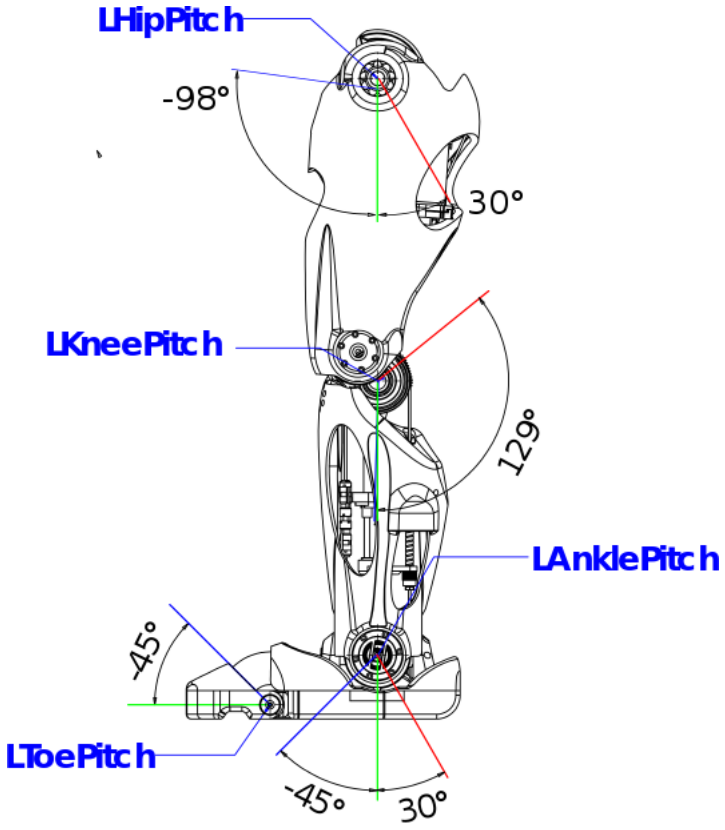

Figure 7.2: Left Leg Pitch Angles (from www.projectromeo.com). Overall there are three pitch degrees of freedom in each leg. (Note that we are not including the unactuated toe pitch joint)

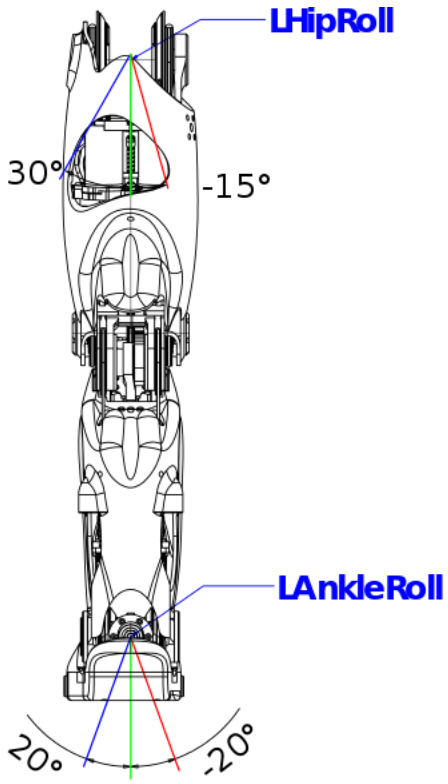

Figure 7.3: Left Leg Roll Angles (from www.projectromeo.com). Overall there are two roll degrees of freedom in each leg

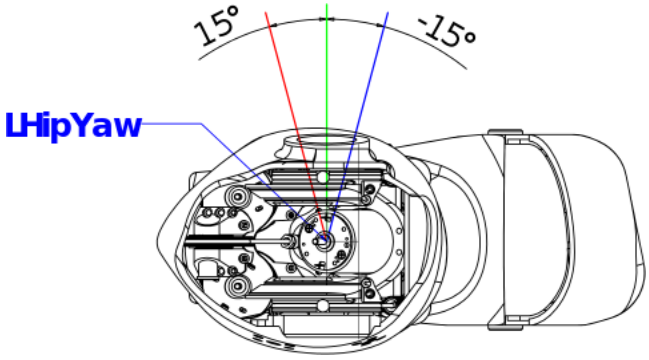

Figure 7.4: Left Leg Yaw (from www.projectromeo.com). Overall there is one yaw degree of freedom in each leg.

Coordinate	Description	Actuator
q_1	right leg ankle roll angle	u_1
q_2	right leg ankle pitch angle	u_2
q_3	right leg knee angle	u_3
q_4	right leg hip pitch angle	u_4
q_5	right leg hip roll angle	u_5
q_6	right leg hip yaw angle	u_6
q_7	left leg hip yaw angle	u_7
q_8	left leg hip roll angle	u_8
q_9	left leg hip pitch angle	u_9
q_{10}	left leg knee angle	u_{10}
q_{11}	left leg ankle pitch angle	u_{11}
q_{12}	left leg ankle roll angle	u_{12}

Table 7.1: Romeo's 12-DOF model coordinates.

simplification of this file, in MATLAB, a structure for the robot is generated which includes all the relevant information of the URDF. From this structure, the *Modified Denviat-Hartenberg (MDH)* parameters[1] are calculated based on the convention of (*Khalil and Dombre*, 1999). Fig. 7.5 shows the MDH coordinate systems.

Having the MDH parameters, the equations of motion are derived using Symoro+[2].

Assuming that the right foot is flat and on the ground, the simplified model of Romeo has 12 DOFs. The generalized coordinates for this 12-DOF model can be considered to be $q = (q_1, q_2, \ldots, q_{12})$, where $q_1, \ldots, q_{12}$ are defined in Table 7.1.

Romeo has 12 actuators in the two legs each directly controlling its corresponding angle listed in Table 7.1. However, we assume that the stance leg ankle is always passive, that is, $u_1 = u_2 = 0$. As a result, the 12-DOF model that we study has only 10 actuators, hence, has two degrees of underactuation.

[1]MDH parameters define the relative location of the coordinate systems attached to each joint. It is assumed that the for the revolute joints the z axis of the joint coordinate system is the axis of rotation of the joint. For a detailed discussion on MDH parameters see (*Khalil and Dombre*, 1999).

[2]Symoro stands for Symbolic Modeling of Robots. Symoro+, which is developed by the robot modeling team of IRCCyN, France, generates computationally optimal forward and inverse kinematics and dynamics given the MDH parameters of the robot (*Khalil et al.*, 1989)

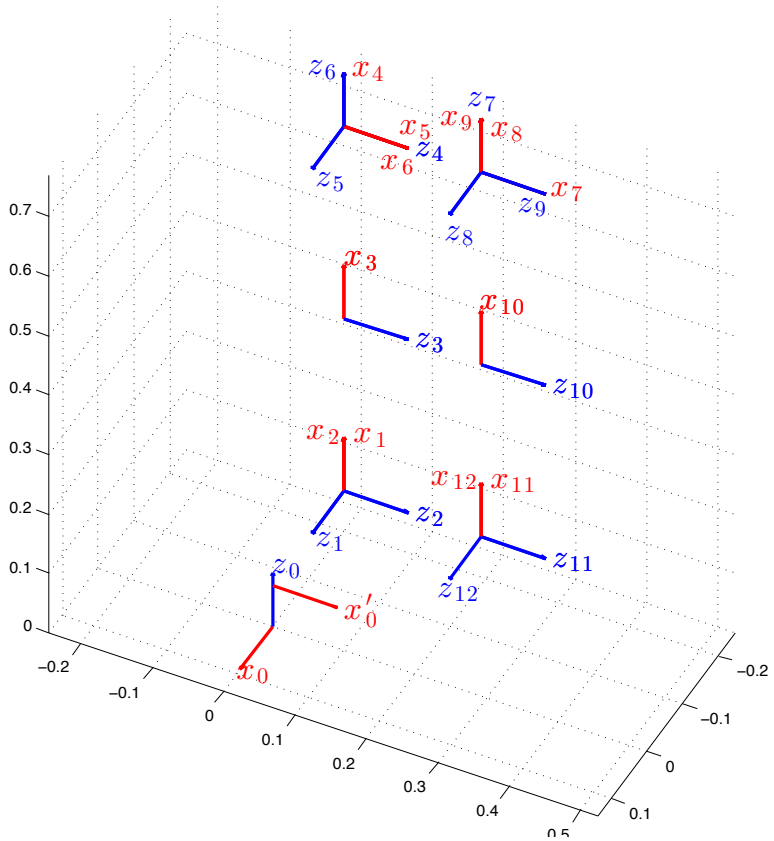

Figure 7.5: The MDH coordinate systems for the 12 joints in the two legs. The coordinate system 0, is the inertial frame which is attached to the right foot tip. By convention the z axis is the axis of rotation of each joint.

7.2 Generating Stable Walking Gaits for Romeo

Due to the asymmetries introduced by the knees and feet, Romeo is not a symmetric biped, however, similar to all other bipedal robots it is almost symmetric. So, to generate stable walking gaits, we start with using PSBPs to design the outputs that need to be driven to zero.

The steps to generate stable walking gaits based on the symmetry method are according to Fig. 1.8. First, we detect the symmetry map of Romeo, ignoring the asymmetries for the moment. Then, we define SBPs to achieve an almost symmetric HZD. Again, ignoring the asymmetries the resulting HZD is an SHS, hence, possesses an infinite number of symmetric solutions that can become symmetric periodic orbits. The last step is to modify the SBPs to get appropriate PSBPs to obtain asymptotically stable limit cycles. Achieving stable limit cycles is verified by simulations.

7.2.1 The Symmetry Map for Romeo and SVCs

As mentioned above, and explained in more details in Section 3.2.2, due to the knees and feet, Romeo is not completely symmetric. However, the asymmetries introduced by knees and feet are small enough that we can use the same theory as if the robot was symmetric.

Let $q = (q_1, q_2, \ldots, q_{12})$, where q_is are defined in Table 7.1. Let G be the map defined on the configuration space of the robot which sends $(q_1, q_2, q_3, q_4, q_5, q_6, q_7, q_8, q_9, q_{10}, q_{11}, q_{12})$ to $(q_1, -q_2, q_3, -q_4, q_5, -q_6, -q_7, -q_8, q_9, -q_{10}, -q_{11}, q_{12})$. Thus, if q_i is denoting a roll angle it is kept unchanged under the map G, otherwise, its sign is reversed. If the legs were acting as a parallelogram as in the robot in Fig. 3.5 and there were no feet, G would be the symmetry map of Romeo. However, we still consider this map as an approximate symmetry map for Romeo[3].

[3]Many bipedal robots have the same structure as that of Romeo, and we believe that the same

Based on the symmetry method, at this point, the SVCs should be determined. Assume that the right leg is the stance leg, and let x_H denote the position of the right leg hip. Let $-x_0 < x_H < x_0$. Define the phase variable s as follows:

$$s = \frac{x_H}{2x_0}.$$

Then s varies between -0.5 and 0.5.

Since the 12-DOF model has only 10 actuators, we define 10 virtual constraints. We choose to control the following outputs.

1. Stance knee angle: $q_k^{st} = h_1(s)$
2. Torso pitch angle in the inertial frame : $\theta_p = h_2(s)$
3. Torso roll angle in the inertial frame: $\theta_r = h_3(s)$
4. Torso yaw angle in the inertial frame : $\theta_y = h_4(s)$
5. Swing leg yaw angle: $\theta_y^{sw} = h_5(s)$
6. Swing foot heel x coordinate with respect to the swing leg hip: $x_{hf} = h_6(s)$
7. Swing foot heel y coordinate with respect to the swing leg hip: $y_{hf} = h_7(s)$
8 . Swing leg knee: $q_k^{sw} = h_8(s)$
9. Swing leg foot pitch angle in the inertial frame $\theta_p^{swf} = h_9(s)$
10. Swing leg foot roll angle in the inertial frame $\theta_r^{swf} = h_{10}(s)$

The symmetry map G which in above was defined in the coordinates $(q_1, q_2, \ldots, q_{12})$ in the coordinates $(q_k^{st}, \theta_p, \theta_r, \theta_y, \theta_y^{sw}, x_{hf}, y_{hf}, q_k^{sw}, \theta_p^{swf}, \theta_r^{swf})$ sends $(q_k^{st}, \theta_p, \theta_r, \theta_y, \theta_y^{sw}, x_{hf}, y_{hf}, q_k^{sw}, \theta_p^{swf}, \theta_r^{swf})$ to $(q_k^{st}, -\theta_p, \theta_r, -\theta_y, -\theta_y^{sw}, -x_{hf}, y_{hf}, q_k^{sw}, -\theta_p^{swf}, \theta_r^{swf})$.

Thus, in order for these virtual constraints (1-10) to be symmetric, based on the symmetry map, the following conditions need to be satisfied:

C1. h_1 is an even function.

symmetry map, G, defined above, is a good approximation of the inherent symmetries of these bipeds.

C2. h_2 is an odd function.

C3. h_3 is an even function.

C4. h_4 is an odd function.

C5. h_5 is an odd function.

C6. h_6 is an odd function.

C7. h_7 is an even function.

C8. h_8 is an even function.

C9. h_9 is an odd function.

C10. h_{10} is an even function.

We assume that the stance leg foot is always flat on the ground (i.e., always is parallel the $x-y$ plane of the inertial frame.). Consequently, right before the impact, θ_p^{swf} and θ_r^{swf} need to be zero. Thus, a simple choice for h_9 and h_{10} is $h_9 = h_{10} = 0$. Also, since we want the robot to walk on a straight line, we pick $h_4 = h_5 = 0$ (i.e., all the yaw angles are driven to zero). Finally, we select $\theta_r = h_3 = 0$. In the next section, we use SBPs to define virtual constraints for the five remaining outputs q_k^{st}, θ_p, x_{hf}, y_{hf} and q_k^{sw}.

Remark VII.1. It is very common that instead of the knee angles the hip height and swing foot height are selected as outputs to be controlled. However, selecting the swing foot height as an output needs careful attention because having z_f as a function of the phase variable s, where $s = x_H/x_0$, means that the impact is only a function of the variable x_H, that is, on the zero dynamics the impact surface is $x_H = x_0$ and has no dependence on y_H. As shown in Corollary 3 in the appendix, for the 3D LIP, the transition surface $x_H = x_0$ leads to unstable symmetric periodic gaits. That is, if impact occurs anytime x_H is equal to x_0, the symmetric periodic orbits are not self-synchronized. Therefore, if z_f is chosen as an output, using a foot placement algorithm is necessary to obtain asymptotically stable limit cycle walking.

7.2.2 SBPs for Romeo

We use SBPs of order 6 to define h_1, h_2, h_6, h_7 and h_8. According to conditions C1-C10 and the discussion of the SBPs in Section 5.4, the coefficients of these SBPs, which are respectively denoted by $\boldsymbol{\alpha}_1$, $\boldsymbol{\alpha}_2$, $\boldsymbol{\alpha}_6$, $\boldsymbol{\alpha}_7$, $\boldsymbol{\alpha}_8$, are in the form

$$\begin{aligned}
\boldsymbol{\alpha}_1 &= [\alpha_{1,0}, \alpha_{1,1}, \alpha_{1,2}, \alpha_{1,2}, \alpha_{1,1}, \alpha_{1,0}], \\
\boldsymbol{\alpha}_2 &= [\alpha_{2,0}, \alpha_{2,1}, \alpha_{2,2}, -\alpha_{2,2}, -\alpha_{2,1}, -\alpha_{2,0}], \\
\boldsymbol{\alpha}_6 &= [\alpha_{6,0}, \alpha_{6,1}, \alpha_{6,2}, -\alpha_{6,2}, -\alpha_{6,1}, -\alpha_{6,0}], \\
\boldsymbol{\alpha}_7 &= [\alpha_{7,0}, \alpha_{7,1}, \alpha_{7,2}, \alpha_{7,2}, \alpha_{7,1}, \alpha_{7,0}], \\
\boldsymbol{\alpha}_8 &= [\alpha_{8,0}, \alpha_{8,1}, \alpha_{8,2}, \alpha_{8,2}, \alpha_{8,1}, \alpha_{8,0}].
\end{aligned} \tag{7.1}$$

In order to achieve an (x_0, y_0)-invariant SHS (see Section 6.2), the following conditions need to be satisfied

$$\alpha_{72} = x_0, \alpha_{82} = y_0.$$

7.2.3 PSBPs for Romeo

As discussed before in Section 6.4, in order to compensate the impact and friction losses, the SBPs must be modified slightly. Similar to the 5-DOF example in Section 6.4 the torso is inclined forward by a small angle $\theta_p^d > 0$; thus,

$$\boldsymbol{\alpha}_2 = [\alpha_{2,0}, \alpha_{2,1}, \alpha_{2,2}, -\alpha_{2,2}, -\alpha_{2,1}, -\alpha_{2,0}] + \boldsymbol{\epsilon}_2,$$

where $\boldsymbol{\epsilon}_2 = [\theta_p^d, \theta_p^d, \theta_p^d, \theta_p^d, \theta_p^d, \theta_p^d]$. Another way we introduce asymmetry to the outputs is through the stance and swing knees such that at the end of each step the stance leg length is greater than the swing leg length (see Fig. 7.6). Similar to θ_p^d, this asymmetry is an energy injecting asymmetry. To introduce such asymmetry in the

knees we set[4]

$$\boldsymbol{\alpha}_1 = [\alpha_{1,0}, \alpha_{1,1}, \alpha_{1,2}, \alpha_{1,2}, \alpha_{1,1}, \alpha_{1,0}] + \boldsymbol{\epsilon}_1,$$

for $\boldsymbol{\epsilon_1} = (-\epsilon_{knee}, 0, 0, 0, 0, \epsilon_{knee})$ for $\epsilon_{knee} > 0$. Also, for the swing leg knee,

$$\boldsymbol{\alpha}_8 \;\; = \;\; [\alpha_{8,0}, \alpha_{8,1}, \alpha_{8,2}, \alpha_{8,2}, \alpha_{8,1}, \alpha_{8,0}] - \boldsymbol{\epsilon}_1.$$

Moreover, since at the end of each step the swing leg and stance leg are swapped, the knee angle of the swing leg at the end of each step needs to be equal to the knee angle of the stance leg at the beginning of the next step. Thus, we require

$$\alpha_{80} = -\alpha_{10}.$$

7.2.4 Simulation Results

In this section, we present a numerical example of the PSBPs for the 12-DOF model of Romeo and verify the existence of asymptotically stable limit cycles. In the example we study here $x_0 = 15\ cm$ and $y_0 = 8\ cm$. The PSBPs for knees, torso pitch, x_{hf} and y_{hf}, which satisfy the conditions presented in the previous section, are selected as in Table 7.2. The graphs of the SBPs and PSBPs for the numerical values given in Table 7.2 are depicted in Fig. 7.7 through 7.9.

Given the outputs, $h = (h_1, \ldots, h_{10})$, and the desired PSBPs, h_d, the virtual constraints can be written as $y = h(s) - h_d(s)$. The next step is to find the controllers that drive y to zero. To this end, rather than using nonlinear controllers, for simple implementation of the controllers on the actual robot, we use simple Proportional-

[4]Note that by our convention of the coordinate systems and positive direction of rotation about the x, y and z axis based on the right-hand rule, the more negative is the stance knee angle the more bent is the stance leg knee, and the more positive the swing leg knee is the more bent is the swing leg knee.

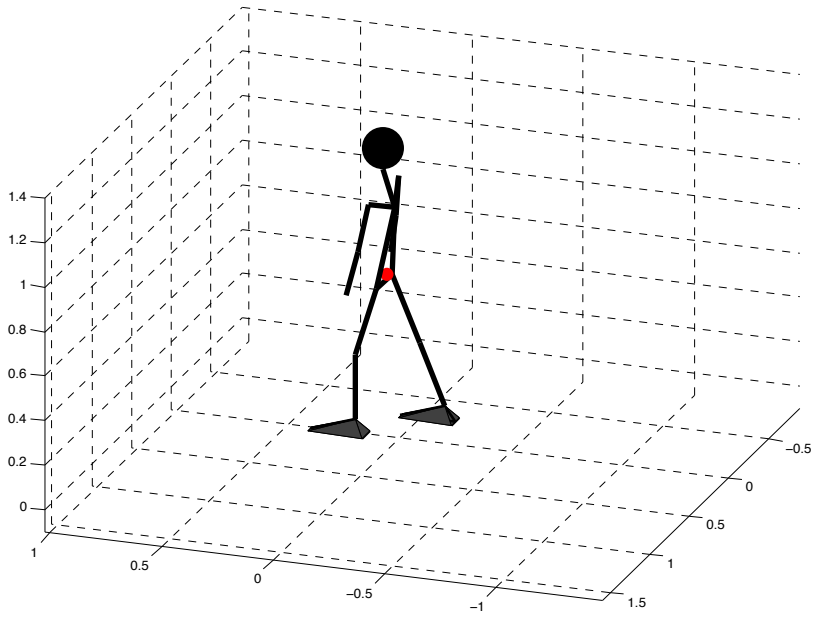

Figure 7.6: Energy injecting asymmetry introduced by the difference in stance and swing leg knee angles. At the beginning of the step the stance leg is bent, and as a result, the COM is closer to the stance point. Consequently, the COM spends more time in front of the stance point, thus, generating a net positive acceleration.

Output			PSBP					
q_k^{st}	$\boldsymbol{\alpha}_1$	= [	-0.6	-0.6	-0.5	-0.5	-0.4	-0.4]
θ_p	$\boldsymbol{\alpha}_2$	= [	0.025	0.025	0.025	0.025	0.025	0.025]
θ_r	$\boldsymbol{\alpha}_3$	= [	0	0	0	0	0	0]
θ_y	$\boldsymbol{\alpha}_4$	= [	0	0	0	0	0	0]
θ_y^{sw}	$\boldsymbol{\alpha}_5$	= [	0	0	0	0	0	0]
x_{hf}	$\boldsymbol{\alpha}_6$	= [	$-x_0$	$-x_0$	$-x_0 - 0.1$	$x_0 + 0.1$	x_0	x_0]
y_{hf}	$\boldsymbol{\alpha}_7$	= [	y_0	y_0	y_0	y_0	y_0	y_0]
q_k^{sw}	$\boldsymbol{\alpha}_8$	= [	0.4	0.6	1	1	0.6	0.6]
θ_p^{swf}	$\boldsymbol{\alpha}_9$	= [	0	0	0	0	0	0]
θ_r^{swf}	$\boldsymbol{\alpha}_{10}$	= [	0	0	0	0	0	0]

Table 7.2: PSBPs for Romeo.

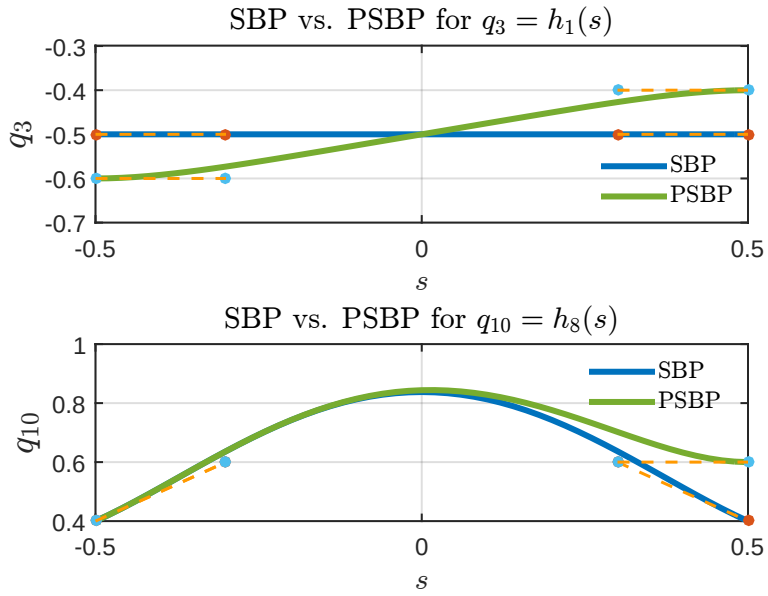

Figure 7.7: SBP vs PSBP for the stance leg knee and swing leg knees. With Bézier polynomials for the knee angles, the stance (swing) leg knee is more (less) bent at the beginning of the step compared to the end of the step.

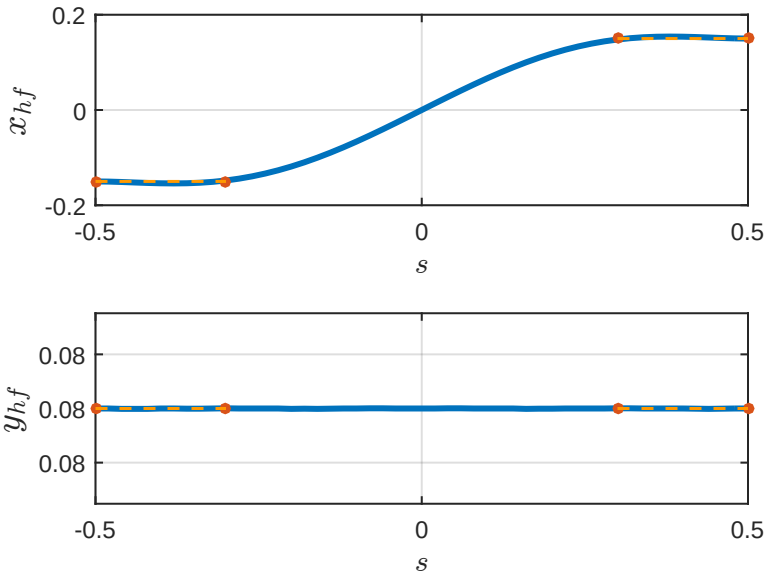

Figure 7.8: SBP and PSBP for x_{hf} and y_{hf}. Note that SBP and PSBP are the same in this case.

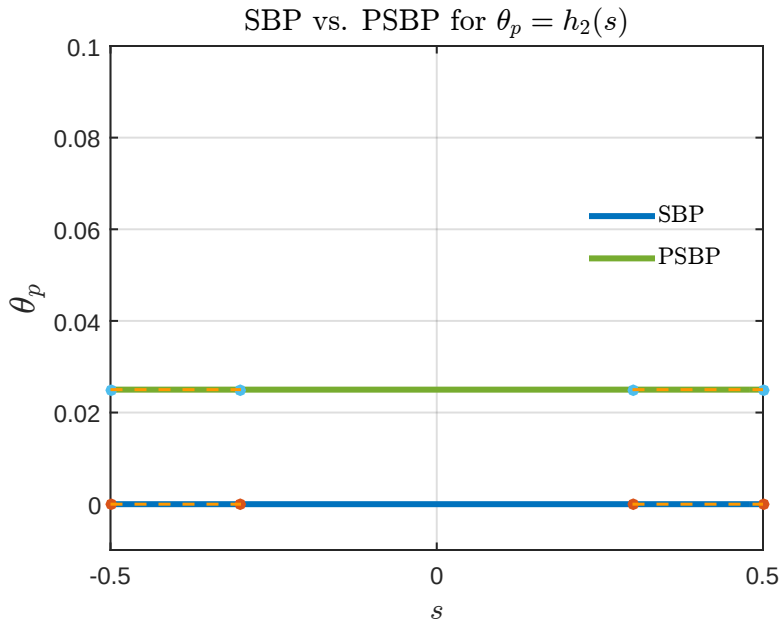

Figure 7.9: SBP vs PSBP for the pitch angle. The pitch angle in the PSBP case is greater than zero to generate energy injecting asymmetry.

Derivative (PD) controllers as discussed below.

To decompose the role of actuators, for each output we use one specific and independent actuator. For example, for the torso pitch angle, h_2, we only use the actuator u_4 (see Table 7.1). In sum, we get the following relationship between the actuator angles (as described in Table 7.1) and the desired constraint:

$$y = Ae_{act}, \tag{7.2}$$

$$\dot{y} = A\dot{e}_{act}, \tag{7.3}$$

where e_{act} and $\dot{e}_{act}$ are the error and derivative of the error in the actuated angles[5] $q_3, \ldots, q_{12}$, where

$$\begin{aligned} A_{1,1} &= 1, \quad A_{2,2} = 1, \quad A_{3,3} = 1, \quad A_{4,4} = 1, \quad A_{5,5} = 1, \\ A_{6,7} &= -1, \quad A_{7,6} = 1, \quad A_{8,8} = 1, \quad A_{9,9} = 1, \quad A_{10,10} = 1. \end{aligned}$$

[5]Note that q_1 and q_2 are assumed not to be actuated.

and other components of A are all zero. From (7.2) and (7.3),

$$e_{act} = A^{-1}y,$$
$$\dot{e}_{act} = A^{-1}\dot{y}.$$

A simple PD control is used to drive these errors to zero:

$$\boldsymbol{u} = -K_p e_{act} - K_d \dot{e}_{act},$$

where $\boldsymbol{u} = [u_3; u_4; \ldots; u_{12}]$, and $K_p, K_d > 0$.

The top plot in Fig. 7.10 shows $\dot{x}_{COM}$, the velocity of the COM in the x direction of the inertial frame, at the beginning of each step vs. step number, and the bottom plot shows $\dot{y}_{COM}$ at $x_{COM} = 0$ vs. step number. Convergence of $\dot{y}_{COM}$ in this figure confirms the self-synchronization of the limit cycle. Fig. 7.11 shows the resulting $\dot{y}_{COM}$ vs. x_{COM} on the limit cycle. In these simulations, the robot is given a small initial velocity (as low as 0.1 m/s), and then it automatically approaches a limit cycle which is far from the initial state of the robot. The convergence to a limit cycle with such simple initial conditions suggests that the basin of attraction of the emerged limit cycle is relatively large.

From Fig. 7.11, the average position of the COM in the x direction is greater than zero; the energy injecting asymmetry that causes this positive average position mostly comes from the difference in the stance leg knee and swing leg knee angles as explained in Fig. 7.6.

Fig. 7.12 shows a few snapshots of the simulation together with the path of the COM.

We note that in all of the simulations, torque limits and friction limits on ground reaction forces (with a friction coefficient of $\mu = 0.6$) have been satisfied.

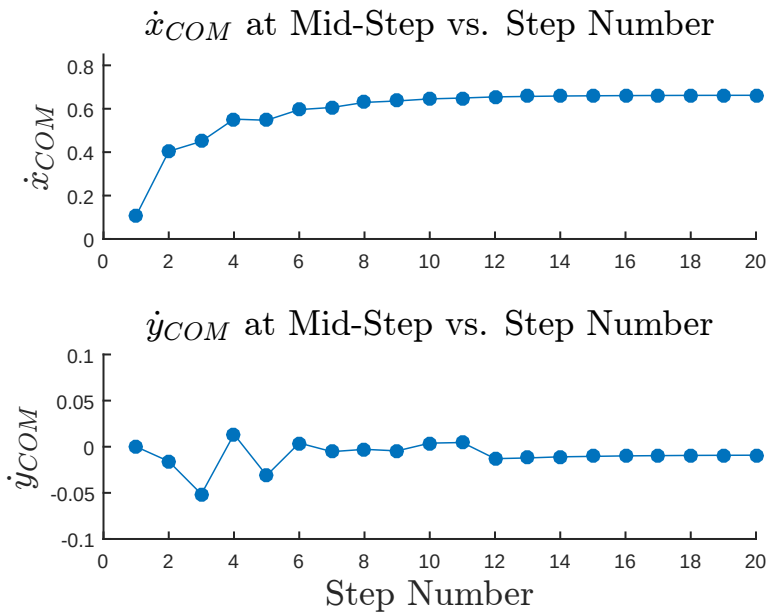

Figure 7.10: $\dot{x}_{COM}$ and $\dot{y}_{COM}$ at the Middle of Each Step vs. Step Number for $x_0 = 0.15$ and $y_0 = 0.08$ without foot placement. The initial velocity in the x direction, as seen in the top plot, is as low as 0.1 m/s. The convergence of $\dot{y}_{COM}$ at the mid-step confirms the self-synchronization.

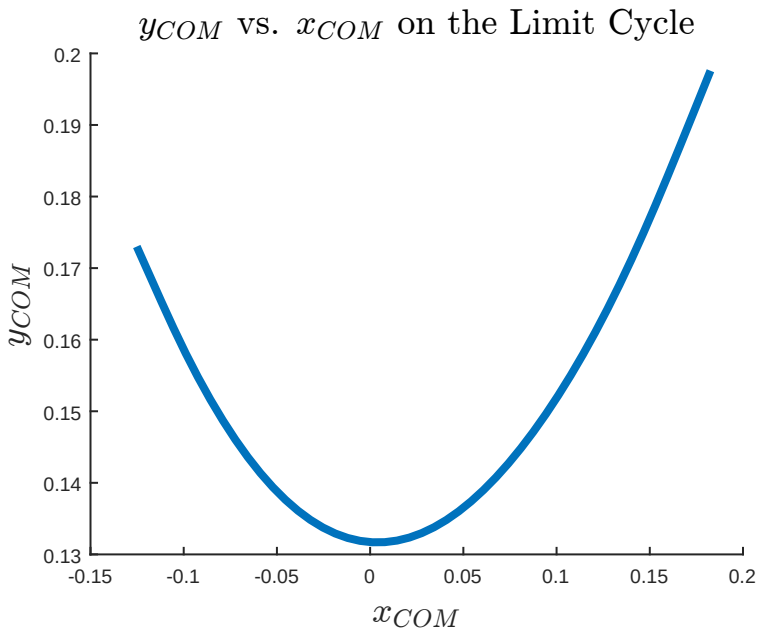

Figure 7.11: y_{COM} vs. x_{COM} on the limit cycle for . y_{COM} is an almost symmetric (even) function of x_{COM} as expected.

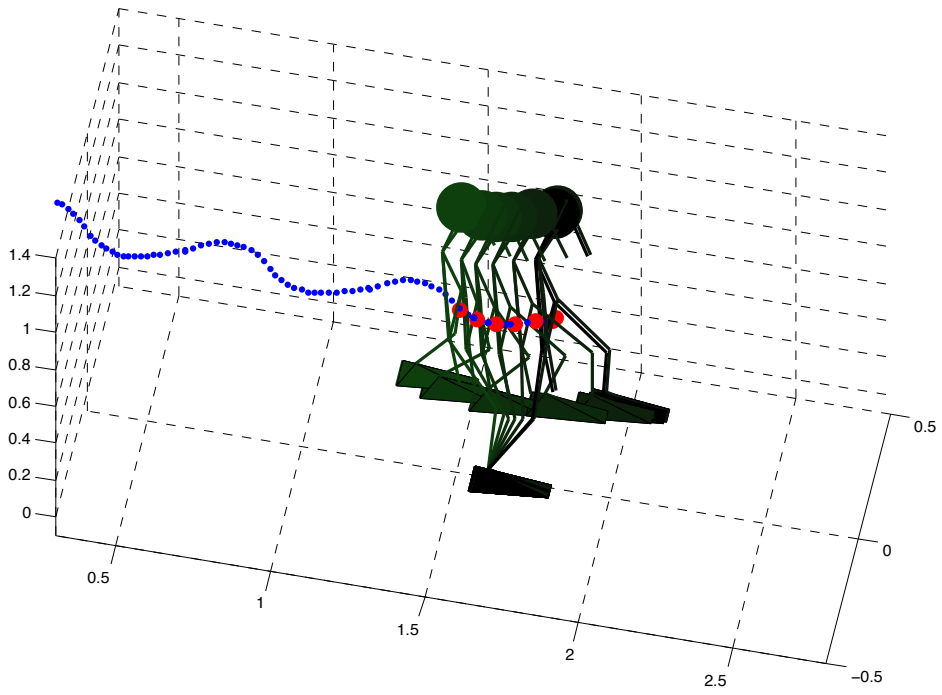

Figure 7.12: A few Snapshots of the Animation. The blue line is the path of COM.

7.2.5 Augmenting Foot placement

In the last section, stable limit cycle walking was achieved by symmetry method without any foot placement algorithm. In this section, we present a simple foot placement algorithm that can improve the stability of the walking. Moreover, by numerical simulations we observed that with the specific PSBPs that we used, in order for the gait to be stable without foot placement for $x_0 = 0.15\ m$, y_0 has to be greater than or equal to $0.08m$. Here, with a foot placement algorithm we obtain asymptotically stable limit cycle walking gaits with $x_0 = 0.15\ m$ and y_0 as low as 0. Therefore, some of the gaits which were unstable without foot placement, can become stable with foot placement.

The foot placement algorithm used is similar to that of the 3D LIP in Section 6.3.2.1. Let $x_{0_{nom}}$ and $y_{0_{nom}}$ be the nominal values of x_{hf} and y_{hf} at the end of each

step, respectively. At the middle of step, that is, when[6] $x_H = 0$, we implement the following event-based control for the foot placement:

$$\begin{aligned} x_0 &= x_{0_{nom}} + k_x(\dot{x}_{COM} - \dot{x}^d), \\ y_0 &= \max\{y_{0_{nom}}, y_{0_{nom}} + k_y \dot{y}_{COM}\}, \end{aligned}$$

for $k_x, k_y > 0$ and a desired forward velocity $\dot{x}^d > 0$. The foot placement in the lateral direction is done as if the desired velocity in the y direction in the middle of the step is 0. The reason that we set $\dot{y}^d = 0$ is that for pure symmetric walking gaits $\dot{y} = 0$ when $x = 0$ (for instance, recall the 3D LIP symmetric orbits in Fig. 3.3). Moreover, based on the foot placement algorithm above, y_0 is always greater than or equal to $y_{0_{nom}}$. The Bezier polynomials for x_{hf} and y_{hf} are updated based on the value of x_0 and y_0 in each step. In particular, based on Table 7.2, $\boldsymbol{\alpha}_6 = [-x_0, -x_0, -x_0-0.1, x_0+0.1, x_0, x_0]$ and $\boldsymbol{\alpha}_7 = [y_0, y_0, y_0, y_0, y_0, y_0]$.

Figs. 7.13 through 7.14 show the simulation results for $x_{0_{nom}} = 0.15$, $y_{0_{nom}} = 0$, $k_x = 0.1$ and $k_y = 0.25$. An asymptotically stable periodic walking gait is successfully achieved. We note that for many other nominal values for x_0 and y_0 or different k_x and k_y values asymptotically stable limit periodic walking was achieved as well.

Remark VII.2. We note that all the asymptotically stable walking gaits here were achieved without any search for fixed points of the Poincaré map. Simply, in the simulations the biped is set at an initial pose and then is given a very small initial velocity[7]. It automatically converges to an almost symmetric asymptotically stable periodic orbit. The fact that the robot can start walking with such simple initial conditions also shows the robustness of the symmetry method for limit cycle walking.

[6]One could define $x_{COM} = 0$ or $x_H = 0$ as the mid-step, the results of the foot-placement algorithm are almost the same in either case because x_H is very close to x_{COM}.

[7]We note that the convergence to the limit cycle is not very sensitive to the value of the initial velocity.

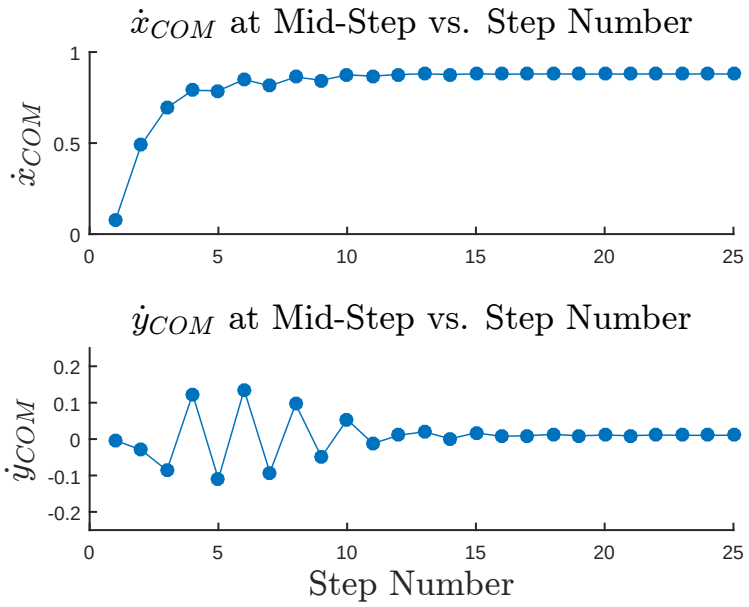

Figure 7.13: $\dot{x}_{COM}$ and $\dot{y}_{COM}$ at the middle of each step vs. step number for $x_{0_{nom}} = 0.15$ and $y_{0_{nom}} = 0$ with foot placement. The initial $\dot{x}_{COM}$ is as low as 0.1 m/s. Without foot-placement, with these nominal values, the periodic gait is not self-sychronized. However, with foot-placement $\dot{y}_{COM}$ at the mid-step converges to a small value which confirms that synchronization is achieved with foot-placement.

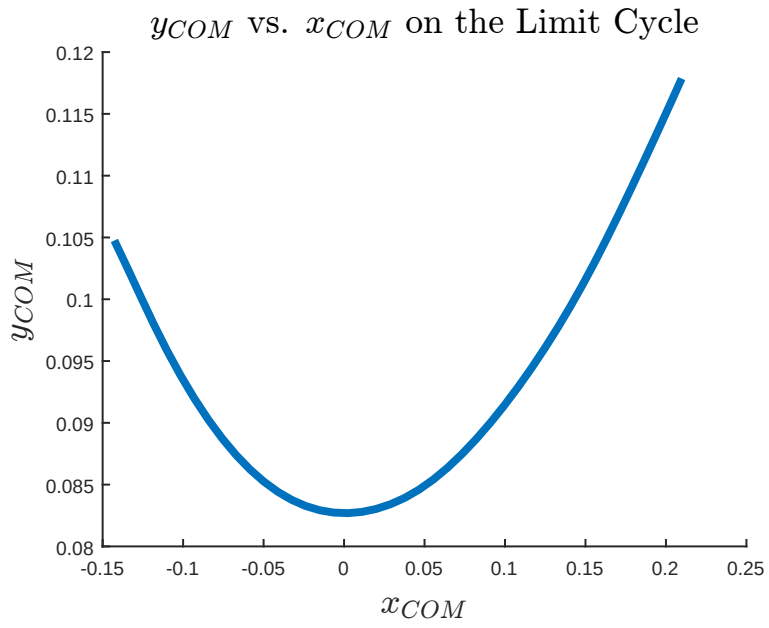

Figure 7.14: y_{COM} vs. x_{COM} on the limit cycle for $x_{0_{nom}} = 0.15$ and $y_{0_{nom}} = 0$ with foot placement. y_{COM} is an almost symmetric (even) function of x_{COM} as expected.

CHAPTER VIII

Conclusions

8.1 Summary

Even though the ZMP method has been a common way of generating walking gaits for legged robots, the achieved performance is far from being human/animal-like. In particular, the current ZMP walking gaits have not been capable of demonstrating the full extent of agility that a legged robot can achieve. In contrast to ZMP walking, limit cycle walking is capable of demonstrating agility in dynamic legged locomotion. However, given a legged robot, obtaining limit cycle walking is not always straightforward. The common method for obtaining stable periodic orbits of a legged robot is to conduct a numerical search for the fixed points of a Poincaré map associated with a hybrid system that models the legged robot. However, this method is computationally expensive as in each search trial the differential equations representing the robot need to be integrated. Moreover, the resulting walking gait may not be robust enough because the numerical search is conducted based on a model of the robot, and it remains to be seen if with model errors the periodic orbit remains a periodic orbit of the actual robot.

To overcome these issues, we have presented the *Symmetry Method for Limit Cycle Walking* which allows for obtaining stable limit cycles without the need for a numerical search for periodic orbits. Moreover, since the method only relies on basic

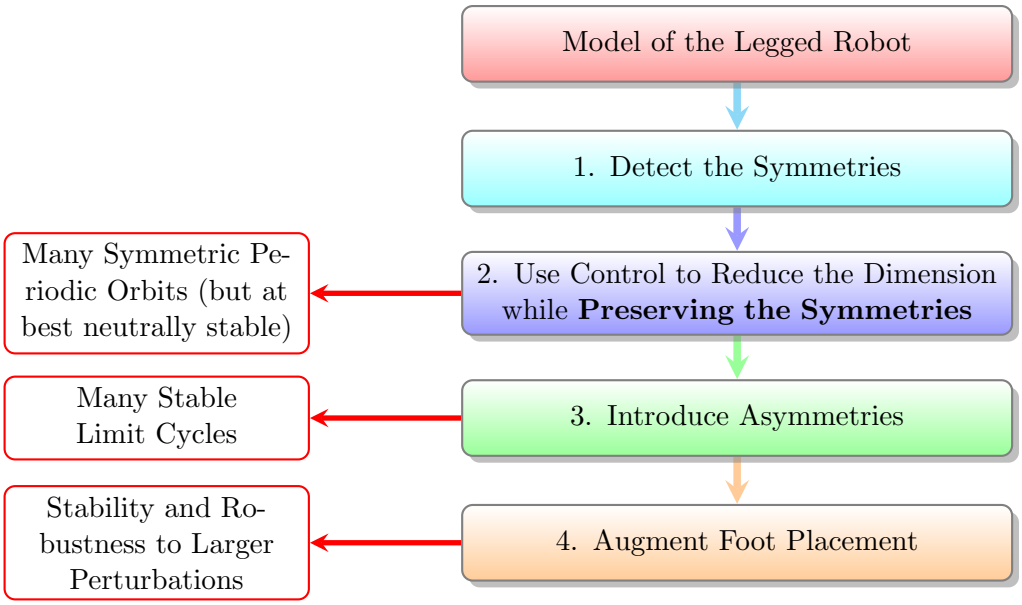

Figure 8.1: High-level control algorithm of the symmetry method for stable limit cycle walking.

symmetry properties that almost all legged robots have, it is by nature robust to model errors.

As shown in Fig. 8.1, the symmetry method for stable limit cycle walking of legged robots consists of four steps: First, given the legged robot, the symmetries are identified; this is done by determining the symmetry map of the robot. We have shown that because of the existing symmetries the system can have as many symmetric periodic orbits as the fixed points of the symmetry map. It should be noted that, even though the robot might not be completely symmetric (e.g., due to the feet, friction or uneven mass distribution), since asymmetries are generally small compared to the overall symmetry of the legged robot, the symmetry map is determined as if the asymmetries did not exist. Moreover, in the third step of the symmetry method for limit cycle walking, such asymmetries turn out to help achieving asymptotic stability of the resulting limit cycles. Second, based on the symmetry map, the virtual constraints are designed so that when control laws enforce the virtual constraints the resulting reduced order system remains symmetric and

hence, has symmetric periodic orbits which can be identified without any numerical search. The class of such virtual constraints which are called Symmetric Virtual Constraints (SVCs) is large enough that allow optimization (e.g., on torque limits) while respecting the symmetry of the system.

The third step is the introduction of asymmetries which include energy injecting (e.g., extension of the stance leg after mid-step) and energy dissipating asymmetries (e.g., impact loss or friction). We have shown that such asymmetries can stabilize the neutrally stable symmetric periodic orbits of the legged robot, but for unstable symmetric periodic orbits, augmenting foot placement, which is the last step in the symmetry method, is necessary. We have presented a simple foot placement strategy that renders the unstable symmetric periodic orbits stable and makes the basin of attraction of the already-stable periodic orbits larger.

The symmetry method for limit cycle walking is successfully tested on a 12-DOF 3D model of the humanoid robot Romeo.

8.2 Future Work

Experimental Validation: Even though the symmetry method for limit cycle walking has been successfully tested on different models of bipedal robots such as Romeo (see Chapter VII) and MARLO, it has not been tested in experiments. We hope that the symmetry method will be tested and experimentally validated on the humanoid robot Romeo in the near future.

Theoretical Work on Stabilization: While two methods for stabilization of the symmetric periodic orbits of an SHS were given and verified in a few examples, more theoretical work on these methods is needed. In this regard, for instance, future work can involve developing conditions under which introducing asymmetries can lead to asymptotic stability of the limit cycle merging out of the symmetric periodic orbits.

Other Types of Legged Robots: As future work, one can apply the symmetry method to other models of legged robots such has quadrupeds.

Optimization: SVCs provide the flexibility of gait design and optimization (e.g., on torque limits). While we have studied the problem of stable periodic walking, it is interesting to demonstrate how optimization and symmetry method can be paired together.

Other Modes of Locomotion: Models of legged locomotion considered here all assume instantaneous impact. A future direction could be generalization of the theory of symmetry to more general modes of locomotion, for instance, when a double support phase is involved.

APPENDIX

Rest of Proof of Proposition II.3: We show that the maximal solution $x_M(t)$ of X for which $x_M(0) = x^*$, is defined on a symmetric interval of the form $I_{x^*} = (-a_M, a_M)$.

Suppose that x_M is defined on an interval of the form $(-\alpha, \beta)$. If $\beta = \alpha$ we are done by setting $a_M = \beta$. Assume that $\beta > \alpha$. The case of $\alpha > \beta$ will be similar. By Proposition II.3,

$$G(x_M(-t)) = x_M(t), \quad \forall t \in (-\alpha, \alpha).$$

Suppose that $x_\alpha(t)$ is a solution of X with the initial condition $x_\alpha(-\alpha) = G(x_M(\alpha))$. There exists $\epsilon > 0$ such that $x_\alpha(t)$ is defined on $(-\alpha - \epsilon, \alpha + \epsilon)$. Define $\hat{x}_M(t)$ on $(-\alpha - \epsilon, \beta)$ as follows:

$$\hat{x}_M(t) = \begin{cases} x_M(t), & t \in (-\alpha, \beta) \\ x_\alpha(t), & t = (-\alpha - \epsilon, -\alpha] \end{cases}$$

We show that $\hat{x}_M(t)$ is a solution of X. To this end, since $x_M(t)$ and $x_\alpha(t)$ are both

solutions of X, it suffices to show the continuity of $x_M(t)$ at $t = -\alpha$.

$$\begin{aligned}
\lim_{t\to-\alpha^+} \hat{x}_M(t) &= \lim_{t\to-\alpha^+} x_M(t), \\
&= \lim_{t\to-\alpha^+} G(x_M(-t)), \\
&= \lim_{t\to\alpha^-} G(x_M(t)), \\
&= G(x_M(\alpha)), \\
&= x_\alpha(-\alpha).
\end{aligned}$$

This proves the continuity of $\hat{x}_M(t)$. Therefore, $\hat{x}_M(t)$ is a solution of X defined on the interval $(-\alpha - \epsilon, \beta)$, however, this is a contradiction to the maximality of x_M. Therefore, we conclude that $\beta \leq \alpha$. However, similarly it can be shown that $\beta < \alpha$ leads to a contradiction. Consequently, $\beta = \alpha$; hence, defining $a_M = \alpha$, the maximal solution $x_M(t)$ is necessarily defined the maximal interval $(-a_M, a_M)$.

Proof of Lemma VI.1: Since $\dot{x}(0) = X(x_s(0))$, if $\dot{x}_s(0) = 0$, then $X(x_s(0)) = 0$; thus $X(x^*) = 0$. As a result, $x_s(t) = x^*$ is the unique solution of X passing through x^*. However, since $x_s(t)$ crosses the switching surface $\mathcal{S}$ at $t_I \neq 0$, we conclude that $\dot{x}_s(0) \neq 0$. Moreover, since $\dim(S_G) < \dim(\mathcal{X})$, there exists a hypersurface $\mathcal{S}_{x^*}$ at x^* such that $T_{x^*}S_G \subset T_{x^*}\mathcal{S}_{x^*}$. If $\dim(S_G) < \dim(\mathcal{X}) - 1$, then noting $\dot{x}_s(0) \neq 0$, clearly $\mathcal{S}_{x^*}$ can be chosen to be transversal to $\dot{x}_s(0)$. If $\dim(S_G) = \dim(\mathcal{X}) - 1$, then we pick $\mathcal{S}_{x^*} = \mathcal{O} \subset S_G$, where $\mathcal{O}$ is an open subset of S_G including x^*. Since $\mathcal{O}$ is an open subset of S_G, we have $T_{x^*}\mathcal{S}_{x^*} = T_{x^*}S_G$. We show that $\dot{x}_s(0)$ is transversal to $T_{x^*}S_G$, and hence $T_{x^*}\mathcal{S}_{x^*}$. If $\dot{x}_s(0)$ is not transversal to $T_{x^*}S_G$, then $\dot{x}_s(0) \in T_{x^*}S_G$. However, by symmetry of $x_s(t)$,

$$\dot{x}_s(0) = -\mathrm{d}G \cdot \dot{x}_s(0).$$

By definition of S_G, since $\dot{x}_s(0) \in T_{x^*}S_G$, we conclude that $\mathrm{d}G \cdot \dot{x}_s(0) = x_s(0)$; thus, by the above equation, $\dot{x}_s(0) = -\dot{x}_s(0)$, which yields $\dot{x}_s(0) = 0$. However, this is a contradiction because we already showed that $\dot{x}_s(0) \neq 0$. Consequently, $\dot{x}_s(0)$ is transversal to $T_{x^*}S_G$.

Proposition 1. *Suppose that the SHS has a synchronized solution $(X(t), Y(t))$ with initial conditions $(X(0), Y(0)) = (-x_0, y_0)$ and $(\dot{X}(0), \dot{Y}(0)) = (\dot{X}_0, \dot{Y}_0)$. Suppose that $t = t_m$ is the time for which $X(t_m) = 0$ and $\dot{Y}(t_m) = 0$ such that $\dot{X}(t_m) \neq 0$. Let $\chi(\dot{x}_0, \dot{y}_0, t)$ be the flow map of the (x_0, y_0)-invariant SHS. Therefore, $\chi(\dot{x}_0, \dot{y}_0, 0) = (-x_0, y_0, \dot{x}_0, \dot{y}_0)$ for every $(\dot{x}_0, \dot{y}_0) \in \mathcal{T}_{(-x_0,y_0)}\mathcal{Q}$. Let $\chi = (x, y, \dot{x}, \dot{y})$. Since $(X(t), Y(t))$ is synchronized,*

$$x(\dot{X}_0, \dot{Y}_0, t_m) = 0,\ \dot{y}(\dot{X}_0, \dot{Y}_0, t_m) = 0.$$

If the Jacobian of $(x, \dot{y})$ with respect to $(\dot{x}_0, \dot{y}_0)$ is invertible at $(\dot{X}_0, \dot{Y}_0, t_m)$, then there exists a smooth function $L : \mathcal{T}_{(-x_0,y_0)}\mathcal{Q} \to \mathbb{R}^{m+n-1}$ such that if $L(\dot{x}_0, \dot{y}_0) = 0$, the solution starting from $(-x_0, y_0)$ with initial velocity $(\dot{x}_0, \dot{y}_0)$ is synchronized.

Proof. Based on the definition of a synchronized solution, we are interested in the values of $(\dot{x}_0, \dot{y}_0, t)$ for which

$$x(\dot{x}_0, \dot{y}_0, t) = 0,\ \dot{y}(\dot{x}_0, \dot{y}_0, t) = 0.$$

Since $(\dot{X}_0, \dot{Y}_0, t_m)$ is a solution to this system, we have

$$x(\dot{X}_0, \dot{Y}_0, t_m) = 0,\ \dot{y}(\dot{X}_0, \dot{Y}_0, t_m) = 0.$$

Because the Jacobian of $(x, \dot{y})$ with respect to $(\dot{x}_0, \dot{y}_0)$ is invertible at $(\dot{X}_0, \dot{Y}_0, t_m)$, by implicit function theorem there exists a smooth function F defined in a neighborhood

of t_m such that in this neighborhood

$$x(F(t),t)=0,\ \dot{y}(F(t),t)=0. \tag{.1}$$

The function $t \mapsto F(t)$ defines a smooth curve in the manifold $\mathcal{T}_{(-x_0,y_0)}\mathcal{Q}$, where $F(t_m) = (\dot{X}_0, \dot{Y}_0)$. Differentiating the two equations in (.1) with respect to t at $t = t_m$, since $\dot{X}(t_m) \neq 0$, we can show that $\dot{F}(t_m) \neq 0$. Therefore, the parametrization $t \mapsto F(t)$ is a regular parametrization in a neighborhood of t_m, and, hence, the image of $t \mapsto F(t)$ defines an embedded 1-dimensional submanifold $\mathcal{K}$ of $\mathcal{T}_{(-x_0,y_0)}\mathcal{Q}$ (*Lee*, 2003). Thus, there exists a smooth function $L : \mathcal{T}_{(-x_0,y_0)}\mathcal{Q} \to \mathbb{R}^{m+n-1}$ with rank $m + n - 1$ such that

$$\mathcal{K} = \{(\dot{x}_0, \dot{y}_0) \in \mathcal{T}_{(-x_0,y_0)}\mathcal{Q} | L(\dot{x}_0, \dot{y}_0) = 0\}.$$

Consequently, if $L(\dot{x}_0, \dot{y}_0) = 0$, the solution starting from $(-x_0, y_0)$ with initial velocity $(\dot{x}_0, \dot{y}_0)$ is synchronized. □

Proposition 2. *Let $\mathcal{Q}$ denote the configuration space of the (x_0, y_0)-invariant 3D LIP biped. Assume that the switching surface is*

$$\mathcal{S} = \{(x, y, \dot{x}, \dot{y}) | h(x, y) = h(x_0, y_0)\},$$

where $h : Q \to \mathbb{R}$ is a smooth function and $\partial h/\partial y(x_0, y_0) \neq 0$. Let $(\dot{x}_*, \dot{y}_*)$ be a fixed point of the restricted Poincaré map $P : \mathcal{T}_{(-x_0,y_0)}\mathcal{Q} \to \mathcal{T}_{(-x_0,y_0)}\mathcal{Q}$. The eigenvalues of P at $(\dot{x}_*, \dot{y}_*)$ are $\{\lambda, 1\}$ with

$$\lambda = -1 + \frac{2\omega^2(y_0^2 - Cx_0^2)}{CE_x^* - E_y^*}, \tag{.2}$$

where

$$C = \frac{y_0}{x_0}\left(\frac{\partial h}{\partial y}(x_0, y_0)\right)^{-1}\frac{\partial h}{\partial x}(x_0, y_0),$$

and

$$E_x^* = \dot{x}_*^2 - \omega^2 x_0^2,\ E_y^* = \dot{y}_*^2 - \omega^2 y_0^2$$

are the orbital energies in the x and y directions.

Proof. Let $L : \mathcal{T}_{(-x_0,y_0)}\mathcal{Q} \to \mathbb{R}$ be the synchronization measure of the 3D LIP. By Proposition VI.7, $\lambda = \partial L_1/\partial L_0(0, K^*)$, where $K^* = (1/2)((\dot{x}_*)^2 + (\dot{y}_*)^2)$. Assume that $(-x_0, y_0, \dot{x}_* + \delta\dot{x}_0, \dot{y}_* + \delta\dot{y}_0)$ is the initial state of a solution of the system at the beginning of the step, and let $(-x_0, y_0, \dot{x}_* + \delta\dot{x}_1, \dot{y}_* + \delta\dot{y}_1)$ be its state at the beginning of the next step. Define $L_0 = L(\dot{x}_* + \delta\dot{x}_0, \dot{y}_* + \delta\dot{y}_0)$ and $L_1 = L(\dot{x}_* + \delta\dot{x}_1, \dot{y}_* + \delta\dot{y}_1)$. We have

$$\lambda = \lim_{L_0 \to 0} \frac{L_1}{L_0}.$$

Denote the state of the system right before the transition by $(x_0 + \delta x_1, y_0 + \delta y_1, \dot{x}_* + \delta\dot{x}_1, -(\dot{y}_* + \delta\dot{y}_1))$. Since $L = \dot{x}\dot{y} - \omega^2 xy$ is a conserved quantity for the 3D LIP in the continuous phase of motion, we have

$$L_0 = -(\dot{x}_* + \delta\dot{x}_1)(\dot{y}_* + \delta\dot{y}_1) - \omega^2(x_0 + \delta x_1)(y_0 + \delta y_1).$$

Moreover, since the system is (x_0, y_0)-invariant,

$$L_1 = (\dot{x}_* + \delta\dot{x}_1)(\dot{y}_* + \delta\dot{y}_1) + \omega^2 x_0 y_0.$$

Adding this equation to the previous one,

$$L_1 + L_0 = -\omega^2(x_0\delta y_1 + y_0\delta x_1). \tag{.3}$$

By definition of the switching surface, $h(x_0 + \delta x_1, y_0 + \delta y_1) = h(x_0, y_0)$, from which,

$$\frac{\partial h}{\partial x}(x_0, y_0)\delta x_1 = -\frac{\partial h}{\partial y}(x_0, y_0)\delta y_1. \tag{.4}$$

By definition of C, $\delta y_1 = -C\frac{x_0}{y_0}\delta x_1$. Substituting this into equation (.3) results in

$$L_1 + L_0 = -\omega^2(-C\frac{x_0^2}{y_0} + y_0)\delta x_1.$$

Therefore, from the equation above,

$$\lim_{L_0\to 0}\frac{L_1}{L_0} = -1 - \omega^2(-C\frac{x_0^2}{y_0} + y_0)\lim_{L_0\to 0}\frac{\delta x_1}{L_0}. \tag{.5}$$

Thus, to find the limit on the left-hand side we need only find the limit on the right-hand side. Since in the continuous phase of motion the orbital energies, $\dot{x}^2 - \omega^2 x^2$ and $y^2 - \omega^2 y^2$, are conserved quantities, we have

$$\begin{aligned}(\dot{x}_* + \delta\dot{x}_0)^2 - \omega^2 x_0 &= (\dot{x}_* + \delta\dot{x}_1)^2 - \omega^2(x_0 + \delta x_1),\\ (\dot{y}_* + \delta\dot{y}_0)^2 - \omega^2 y_0 &= (\dot{y}_* + \delta\dot{y}_1)^2 - \omega^2(y_0 + \delta y_1).\end{aligned}$$

From these two equations and definition of C,

$$\dot{x}_*(\delta\dot{x}_1 - \delta\dot{x}_0) = \omega^2\delta x_1,\ \dot{y}_*(\delta\dot{y}_1 - \delta\dot{y}_0) = -C\omega^2\frac{x_0}{y_0}\delta x_1. \tag{.6}$$

Since $L = \dot{x}\dot{y} - \omega^2 xy$ is a conserved quantity in the continuous phase of the motion, we can write L_0 in terms of the states at the beginning of step, that is, $(-x_0, y_0, \dot{x}_* +$

$\delta\dot{x}_0, \dot{y}_* + \dot{y}_0)$ or at end of the step, that is, $(x_0 + \delta x_1, y_0 + \delta y_1, \dot{x}_* + \delta\dot{x}_1, \dot{y}_* + \dot{y}_1)$. Hence,

$$\begin{aligned} L_0 &= (\dot{x}_* + \delta\dot{x}_0)(\dot{y}_* + \delta\dot{y}_0) + \omega^2 x_0 y_0, \\ L_0 &= -(\dot{x}_* + \delta\dot{x}_1)(\dot{y}_* + \delta\dot{y}_1) - \omega^2(x_0 + \delta x_1)(y_0 + \delta y_1). \end{aligned}$$

From (.6) and the two equations above,

$$\frac{2L_0}{\delta x_1} = -\omega^2 \frac{x_0 y_0(-C\dot{x}_*^2 + \dot{y}_*^2) + (\dot{x}_*\dot{y}_*)(-Cx_0^2 + y_0^2)}{y_0\dot{x}_*\dot{y}_*}.$$

Substituting this into equation (.5), we have

$$\begin{aligned} \lim_{L_0 \to 0} \frac{L_1}{L_0} &= -1 + \frac{1}{\omega^2} \\ &\cdot \quad \frac{2(-Cx_0^2 + y_0^2)(\dot{x}_*\dot{y}_*)}{x_0 y_0(-C\dot{x}_*^2 + \dot{y}_*^2) + (\dot{x}_*\dot{y}_*)(-Cx_0^2 + y_0^2)}. \end{aligned}$$

The limit on the left-hand side is λ. Since $L(\dot{x}_*, \dot{y}_*) = 0$, we have $\dot{x}_*\dot{y}_* = -\omega^2 x_0 y_0$. Therefore, if we replace $\dot{x}_*\dot{y}_*$ with $-\omega^2 x_0 y_0$ in the equation above, we obtain

$$\begin{aligned} \lambda &= -1 + \frac{1}{\omega^2} \\ &\cdot \quad \frac{2(-Cx_0^2 + y_0^2)(-\omega^2 x_0 y_0)}{x_0 y_0(-C\dot{x}_*^2 + \dot{y}_*^2) + (-\omega^2 x_0 y_0)(-Cx_0^2 + y_0^2)}. \end{aligned}$$

After simplification

$$\lambda = -1 + \frac{2\omega^2(y_0^2 - Cx_0^2)}{C\dot{x}_*^2 - \dot{y}_*^2 + \omega^2(y_0^2 - Cx_0^2)}.$$

By definition of E_x^* and E_y^* this equation is equivalent to equation (.2). □

Corollary 3. *In Proposition 2, if* $h(x, y) = x^2 + a^2 y^2$ *then*

$$\lambda = -1 + \frac{2\omega^2(a^2 y_0^2 - x_0^2)}{E_x^* - a^2 E_y^*}.$$

In particular, if $a = 1$*, then*

$$\lambda = -1 + \frac{2\omega^2(y_0^2 - x_0^2)}{E_x^* - E_y^*},$$

and, if $a = 0$*, that is, if impact occurs when* $x = x_0$ *(so, with no dependence on* y*), then*

$$\lambda = -1 - \frac{2\omega^2 x_0^2}{E_x^*} < -1.$$

Thus, when the impact surface is $\mathcal{S} = \{(x, y, \dot{x}, \dot{y}) | x = x_0\}$*, we have* $|\lambda| > 1$*.*

BIBLIOGRAPHY

Altendorfer, R., D. E. Koditschek, and P. Holmes (2004), Stability analysis of legged locomotion models by symmetry-factored return maps, *The International Journal of Robotics Research*, *23*(10-11), 979–999.

Bloch, A., J. Baillieul, P. Crouch, J. E. Marsden, and D. Zenkov (2003), *Nonholonomic mechanics and control*, vol. 24, Springer.

Buono, P. L., J. S. Lamb, and M. Roberts (2008), Bifurcation and branching of equilibria in reversible-equivariant vector fields, *Nonlinearity*, *21*(4), 625.

Buss, B. G., A. Ramezani, K. A. Hamed, B. A. Griffin, K. S. Galloway, and J. W. Grizzle (2014), Preliminary walking experiments with underactuated 3d bipedal robot marlo, in *Intelligent Robots and Systems (IROS 2014), 2014 IEEE/RSJ International Conference on*, pp. 2529–2536, IEEE.

Chevallereau, C., A. Gabriel, Y. Aoustin, F. Plestan, E. Westervelt, C. C. de Wit, and J. Grizzle (2003), Rabbit: A testbed for advanced control theory, *IEEE Control Systems Magazine*, *23*(5), 57–79.

Da, X., O. Harib, R. Hartley, B. Griffin, and J. Grizzle (2016), From 2d design of underactuated bipedal gaits to 3d implementation: Walking with speed tracking, *IEEE Access*.

Dingwell, J. B., and H. G. Kang (2007), Differences between local and orbital dynamic stability during human walking, *Journal of Biomechanical Engineering*, *129*(4), 586–593.

Garcia, M., A. Chatterjee, A. Ruina, and M. Coleman (1998), The simplest walking model: stability, complexity, and scaling, *Journal of Biomechanical Engineering*, *120*(2), 281–288.

Geng, T., B. Porr, and F. Worgotter (2006), Fast biped walking with a sensor-driven neuronal controller and real-time online learning, *The International Journal of Robotics Research*, *25*(3), 243–259.

Goswami, A. (1999), Postural stability of biped robots and the foot-rotation indicator (fri) point, *The International Journal of Robotics Research*, *18*(6), 523–533.

Goswami, A., B. Espiau, and A. Keramane (1997), Limit cycles in a passive compass gait biped and passivity-mimicking control laws, *Autonomous Robots*, *4*(3), 273–286.

Gregg, R. D., and L. Righetti (2013), Controlled reduction with unactuated cyclic variables: Application to 3d bipedal walking with passive yaw rotation, *Automatic Control, IEEE Transactions on*, *58*(10), 2679–2685.

Gregg, R. D., T. Lenzi, L. J. Hargrove, and J. W. Sensinger (2014), Virtual constraint control of a powered prosthetic leg: From simulation to experiments with transfemoral amputees.

Griffin, B., and J. Grizzle (2015), Nonholonomic virtual constraints for dynamic walking, in *54th IEEE Conference on Decision and Control (CDC)*, pp. 4053–4060, IEEE.

Grizzle, J., J. Hurst, B. Morris, H.-W. Park, and K. Sreenath (2009), Mabel, a new robotic bipedal walker and runner, in *American Control Conference, 2009. ACC'09.*, pp. 2030–2036, IEEE.

Grizzle, J. W., G. Abba, and F. Plestan (2001), Asymptotically stable walking for biped robots: Analysis via systems with impulse effects, *Automatic Control, IEEE Transactions on*, *46*(1), 51–64.

Grizzle, J. W., C. Chevallereau, and C.-L. Shih (2008), Hzd-based control of a five-link underactuated 3d bipedal robot, in *Decision and Control, 2008. CDC 2008. 47th IEEE Conference on*, pp. 5206–5213, IEEE.

Ijspeert, A. J. (2014), Biorobotics: Using robots to emulate and investigate agile locomotion, *Science*, *346*(6206), 196–203.

Isidori, A. (1995), *Nonlinear control systems*, Springer Science & Business Media.

Kajita, S., F. Kanehiro, K. Kaneko, K. Yokoi, and H. Hirukawa (2001), The 3d linear inverted pendulum mode: A simple modeling for a biped walking pattern generation, in *Intelligent Robots and Systems, 2001. Proceedings. 2001 IEEE/RSJ International Conference on*, vol. 1, pp. 239–246, IEEE.

Khalil, W., and E. Dombre (1999), *Modélisation, identification et commande des robots*, Hermès science publ.

Khalil, W., F. Bennis, C. Chevallereau, and J. Kleinfinger (1989), Symoro: A software package for the symbolic modelling of robots, in *Proceedings of the 20th ISIR*.

Koolen, T., T. De Boer, J. Rebula, A. Goswami, and J. Pratt (2012), Capturability-based analysis and control of legged locomotion, part 1: Theory and application to three simple gait models, *The International Journal of Robotics Research*, *31*(9), 1094–1113.

Lee, J. M. (2003), *Introduction to Smooth manifolds*, Springer.

McGeer, T. (1990), Passive dynamic walking, *The International Journal of Robotics Research*, *9*(2), 62–82.

McGhee, R. B. (1985), Vehicular legged locomotion, *Advances in Automation and Robotics*, *1*, 259–284.

Merker, A., J. Rummel, and A. Seyfarth (2011), Stable walking with asymmetric legs, *Bioinspiration & biomimetics*, *6*(4), 045,004.

Merker, A., D. Kaiser, A. Seyfarth, and M. Hermann (2015), Stable running with asymmetric legs: A bifurcation approach, *International Journal of Bifurcation and Chaos*, *25*(11), 1550,152.

Raibert, M. H. (1986a), Legged robots, *Communications of the ACM*, *29*(6), 499–514.

Raibert, M. H. (1986b), *Legged robots that balance*, vol. 3, MIT press Cambridge, MA.

Razavi, H., A. M. Bloch, C. Chevallereau, and J. W. Grizzle (2015), Restricted discrete invariance and self-synchronization for stable walking of bipedal robots, in *American Control Conference (ACC), 2015*, pp. 4818–4824, IEEE.

Razavi, H., A. M. Bloch, C. Chevallereau, and J. W. Grizzle (2016), Symmetry in legged locomotion: A new method for designing stable periodic gaits, *under review, Journal of Autonomous Robots*.

Sreenath, K., H.-W. Park, I. Poulakakis, and J. W. Grizzle (2011), A compliant hybrid zero dynamics controller for stable, efficient and fast bipedal walking on mabel, *The International Journal of Robotics Research*, *30*(9), 1170–1193.

Sreenath, K., H.-W. Park, I. Poulakakis, and J. Grizzle (2013), Embedding active force control within the compliant hybrid zero dynamics to achieve stable, fast running on mabel, *The International Journal of Robotics Research*, *32*(3), 324–345.

Westervelt, E. R., J. W. Grizzle, C. Chevallereau, J. H. Choi, and B. Morris (2007), *Feedback control of dynamic bipedal robot locomotion*, Taylor & Francis/CRC.

Wisse, M., A. L. Schwab, R. Q. Van der Linde, and F. C. van der Helm (2005), How to keep from falling forward: elementary swing leg action for passive dynamic walkers, *Robotics, IEEE Transactions on*, *21*(3), 393–401.